INVESTIGATION OF BIOMATERIALS-BASED STRATEGIES FOR CORNEAL RECONSTRUCTION

By
Jemin J. Chae

A dissertation submitted to Johns Hopkins University in conformity with the requirements for the degree of Doctor of Philosophy

Baltimore, Maryland

February, 2016

Abstract

Corneal blindness, resulting from corneal disease or injury, is the fourth leading cause of blindness worldwide. Corneal transplantation is the current standard treatment for restoring vision in many cases with a high success rate. However, high quality donors are in limited supply globally. In certain severe trauma cases, prompt treatment of the damaged cornea to preserve the corneal structure is critical. We address corneal blindness using two paradigms of reconstruction: replacement of the diseased cornea and prompt repair of the severely damaged cornea.

For replacement strategies, we evaluated the clinically available gamma-irradiated cornea through physical and biological characterization. In addition, we developed a xenotransplantable corneal substitute using decellularizing methods and structural reconstruction technologies. For prompt repair of severely damaged corneas, we treated severe blast ocular injuries with our novel collagen-based membrane and sulfate-based hydrogel adhesive. In addition, cellulose contact lenses were developed for application in the event of severe corneal damage. The biocompatibility of the contact lens was evaluated with *in vitro* methods and two animal models. Moreover, we developed a surgical technique that improved application of the biomaterial onto the corneal surface with a rabbit model.

The gamma-irradiated human cornea shared similar properties with the fresh human cornea. This suggests the gamma-irradiated human cornea would be a suitable corneal substitute in various ophthalmic applications. The animal tissue-based corneal substitute was macro- and microscopically reconstructed with our novel structural reconstruction technologies following invasive decellularization processes. In addition, the animal

tissue-based cornea showed ideal properties and demonstrated its potential as a corneal transplantation substitute in interlamellar and anterior lamellar keratoplasty animal models. The severe ocular blast injuries were effectively repaired with our collagen-based membrane and sulfate-based hydrogel adhesive. In addition, the cellulose bandage contact lens was developed and demonstrated its biocompatibility with both the rat subcutaneous implantation and the rabbit ocular irritation models. And the animal model for the contact lens application was greatly improved by our novel surgical technique.

In conclusion, we have investigated biomaterial-based approaches to reconstruct the damaged cornea which may serve to reduce corneal blindness and restore vision.

Advisor: Dr. Jennifer H. Elisseeff (Principle investigator, Reader)

Thesis Committee: Drs. Hai-Quan Mao (Chair), Albert S. Jun, Peter L. Gehlbach (Reader)

Acknowledgments

I have been greatly blessed to conduct my doctoral training with many people who deserve to be specially mentioned for their help and contributions that made this work possible. First, I would like to thank my PI, Dr. Jennifer Elisseeff for allowing me to be a member of such a wonderful group, and for supporting my research interests in corneal blindness. She has always provided keen insights and guidance that have inspired me to overcome challenges during my research. In addition, her extraordinary enthusiasm and unwavering dedication have taught me about the responsibilities of a scientist to the community and society. I am also deeply grateful for Professors Hai-Quan Mao, Albert Jun and Peter Gehlbach for their valuable comments, constructive suggestions and assessments from time to time, up to the last stages of my dissertation as members of my thesis committee. Furthermore, I am thankful for my former advisors, Professors Roy Chuck and Kangmoon Seo. They remain my best role models as clinician scientists, mentors and educators.

I would like to thank all the members past and present from the Elisseeff lab. Their numerous technical and intellectual supports were significant in the development of my academic ability. Dr. Winnette McIntosh-Ambrose introduced me to the field of tissue engineering and this lab as I searched for a field that could solve the problem of corneal blindness. Dr. Qiongy Guo and Qiaozhi Lu taught me fundamental techniques for conducting biomaterial research when I embarked into this field of study. Dr. Chaekyu Kin and Okhee Jun always showed me their sincerity and diligence with their contagious enthusiasm and love for the research. In addition, Dr. Kim was willing to share his experience, thoughts and philosophies of research that were tremendously helpful in

developing my own ideas. I also thank the eye team including Shoumyo Majumdar, Dr. Huifang Zhou, Freddy Espinoza and Daniel Mulreany.

It was incredibly joyful to work with my undergraduate students, Joseph Choi, Justin Lee and Yujung Shin. They are always contributing voluntarily to go the extra mile through intense and hard working hours. I could not forget their integrity, sincerity, effort, patience and dedication. In addition, I immensely appreciate the many animals for their sacrifice. They have been valuable in the fight against blindness.

I must also send my most sincere thanks to our collaborators. Drs. Morgana Trexler, Xiomara Calderon-Colon, Marcia Patchan and other Applied Physics Lab members opened my eyes to the mechanical aspects of biomaterials. I am thrilled to have worked and published with them and our manuscripts have shown our great relationship and productive collaborations. Professor Jin U. Kang generously allowed me to work with his great graduate student, Gyeongwoo Chon and supported my work by allowing me to use one of the most advanced optical coherence tomography systems in the US.

I am deeply grateful for all my friends and community for their support, encouragement, and prayer. I am especially thankful to Drs. Daero Na, Eunchul Kim, Jungsoo Suk and Jisuk Choi, and Jaeyoung Kim, Changkyu Yoon, Mrs. Ruth Cho, and the Maryland Christian Church fellowship. Finally, I would like to express my deepest gratitude to my family in Korea; especially my parents. Although they grew up me in the poorest place of Seoul, their love, sacrifice and support are greater than any others'. Most of all, I appreciate my God for His driven purposes.

Contents

Title i

Abstract ii

Acknowledgements iv

Content vi

List of Tables vii

List of Figures viii

Chapter 1: Introduction 1

Chapter 2: Background 4

Chapter 3: Application of a collagen-based membrane and chondroitin sulfate-based hydrogel adhesive for the potential repair of severe ocular surface injuries 22

Chapter 4: Physical and biological characterization of the gamma-irradiated human cornea 42

Chapter 5: Reconstructed decellularized tissue for corneal regeneration 63

Chapter 6: Nictitating membrane fixation improves stability of the contact lens on the animal corneal surface 114

Chapter 7: Evaluation of the biocompatibility of regenerated cellulose hydrogels with high strength and transparency for ocular applications 126

Bibliography 150

Curriculum Vitae 164

List of Tables

Table 5. 1. Information about antibodies ……... 113

Table 7. 1. Oxygen permeability measured for rigid gas permeable reference materials …... 146

Table 7. 2. Oxygen permeability and confidence limits for regenerated cellulose hydrogel ... 147

Table 7. 3. Ophthalmic observation by slit lamp biomicroscopy with the McDonald-Shadduck score system ……. 148

Table 7. 4. Gross ocular observation by the Draize Scale ..……..…… 149

List of Figures

Figure 3. 1. Curved vitrigel preparation procedures, wound repair model and burst test, and KBBI test …… 37

Figure 3. 2. The representative combat injuries on the ocular surface and their repair by suture, CS-PEG + CV and CS-PEG adhesive in a porcine eye model …… 38

Figure 3. 3. Maximum reparable wound size depended on the method of treatment and characteristics of the wound: in linear and round types of defects …… 39

Figure 3. 4. Vancomycin release kinetics and zones of inhibition measured for vancomycin released with encapsulated vancomycin hydrochloride (V-HCl) and vancomycin free base (V-FB) …… 40

Figure 3. 5. An external view of curved collagen vitrigel (CV) with blue dye, and a comparison between curved and flat collagen vitrigels on rabbit eyes …… 41

Figure 4. 1. Light transmission, compressive modulus, and hydration of fresh gamma-irradiated corneas, and outdated gamma-irradiated corneas …… 58

Figure 4. 2. Thermal properties of fresh and gamma-irradiated corneas …… 59

Figure 4. 3. Histology of fresh and gamma-irradiated corneas …… 60

Figure 4. 4. Transmission electron micrographs of fresh and gamma-irradiated human corneas in the mid-peripheral region …… 61

Figure 4. 5. Biological characterization of fresh and gamma-irradiated corneas …… 62

Figure 5. 1. Schema for generating the concave shape of the reconstructed cornea ... 93

Figure 5. 2. The method to evaluate curvature of the shaped reconstructed cornea using an optical coherence tomography (OCT) imaging system …… 94

Figure 5. 3. Schematic feature of the procedure of interlamellar keratoplasty …… 95

Figure 5. 4. Evaluation of the efficiency of conventional decellularized methods for porcine corneas ..…..…. 96

Figure 5. 5. Alteration of transparency of porcine corneas after each decellularization process ..……..……..…….…….…….. 97

Figure 5. 6. Effects of the combine decellularization protocol (I) ……. 98

Figure 5. 7. Effect of the combined decellularization protocol (II) ……. 99

Figure 5. 8. Effect of the reconstruction process for transparency of corneas ……... 100

Figure 5. 9. Macrostructural evaluation for native, decellularized and reconstructed corneas with H&E and Alcian blue staining ……... 101

Figure 5. 10. Ultrastructural evaluation for native, decellularized and reconstructed corneas …….. 102

Figure 5. 11. Characterization of corneas …….. 103

Figure 5. 12. Thermal properties of corneas …….. 104

Figure 5. 13. Mechanical characterization and degradation profile of corneas …….. 105

Figure 5. 14. Cytotoxicity analysis with Live/Dead cell staining for tissue culture plate, native, decellularized and reconstructed corneas …… 106

Figure 5. 15. Proliferation prolife of three corneal cell types on corneas …….. 107

Figure 5. 16. Immunocytochemistry for human epithelial cells, human keratocyte and bovine endothelial cells on tissue culture plate, native, decellularized and reconstructed corneas ……..… 108

Figure 5. 17. Representative gloss feature, 3D and 2D optical coherence tomography images for the mold and the shaped reconstructed cornea ……. 109

Figure 5. 18. Intrastromal implantation of the reconstructed cornea for rabbits ….. 110

Figure 5. 19. Implantation of the reconstructed cornea into rabbits with anterior lamellar keratoplasty ……. 111

Figure 5. 20. Pathological examination for the rabbit cornea implanted the reconstructed cornea with anterior lamellar keratoplasty …….. 112

Figure 6. 1. Surgical procedure for nictitating membrane fixation …… 122

Figure 6. 2. Evaluation of tear quantity and quality …….. 123

Figure 6. 3. Gross observation for untreated and NM-fixed eyes …….. 124

Figure 6. 4. Pathological examination for experimental and control corneas ……. 125

Figure 7. 1. Oxygen permeability measurements ……..… 141

Figure 7. 2. Bacterial endotoxin level for cellulose-based hydrogels ……..... 142

Figure 7. 3. Pathological examination of material implanted rats ……. 143

Figure 7. 4. Hydrogels with contact lens geometry and *in vivo* ocular irritation study …. 144

Figure 7. 5. Pathological examination for the native cornea, cellulose-derived and conventional contact lens (control) applied corneas …… 145

1. Introduction

The cornea is the outermost layer of the eye and a highly organized transparent tissue. The cornea is vulnerable to damage via various traumatic, degenerative, dystrophic, infectious and inflammatory corneal disorders. However, the cornea is limited in its ability to self-repair and cannot fully regenerate without proper treatments. Insufficient treatment for a damaged cornea will mostly cause a deformation of the organized corneal structure, which if left untreated leads to corneal blindness. Clinically, corneal transplantation remains the standard method to restore vison and is relied upon to cover a wide range of corneal disorders. However, donor shortages limit the application of this largely successful treatment world-wide. In addition, in cases of severe corneal damage such as corneal penetration, prompt surgical closure is paramount to restore vision. Delayed structural reconstruction of the severely damaged cornea will result in visual impairment and may preclude a corneal transplantation. Biomaterials have the potential to restore vision by reconstructing the damaged cornea. As a corneal substitute, novel materials could replace the damaged cornea and overcome the donor shortage issue. In addition, specifically designed biomaterials could provide a method to promptly reconstruct the damaged cornea to prevent visual impairment and act as a bridge-to-therapy to secondary reconstructive surgery including corneal transplantation.

In the following dissertation, the author addresses corneal blindness with two reconstruction strategies paradigms: replacement of the diseased cornea and prompt repair of the severely damaged cornea using various biomaterials. Chapter 2 of this thesis reviews the structure and composition of the cornea, corneal blindness and its treatments

as well as contemporary biomaterial-based approaches for corneal reconstruction. In Chapter 3, we propose a biomaterial-based method to promptly repair severe blast ocular injury using our novel collagen-based membrane and sulfate-based hydrogel adhesive. In addition, we attempt to develop these materials by creating a 3D scaffold of collagen and incorporating antibiotics into the hydrogel adhesive. This method efficiently repairs severe war-type ocular damage for preservation of corneal structure and the two developed technologies improve their applicability to the battlefield.

In Chapters 4 and 5, we investigate two tissue-derived biomaterials. We characterize the gamma-irradiated human cornea and the fresh human cornea to compare their physical and biological properties in chapter 4. The gamma-irradiated cornea is clinically available and could alleviate the donor shortage issue by reusing unsuitable donor corneas through engineering methods. Physical and biological characterization of the gamma and native corneas reveal similar properties, implying the gamma-irradiated human cornea could be a suitable corneal substitute.

Chapter 5 describes how we develop an animal tissue-based corneal substitute with decellularization methods through our novel vitrification and material shaping methods from Chapter 3. Using established characterization methods from Chapter 4, we demonstrate our novel vitrification and two-mold method successfully reconstruct the damaged decellularized cornea after the decellularization process both macro- and microstructurally. In addition, two animal models support the conclusion that our engineered cornea has the potential to act as a xenotransplantable corneal substitute.

Chapter 6 describes a surgical technique I developed as a veterinary surgeon to address the reduced stability of biomaterials on the animal cornea because of the nictitating membrane. By fixing the nictitating membrane on the upper eyelid, stability of the biomaterial, especially the contact lens, is markedly increased and this technique contributes to a successful study documented in the following chapter. In Chapter 7, we describe the development of a cellulose bandage contact lens for preserving vision in the event of severe corneal damage that is applicable both in the battlefield and for civilians. In addition, we establish the biocompatibility of the cellulose hydrogels which may improve the healing process of the cornea as shown in other applications.

2. Background[1]

2. 1. Cornea

2. 1. 1. Anatomy and Physiology

The cornea is a transparent fibrous tunic, connected with the conjunctiva and the sclera in the limbus area. The tissue compromises 1/6 of the total surface of globe that covers the anterior chamber, iris and pupil [1]. Eye lids protect the cornea from the external environment and the nictitating membrane shares the protective function with eyelids in animals except in primates and humans [2]. The cornea is an avascular tissue. Instead of a vascular system, the supply of oxygen and nutrition, and the excretion of waste products are provided by the aqueous humor and tears. Sensory nerves, especially pain receptors, are richly distributed in the cornea and help to protect this tissue through their high sensitivity. Tear fluid always covers the corneal surface, which helps to maintain homeostasis of the corneal epithelium and prevents dehydration of cornea.

In humans, the cornea consists of five morphologically recognized layers. From outside to inside, they are the epithelium, Bowman's layer (absent in some animals), stroma, Descemet's membrane and endothelium. The epithelium is comprised of 5-7 layers of non-keratinized epithelial cells which cover the anterior corneal surface. The epithelium has 3 different types of cells: superficial cells, wing cells and basal cells.

[1] Part of this chapter was previously published as a paper here: Elisseeff JE, Madrid MG, Lu Q, Chae JJ, Guo Q. (2013) "Future perspectives for regenerative medicine in ophthalmology" **Middle East African journal of ophthalmology** 20 (1): 38–45.

Unlike other types of epithelial cells, the columnar basal cells possess mitotic and proliferative activity [3, 4]. The columnar cells are hypothesized to drive their regenerative activity from limbal stem cells [5, 6]. After migration, columnar cells differentiate to wing cells and ultimately to superficial cells [3]. Each corneal epithelial cell is tightly connected with neighboring epithelial cells or corneal matrix that functionally prevents invasion of pathogens to the stroma. The Bowman's layer (or Bowman's membrane) is an acellular layer at the interface between the corneal epithelium and stroma and is considered a condensate of the most anterior portion of the stroma [7]. The function of this layer is not fully understood but the layer may contribute to maintaining corneal shape. This layer has some regenerative ability, but damage may lead to scarring.

The corneal stroma comprises approximately 85% of the thickness of the cornea with an organized layer-by-layer connective tissue [7]. The main composition of the stroma is collagen (mainly type I collagen) and proteoglycans (dominantly decorin and lumican) [8] which work together to keep the stroma precisely organized and transparent. The collagen fibrils, consisting of collagen fibers, are uniformly positioned into lamellar and transverse layers that allow light transmittance without scattering [9, 10]. The stroma cell, the keratocyte, is sparsely distributed in the layer and is quiescent. However, when the cornea is injured, the cell can transform into a fibroblast that reconstructs the damaged cornea. In case of deep corneal injury, the fibroblast may form scar tissue that reduces transparency of the cornea [11]. The cornea is 75% to 85% water which is closely related to its transparency. When epithelium and endothelium is functionally damaged, deturgescence could be affected which allows an increase of 200% (epithelium)

and 500% (endothelium) in corneal thickness after 24 hours because of the influx of water [12]. Descemet's membrane is the basement membrane of the corneal endothelium. Damage to this layer could result in the corneal rupture that would be expected to cause corneal edema. Although the ruptured area is covered by endothelial cells, the membrane is not regenerated.

Endothelium is the innermost layer of the cornea with a monolayer of flattened endothelial cells [13]. Approximately 400,000 endothelial cells are arranged with a hexagonal mosaic pattern in this layer. The main function of this layer is pumping out water from the stromal layer using energy-dependent Na+/K+ adenosine triphosphatase (ATPase) pumps and other associated complexes [14, 15]. The compensatory ability is available with enlargement and migration of the remaining neighboring cells that covers the defective area after the loss of endothelial cells [16]. However, due to their limited regenerative ability, normal age-related loss or damage of endothelial cells could allow increased imbibition of water into stroma and lead to corneal swelling and finally to corneal blindness [15, 17].

2. 1. 2. Function of cornea

The main roles of the cornea could be simplified to protection, light transmission and refraction. The protective function from corneal structure integrity is critical since intraocular contents are vulnerable to the external environment. Mechanically, the highly organized corneal stroma consists of collagen lamellae which produce mechanical elasticity. This property of the cornea confers the ability to withstand biaxial load which renders mechanical protection. In addition, the cornea could protect the eye from

chemical and pathological insults with its specific epithelial structure. As described above, corneal epithelial cells are tightly connected to each other with tight junction complexes including desmosomes, adherens junctions and tight junctions, which prevent the passage of substances through the intercellular space. Moreover, the cornea has a light protective function. UV irradiation induces retinal damage by disruption of homeostasis, oxidative stress and DNA damage which leads to impairment of photoreceptors [18]. By blocking the UV light, the cornea associates with the lens to protect retina [19]. Optical clarity is one of fundamental properties of the cornea. The cornea allows transmittance of approximately 95% of light in the visible spectrum which activates photoreceptors of the retina. Ultra-structurally, small and nearly identical diameter collagen fibrils and symmetric interfibrillar spaces contribute to produce this great light transmittance ability. In addition, the highly organized and flattened lamellar structure of cornea transmits the light only in the forward direction which prevents light scattering [10]. Functionally, the corneal endothelium and epithelium maintain corneal deturgescence which prevents corneal swelling and increasing opacity. The cornea is the principle refractive tissue in the eye, contributing about 75% of total refraction [1]. The novel concave shape of cornea produces the refractive power that ensures visual acuity. Corneal curvature is governed by the intrinsic structure and extrinsic environment [7]. The rigidity of the anterior corneal stroma appears to have an especially important role in maintaining the corneal curvature [20]. When the cornea has an unfavorable curvature, refractive errors would reduce the quality of vision. However, several reports presented that corneal shape could be corrected over time with other ocular geometric changes [21-23]. The

mechanism concerning this correction is not clear but the anterior interweaving is considered to play some role in controlling curvature [1].

2. 2. Corneal blindness and treatment

2. 2. 1. Corneal blindness and diseases

The vulnerable cornea can be damaged through various reasons and it is well known that corneal blindness is the fourth leading cause of blindness worldwide [24]. The epidemiology of corneal blindness is complicated and varies with infectious, nutritional, inflammatory, inherited, iatrogenic and degenerative corneal diseases. Those disorders could cause inappropriate corneal structure such as corneal scar formation that ultimately leads to visual impairment and corneal blindness [25].

Corneal trauma causes various degrees of corneal damage from corneal erosion to corneal rupture. A good prognosis can be expected after mild corneal damage without surgical treatments if it is well controlled and treated. However, a moderate to deep traumatic corneal wound leads to corneal haze or scar formation during the natural healing process even when standard treatments are applied. In addition, severe corneal damage by trauma, such as a penetrating corneal wound or a blast injury leads to corneal blindness with high incidence and a bad prognosis can be expected. In those cases, surgical repair should be conducted in a timely manner to preserve the eye from endophthalmitis, tissue necrosis and ultimately visual impairment.

Trachoma is a typical infection and the most common cause of blindness worldwide [26]. It is predominant in developing countries in Asia and Africa, and easily

controlled through public health interventions. However, trachoma is commonly found in children of developing countries and presents its specific symptom, recurrent follicular conjunctivitis. The symptom is problematic because it leads to corneal irritation with entropion and trichiasis, causing scarring and ultimately corneal blindness.

Keratoconus is a bilateral, non-inflammatory and progressive corneal dystrophy with a high incidence, approximately 1 per 2000, in the general population [27]. The main symptom of keratoconus is the cornea becomes thinner and more concave shaped. This symptom alters corneal curvature and induces improper refractive power, astigmatism and nearsightedness. In addition, keratoconus causes corneal swelling which increases corneal opacity and scarring. Specifically designed contact lens would reduce astigmatism and somewhat improve visual quality. In addition, riboflavin crosslinking could slow the progression of the disease. However, the cornea will ultimately be opaque and lead to corneal blindness.

Fuchs' dystrophy is the most common corneal endotheliopathy in the US [28]. The main symptom of this disorder is gradual endothelial cells deterioration without any specific incidents. When the compensatory ability is exhausted, the endothelium does not efficiently pump out water from the stromal layer and finally results in corneal swelling and visual distortion. In addition, the epithelium is damaged which would accelerate visual impairment.

Furthermore various inflammatory corneal diseases including Mooren’s ulcer and Steven’s Johnson Syndrome, nutritional diseases such as vitamin A deficiency and secondary ocular surfaces diseases cause corneal blindness.

2. 2. 2. Corneal transplantation

Although other treatments may be able to alleviate symptoms and reduce disease progress, corneal transplantation is the fundamental and gold standard treatment to restore vision from corneal blindness. The cornea is the most commonly transplanted tissue worldwide [25]. Due to its unique immune privilege, the success rate is relatively high [29]. However, the eye bank cannot provide a sufficient amount of high quality of donor tissue except in North America, resulting in long waiting lists for corneal transplantation in most countries [30]. Various corneal transplantation techniques are available depending on the clinical indication. Penetrating keratoplasty, anterior lamellar keratoplasty and endothelial keratoplasty are mostly applied and each method has its specific purpose.

Penetrating keratoplasty (PK) is the replacement of all five layers of the cornea whereas lamellar keratoplasty targets replacement of only diseased corneal layers [31]. Although this technique has been replaced by other lamellar keratoplasty techniques, PK remains the most common keratoplasty procedure worldwide [25, 31]. The procedure can be used in many indications of corneal diseases without limitations. In addition PK potentially provides the best optical or therapeutic results since this technique does not produce a lamellar interface between the donor and host tissue. However, PK increases the risk of many complications including epithelial and endothelial rejection, donor endothelial cell loss and astigmatism. Endothelial cell loss resulting in future corneal failure is especially common which led to the rapid adoption of other new procedures to replace PK [32, 33].

Anterior lamellar keratoplasty (ALK) is the standard procedure used to replace epithelium and stromal tissue. Since host endothelial cells are retained and relatively unaffected after the procedure, ALK has significant merit concerning endothelial cell loss. In addition, this technique eliminates endothelial allograft rejection which is one of major complications in PK. However, technical difficulties including separation of anterior stroma layers from Descemet's membrane limits widespread adoption of this procedure [25]. Remaining anterior stroma may reduce visual acuity by haze formation during the stromal healing process and astigmatism remains disadvantages of ALK. Deep anterior lamellar keratoplasty (DALK) is an advanced procedure that removes the entire corneal stroma with minimal damage to corneal endothelium. Due to the removal of whole stroma, this procedure could reduce the incidence of the remaining stroma-to-stroma interface which might limit the optimal visual quality in ALK. Using the big bubble technique, injection of air to separate Descemet's membrane from the stroma, DALK procedure may allow full removal of corneal stroma.

Endothelial keratoplasty has replaced PK as a favorable procedure for treating endotheliopathy such as Fuch's dystrophy. The technique initially strips the Descemet's membrane and endothelium from the recipient cornea. After stripping, donor tissue is attached using air tamponade without sutures. Depending on remaining Descemet's membrane, the technique is classified as Descemet Stripping Endothelial Keratoplasty (DSEK) or Descemet membrane endothelial keratoplasty (DMEK). The best advantage of this procedure is predictable and rapid visual habitation. By elimination of astigmatism after PK, fast visual rehabilitation can be achieved. However, the most common complications of endothelial keratoplasty are endothelial graft rejection, primary graft

failure, and iatrogenic glaucoma [34]. In addition, unpredictable donor lamellar adhesion resulting in dislocation limits widespread of this technique [35].

2. 3. Reconstruction of the cornea using biomaterials and tissue engineering approaches

Biomaterial approaches have attempted to develop corneal substitutes using various approaches to address corneal blindness. Initially, a number of synthetic materials have been explored as biomaterials for the eye. While millions of contact lenses or various devices have been utilized on patients around the world, development of a synthetic corneal substitute has had little success [36]. In the meantime, the field of tissue engineering and regenerative medicine developed into a major force in creating tissue substitutes. The general approach of tissue engineering is to employ biomaterials as temporary scaffolds to support and direct cells to form new tissue. While tissue engineering has reached clinical testing and even commercialization for applications, including skin, bone and cartilage, it has been slow to reach ophthalmology and corneal reconstruction. There are a number of strategies to reconstruct the cornea with a regenerative medicine approach using biomaterials.

2.3.1. Corneal substitutes

For addressing the global shortage of high-quality donors for corneal transplantation, the importance of developing an optimal corneal substitutes are emphasized in the recent tissue engineering field. Optimal corneal substitutes must fulfill the natural function of cornea: maintaining transparency; having an adequate refractive index; protecting the inner ocular structures from external hazards, including pathogens

and ultraviolet (UV) light; having proper mechanical properties to tolerate the intraocular pressure and allowing diffusion of oxygen and nutrients [37]. In addition, as biomaterials, they must be biocompatible, nontoxic, neither immunogenic nor mutagenic and integrate well with the recipients' surrounding tissues and cells [1]. There are two main substitute categories: Synthetic keratoprostheses and tissue-engineered corneal substitutes.

2. 3.1.1. Keratoprostheses

The synthetic keratoprostheses (K-Pro) were the first corneal substitute developed. They consist of two main parts: The transparent optical center and the surrounding skirt designed to support the implant. Depending on the type of K-Pro, additional supporting components may be found [38]. The optical region is commonly made of plastic polymers, including poly (methyl methacrylate) (PMMA), poly(2-hydroxyethyl methacrylate) (pHEMA) and polydimethylsiloxane (PDMS), which do not integrate well with the native tissue. The skirt provides the mechanical stability and biological integration critical to reducing adverse results [30]. The major complications derive from integration problems and include device extrusion, stromal melting, epithelial thinning and persistent epithelial defects. An overview of available prostheses is provided below.

The Boston K-Pro (Dohlman-Doane keratoprosthesis) is FDA approved and is considered the gold standard in synthetic corneal substitutes. Type 1 consists of a central PMMA optical region, a porous back plate and a titanium locking ring that locks on native corneal tissue. The type 2 K-Pro was designed for patients suffering from severe diseases of the ocular surface, such as Stevens–Johnson syndrome (SJS) and ocular cicatricial pemphigoid (OCP), who are unable to maintain eyelid function. With the exception of the additional anterior protruding rod in the central area, the Boston KPro types 1

and 2 have the same structure. Although recent reports indicate good clinical outcomes, there are still relatively high complication rates in the main indications such as SJS [39, 40].

The osteo-odonto keratoprosthesis (OOKP), like the Boston type 2 K-Pro, is primarily used for patients with severe dry eye. The concept of the OOKP was derived from research showing that integration is maximized while immune reactions are minimized through the use of the patient's own tissue, including cartilage [41], and tibial bone [42]. The OOKP uses a canine tooth, its alveolar bone and ligament as a skirt to support the central optic component. A retrospective study of the OOKP shows high retention rates (85%) over 19 years, including in SJS and OCP patients, with low complication rates [43]. Even with the additional complex and invasive surgical procedures and the risk of resorption of the tissue, the OOKP is the most successful and well known K-Pro in use today [36].

The AlphaCor^{TM} K-Pro is manufactured by altering the water content in pHEMA during the polymerization of the optical center and the skirt. Unlike other K-Pros, the design of the AlphaCor^{TM} utilizes the interpenetrating polymer network to permanently connect the two regions. The porous pHEMA allows for the vigorous invasion of keratocytes, resulting in a better integration with host tissue [44]. Because of this stromal skirt repopulation, the retention rate is relatively high [45]. Unfortunately, even though there are promising short-term results, the fixation failures caused by stromal melting and intraoptic deposits still limit the usefulness of the AlphaCore ^{TM} K-Pro in long term applications [36].

2. 3. 1. 2. Bottom-up types of engineered corneal equivalent

Bottom-up types of tissue engineering corneal substitutes promise to overcome the many challenges and deficiencies of synthetic materials. Tissue-engineered corneal substitutes are constructed by naturally generating an extracellular matrix (ECM) component with or without corneal cells. It is well established that the ECM directs the fate of cells, therefore, the fabrication of the proper ECM components could produce an ideal corneal substitute, able to mimic the native corneal function. Since the components of the ECM are natural (biological) polymers, there is higher biocompatibility and integration with host tissues when compared to synthetic polymeric materials, such as those in the different K-Pros. In addition, these substitutes can be used to generate a targeted corneal layer, such as the endothelium for Descemet's stripping endothelial keratoplasty (DSEK). Cosmetically, the tissue-engineered cornea is more similar to native cornea than the K-Pros and has the potential to provide a long-term or even permanent tissue replacement, indistinguishable from the original tissue.

Hydrogels are widely used as substitutes for various types of tissue and ECM. They are highly versatile materials that allow for the diffusion of oxygen and nutrients, have adjustable mechanical properties, can be designed to contain large volumes of water and are relatively biocompatible. The corneal stroma comprises roughly 85% of the corneal thickness and consists of keratocytes and ECM [7]. Since collagen type I is the predominant component of the corneal stromal ECM (approximately 70% of dry weight), it has been considered as the natural component to reconstruct it. As such, a corneal substitute was developed using highly cross- linked collagen hydrogels using N-(3-dimethylaminopropyl)-N'-ethylcarbodiimide (EDC) and N-hydroxysuccinimide (NHS)

technology. It was successfully transplanted into several animal models, including guinea pig, dog and pig, either as a deep lamellar or full thickness keratoplasty [46]. Recently, these collagen-based corneal substitutes were transplanted into 10 patients in a phase I clinical trial [47].After 24 months, there were no severe adverse effects and the implants allowed for epithelial and keratocyte migration in all patients, as well as slow nerve invasion in the younger patients. Eight of the patients, however, developed focal hazing, which may critically reduce vision quality. A long-term clinical study, with a large number of patients and further development of the material, will be needed if the material is to be used in clinical practice.

Non-cross-linked collagen hydrogels are generally composed of loosely packed collagen fibers, strongly contrasting with the highly condensed and well organized collagen fibers found in the stromal layer of the cornea. Recently, Takezawa et al. developed a type I collagen hydrogel membrane using a novel processing method, called vitrification, that we have been optimizing for ocular applications [48, 49]. The collagen hydrogel membrane was named vitrigel, and is made from a type I collagen solution prepared through a three-stage sequence: Gelation, vitrification and rehydration [50]. The vitrification step is unique in that it allows the collagen hydrogel to dry slowly so the collagen fibers can be reorganized and develop new hydrogen bonding interactions with each other. More importantly, unlike the opaque and comparably weak non-cross-linked collagen hydrogels, vitrigels are clear and possess greatly enhanced mechanical properties that are critical for ocular applications. Most important, with this method we begin to approach the more complex structure of the native cornea matrix with collagen fibers that are critical for both physical and biological function of the tissue. Using

vitrigel, we evaluated the reconstruction of the three different corneal layers: Epithelium, stroma and endothelium [51]. Human LSCs were cultured successfully on the vitrigel, demonstrating maintenance and upregulated expression of the putative stem cell markers ABCG2 and p63, respectively, thus indicating that vitrigels can preserve the LSC phenotype. *In vivo*, keratocytes exhibit a characteristic dendritic morphology with extensive intercellular contacts [50]. However, when the corneal stroma is wounded, the cells transform either to wound-healing fibroblasts or to scar-forming myofibroblasts, which form a disorganized and opaque ECM. Therefore, it is desirable to promote the fibroblast phenotype and proliferative activity of keratocyte wound healing. Keratocytes cultured on vitrigels exhibit enhanced dendritic branch density and length, compared to tissue culture plate control. An enhanced expression of aldehyde dehydrogenase (ALDH) and keratocan (important markers of keratocyte phenotype and function) was also observed. These results suggest that the use of vitrigel materials may benefit corneal stromal regeneration, as well as promote better integration and cellular function *in vivo*. Finally, promising results were obtained for endothelial culture on the vitrigels. In short, vitrigels demonstrate unique advantages over other materials; these include optical transparency, mechanical strength and handling convenience. They are also easy to process, store and manipulate. These properties make vitrigels novel and very promising options for corneal tissue engineering and regeneration.

2. 3. 1. 3. Tissue-based corneal equivalent

Engineering a new cornea or subset of the cornea remains a long-term interest. Beside bottom-up approaches, tissue-based top-down ones are emerging as promising strategies. To provide surgeons with a corneal substitute, tissue-based corneal substitute

has a structure similar to native tissue. Xenotransplantation can be employed to obtain corneal substitutes, particularly in developing countries that suffer from low donor rates because of regional, cultural and other institutional issues [52]. Although rejection is the greatest obstacle to widespread use of xenotransplantation, fully decellularized components of the animal tissue may be clinically applied without immune rejection [53]. A good example of this approach is the success of porcine heart valve transplantation [54]. Decellularization can be applied, not only to xenogeneic, but also to allogeneic cornea tissues for transplantation. This could, in theory, improve the clinical outcome and reduce the complications associated with allogeneic corneal transplants.

A decellularized tissue provides a three-dimensional ECM structure for corneal reconstruction that fully mimics the native tissue and can be applied with or without the addition of a cellular component. Corneal decellularization has been performed on porcine corneas using various methods: Sodium dodecyl sulfate (SDS) [55], Triton-X [56], hypertonic NaCl solution [57, 58], and high hydrostatic pressure [59, 60]. These methods have been used by several groups in Asian [55-60], and on bovine corneas by our group [61]. There are various results in the literature, however, with some reports failing to provide proper quantitative data on the presence of cell debris, which may cause immune reactions and affect transparency [62]. The relevance of cell debris can be seen in a recent article reporting that both untreated corneas as well as corneas in which cell debris was not removed experienced immune rejection in a primate model [58, 62] Recently, our group successfully engineered decellularized corneas from both porcine and bovine tissue with a novel method, combining chemical and enzymatic treatments to remove the cellular components, but also incorporating vitrification and cross-linking

steps to improve the optical and structural properties of the device. With this novel procedure, we were able to create acellular porcine and bovine corneas containing almost no cellular debris, while maintaining impressive light transmission rates and biocompatibility. Moreover, the curvature can be manipulated in this novel, engineered decellularized cornea, allowing for control of the refractive index, which is essential to corneal function. Another promising decellularizing method is gamma-radiation. The prosthesis is already on the market, commonly known as the human allogeneic "sterile cornea." A study reported the results of 150 patients who received anterior lamellar keratoplasty with this product. They showed high levels of epithelialization within a few days and no postoperative infection or rejection in all but four cases, all of which occurred in patients with preexisting corneal melting [63]. In addition, we successfully characterized this cornea with biological and mechanical methods. The gamma-irradiated human cornea shared similar properties with the fresh human cornea. It is suggested that the gamma-irradiated human cornea would be a suitable corneal substitute in various ophthalmic applications [64].

2. 3. 2. Corneal adhesive

Some specific ocular injuries or even surgical incisions require highly localized tissue repair. Traumatic defects or even cataract incisions would benefit greatly from a repair strategy that includes both physical apposition (i.e. tissue bonding) and biological stimulation to promote new tissue development. Such technology for local corneal repair includes tissue adhesive (TA) biomaterials that can form chemical, biological or physical bonds with the molecular residues from local tissue. Before the development of TAs for the eye, nylon sutures were the standard method to close corneal wounds caused by

cataract incision, corneal ulcer, trauma or transplant [65]. These new materials offer to improve on the past regenerative results of sutures for surgical and non-surgical wounds by reducing operation time, minimizing scar formation [66] and providing a vehicle for delivery of biological signals that can stimulate tissue development.

Corneal tissue adhesives can be categorized as biologic or synthetic in nature [67]. Fibrin glue is a biologic adhesive that is composed of fibrinogen and thrombin [68]. The material is prepared by processing plasma from autologous blood or from plasma pools of volunteer donations. In corneal surgery, fibrin glue has been employed to seal corneal perforations and it melts along with adhering amniotic membrane to the ocular surface. The adhesive can also be applied in different kinds of keratoplasty and even to temporarily stabilize keratoprosthetics [68]. Fibrin glue is easy to prepare and is highly biocompatible. However, as a blood product, it carries the risk of disease transmission and its low tensile strength and fast degradation are significant drawbacks [67]. Thus, there is a significant need for an ocular adhesive that has the biological benefits and compatibility of a biological adhesive but has the increased mechanical strength and durability specifically needed for ocular applications.

Synthetic adhesives provide faster polymerization (i.e. cure rate) and higher tensile strength, making them good candidates for corneal wound closure devices. Among all of the synthetic adhesives for corneal wound healing, polymeric hydrogels have been proven to be the most effective. For example, a dendritic linear copolymer based on poly (ethylene glycol) (PEG), glycerol and succinic acid was shown to be effective in closing linear, full-thickness corneal incisions [69]. After photo crosslinking using UV light, the adhesive produced a firm seal, matching the strength of sutures. In

vivo studies of this dendrimeric adhesive have shown no toxicity and good biocompatibility [67]. Another version of the material that does not require light has been applied clinically in Europe. While these materials have the strength and durability required clinically, they have little biological activity to stimulate new tissue growth.

To create an ocular adhesive that combines the benefits of both synthetic and biological materials, a biosynthetic ocular adhesive was engineered in our group. The first generation adhesive we developed was composed of a modified chondroitin sulfate (CS), CS-aldehyde that, when combined with polyvinyl alcohol co-vinylamine (PVA-A), cross-linked together and with the surrounding tissue. The aldehyde-amine reaction provided the basis for this adhesive; however, the biocompatibility was not perfect [70]. Therefore, we created a second generation material that combines CS and PEG. In this case, the CS is modified with succinimide groups and is chemically cross-linked with PEG-amine molecules through a Michael Addition [71]. In addition to being more biocompatible, the CS-PEG adhesive formed tight seals on corneal incisions to maintain a normal intraocular pressure. Ultimately, the combination of the biological benefits of the CS, which includes reducing scar formation and inflammation, with the physical benefits of the synthetic PEG, which provides durability, allows the creation of an optimal ocular tissue adhesive. Drugs, such as antibiotics or anti-inflammatory molecules, can also be incorporated into the adhesives based on clinical need [72].

3. Application of a collagen-based membrane and chondroitin sulfate-based hydrogel adhesive for the potential repair of severe ocular surface injuries [2]

3. 1. Introduction

Due to the development of explosive weapons, the risk and severity of eye injuries have been increasing on the battlefield [73, 74]. Although protective goggles help to reduce the incidence of eye injuries, ocular trauma comprised approximately 12% and 5% of injuries in the Persian Gulf War and in the recent Iraqi conflict, respectively [75-77]. Approximately half of all blast trauma in the recent operation was composed of open globe trauma [77], which is characterized by much worse visual outcomes compared to closed globe trauma [78].

Prompt surgical closure using sutures is the accepted method of primary repair for open globe injuries [75]. However, the technique requires trained ophthalmic surgeons, special instruments, a surgical microscope and surgical facilities, all of which could be limited in the battlefield. In addition, suture repair is limited for certain injuries, for example those associated with significant tissue loss. In such injuries wound

[2] Part of this chapter was previously published as a paper here: Chae JJ, Mulreany DG, Guo Q, Lu Q, Choi JS, Strehin I, Espinoza FA, Schein O, Trexler MM, Bower KS, Elisseeff JH. (2014) "Application of a collagen-based membrane and chondroitin sulfate-based hydrogel adhesive for the potential repair of severe ocular surface injuries" **Military medicine** 179 (6): 686-694

apposition may be inadequate which may in turn lead to serious astigmatism. Moreover, critical ophthalmic injuries are usually sustained in conjunction with other life-threatening damage, such as brain and facial damage [74, 79] that can lead to the delay of ophthalmic repair and treatment.

Ocular adhesives can potentially serve as an initial treatment alternative to traditional ophthalmic surgical procedures [80]. Cyanoacrylate and fibrin glue have been used clinically. However, the former is toxic, inhibits the epithelial healing process, may be easily dislodged and is limited in use to very small penetrating wounds. The latter is not strong enough to hold tissue together for repair of open globe injuries and has a high risk of secondary infection by bacteria and fungi [67, 81]. Several other biological and synthetic adhesives as well as laser welding are under development [82-84]. However, these approaches have limitations, including complex application methods, additional required instruments, reduced adhesive coverage and a narrow range of treatable wound types.

Our group has developed an adhesive hydrogel composed of chondroitin sulfate–polyethylene glycol (CS-PEG) and a collagen vitrigel (CV) membrane that can serve as a biological bandage or an eye patch. Previous studies have shown that the CS-PEG adhesive is nontoxic, transparent, flexible, hydrophilic, and can incorporate drug delivery systems [85], making it ideal for use in the eye [71]. When compared to conventional ophthalmic adhesives, the CS-PEG adhesive demonstrated its superior biocompatibility and mechanical properties [86]. Furthermore, those merits were confirmed by the porcine partial keratectomy model [71]. CV is a thin, transparent, and flexible membrane produced by the vitrification of a traditional collagen hydrogel [87]. Previous studies

have shown the membrane has excellent mechanical and biological properties to support the three types of corneal cells as a biomaterial [51, 88]. In addition, our recent data indicated the membrane could support the regeneration of corneal epithelium and stroma.

The main purpose of this study is to evaluate the potential of CS-PEG + CV as a method to repair blast injuries which cause open globe injuries using a cadaver model. In addition, cornea shaped CV was developed to facilitate CV application by matching the eye contour and antibiotic release was incorporated in the CS-PEG adhesive to prevent potential infections.

3. 2. Materials & Methods

3. 2. 1. Synthesis of flat and curved collagen vitrigels

Collagen vitrigels (CVs) were fabricated using a modified method from a previous publication [51]. Briefly, 0.5% collagen type I solution (AteloCell, Koken, Tokyo, Japan) and culture media composed of Dulbecco's modified Eagle's medium, 10% fetal bovine serum, 20 mM 4-(2-hydroxyethyl)-1-piperazineethanesulfonic acid and 1% penn-streptomycin solution were uniformly mixed in a 1:1 (v/v) ratio. 5 ml of the solution was incubated at 37 °C to produce a gel; this gel underwent a vitrification process at 10 °C and 40% of humidity. Finally, the material was rehydrated with phosphate buffered saline (PBS) to form a thin, transparent, flexible collagen membrane. Generally, flat CV is referred to as CV for short, unless otherwise specified.

To enhance the handling convenience of CV, a curved CV was developed. The first two steps were the same as those for traditional, flat CV as mentioned above except that a concave mold assembled in a glass chamber with a small opening, instead of culture dishes, was utilized for curved CV (Figure 3.1A). After gelation, the slow vitrification was first introduced to the gelled collagen in the assembled mold in the same incubation condition for 24 hours. Fast vitrification of the collagen gel was then carried out for two weeks by disassembling the glass chamber from the concave mold (Figure 3.1B). As with flat CV, the curved CV was rehydrated before applying on the corneas (Figure 3.1C).

3. 2. 2. Chondroitin sulfate - succinimidyl succinate synthesis and adhesive preparation

The formation of CS-PEG adhesive was achieved by reacting CS-succinimidyl succinate (CS-NHS) with 6-arm poly(ethylene glycol)-amine (PEG-$(NH_2)_6$, 20.0 kDa, SunBio, Ansan, South Korea). Synthesis of CS-succinimidyl succinate (CS–NHS) was carried out as described previously [86]. Briefly, 10%, 25% and 67% (w/v) PBS solution of CS (chondroitin sulfate A, 25.0 kDa, New Zealand Pharmaceuticals Ltd, Palmerston North, NZ), *N*-hydroxysuccinimide (NHS) (Thermo Fisher Scientific, Rockford, IL), and *N*-(3-Dimethylaminopropyl)-*N'*-ethylcarbodiimide hydrochloride (EDC, Sigma-Aldrich, St. Louis, MO) were combined in a v/v ratio of 6.0:1.5:1.5 and left to react for 10 min at 37 °C. The resulting mixture was frozen and extracted with -20 °C ethanol. Precipitated CS-NHS was then washed nine times with ethanol and dried under high vacuum overnight. The prepared CS-NHS and PEG-$(NH_2)_6$ were both dissolved in the PBS and HEPES buffer to a final concentration of 20% (w/v). The two components were chilled

on ice for 5~30 minutes and then mixed at a 1:1 (v/v) ratio. The mixed adhesive was immediately applied to the ocular surface.

3. 2. 3. Repair of porcine cadaver model for battlefield injuries and burst test

A porcine cadaver eye model was used to simulate linear and circular open wounds in corneal, corneoscleral and scleral regions of the eye. Fresh porcine eyes were obtained from a local abattoir. A type of full thickness injury was made in each eye to mimic open globe injuries: a linear laceration or a circular penetrating wounds representing without or with loss of tissue, respectively. Linear wounds were made by inserting various types of scalpel blades perpendicular to the tissue (Figure 3.1D). In case of a larger wound which could not be made by only inserting scalpels, the wounds were made by inserting the scalpel and then slicing across the tissue until the desired length was achieved. Each linear laceration was measured to confirm the desired dimensions before beginning the repair by ophthalmic caliper. Due to the size limitation of porcine eye, the maximum length of linear laceration in the corneal and corneoscleral areas were set at 16mm and 22mm, respectively, based on references [89, 90]. Circular penetrating wounds were made by inserting a trephine through the tissue perpendicularly. These wounds were made in different sites, including corneal, scleral and corneoscleral regions.

The damaged porcine globes were repaired via one of three treatment modalities: traditional suture closure, CS-PEG adhesive-only, or CS-PEG adhesive + CV membrane. All suture repairs were performed by a surgeon (JJC) using 10-0 nylon sutures for corneal repairs and 8-0 nylon sutures for corneoscleral and scleral repairs, as per routine primary repair on the battlefield [78]. Sutures were not applied in the case of circular wounds

since such wounds cannot be closed by primary apposition. Repairs using CS-PEG adhesive were made by applying the adhesive directly to the wound using the pipette (Figure 3.1E). The surface of the eye around the defect site was dried to get the maximal effect of the adhesive using ophthalmic sponges prior to adhesive application. The volume of adhesive applied to the eye ranged from 30 to 200 µl depending on the size of the defect. Repairs made using both the adhesive and CV membrane were performed in a similar fashion to adhesive-only repairs, except after applying the adhesive, the rehydrated CV membrane was placed over the defect and spread out to remove any wrinkles and assure CV adhesion to the CS-PEG adhesive (Figure 3.1F).

For each tissue, wound and treatment type, repairs on increasing defect sizes were conducted until the critical size was reached. A successful repair was defined as a sealed defect that allowed pressurization of the eye to 35 mmHg or greater. Each wound was determined as repairable if it could be successfully repaired three times in a row or four times within five trials. The eyes were pressurized via a 25 gauge needle inserted through the limbus into the anterior chamber. A syringe pump injected balanced salt solution (BSS) into the anterior chamber of the repaired eyes at a fixed rate of 20 ml/hr. A digital manometer (DigiMano 1000, Netech Systems, Farmingdale, NY) was placed in line with the pump. The manometer was monitored until the intraocular pressure reached 35 mmHg, at which point the syringe pump was stopped and the wound was assessed to determine whether there was leakage of fluid on the ocular surface (Figure 3.1G).

3. 2. 4. *In vitro* antibiotic release test and Kirby-Bauer bacterial inhibition test

To calculate the release kinetics, an antibiotic release test was conducted. CS-PEG adhesive hydrogels were made using a cylindrical mold (100 μL, 4.0 mm thickness × 6.0 mm diameter). Either 2% of vancomycin hydrochloride (V-HCl, Sigma-Aldrich, St. Louise, MO) or vancomycin free base (V-FB) was encapsulated into the CS-PEG adhesive as previously described [91]. Each cylinder shape adhesive was immersed by 1 ml PBS in a 24-well tissue culture plated and then incubated at 37 °C for performing the release study. Three replicates were used in each condition. PBS fractions were collected at various time points up to three weeks and the concentration of vancomycin in each fraction was analyzed using high performance liquid chromatography (HPLC) with an analytical column (XTerra® RP18, Waters, Milford, MA).

The Kirby-Bauer bacterial inhibition (KBBI) test was performed to analyze the potency of the antibacterial effect of vancomycin. Cylindrical CS-PEG adhesives (20 μL, 2.0 mm thickness × 3.6 mm diameter) were made with 2% antibiotics (V-HCl or V-FB) as mentioned above. The adhesive masses were put on PBS for time periods ranging from 0~6 days and then placed on the culture dishes uniformly covered with *Staphylococcus aureus* (*S. aureus*, MicroBiologics, St. Cloud, MN) and Lysogeny broth agar (Sigma-Aldrich). Five replicates were made for each time point and condition. The plates were incubated at 37 °C for 24 hours and the zone of inhibition (ZOI) around each hydrogel was measured (Figure 3.1H). The areas of ZOI were analyzed by the Mann-Whitney test to evaluate the differences between two groups at each time point. Statistical significance was established at p-values < 0.05.

3. 2. 5. Cadaver and *in vivo* application of cornea shaped collagen vitrigel in the rabbit model

To check the usability of curved CV, four rabbit cadaver eyes (Pel-Freez Biologicals, Rogers, AR) were used. Both curved and flat CVs were examined by placing them on top of the cadaver eyes or inserted into the corneal pockets. Cornea pockets were created using an ophthalmic crescent knife (Laseredge, Bausch&Lomb, Rochester, NY), and then either flat or curved CV was inserted into the cornea with 20 μl of CS-PEG adhesive on both sides. To improve visibility, CVs were stained by trypan blue (trypan blue stain 0.4%, Gibco, Grand Island, NY) before applying it. A routine cryosection was performed for making slides which were subsequently stained with hematoxylin and eosin (H&E). Following the *in vitro* cadaver work, an *in vivo* study was performed. All animals (n = 2) were treated under the approval of the Animal Care and Use Committee at Johns Hopkins University and the ARVO Statement for the Use of Animals in Ophthalmic and Vision Research. Curved and flat CVs were tested and compared using two male New Zealand White rabbits weighing 3.5 kg. Superficial keratectomy was performed using 8 mm Hessburg-Barron vacuum trephine and an ophthalmic crescent knife. After applying 20 μl of CS-PEG adhesive, the corneas were covered with either a curved or flat CV (8 mm diameter).

3. 3. Results

3. 3. 1. Repair of porcine cadaver model for battlefield injuries and burst test

Combat-related ocular wounds treated and photographed at the Walter Reed Medical Center were modeled in cadaveric eyes (Figure 3.2). The application of adhesive generally created a smooth and raised cap of hydrogel above the injury, except in cases when excessive moisture, which impeded the attachment of the adhesive, was still present on the eye. In contrast to adhesive alone, the CS-PEG + CV treatment conformed to the shape of the eye, creating a smooth surface. The CS-PEG adhesive + CV maintained sufficient transparency to observe the wound.

CS-PEG + CV and suture methods were able to repair the maximum size laceration wounds that we could make in both corneal (16 mm) and corneoscleral (22 mm) regions, whereas CS-PEG alone could only repair wounds as long as 5 mm in the corneal region and 6 mm in the corneoscleral regions (Figure 3.3A). In our experimental model, we found the linear injury model in the scleral region rarely leaked at the pressure of repair criteria due to the self-sealing by thick vitreous humor. For this reason, we excluded the linear sclera wounds in this study. On the other hand, the CS-PEG adhesive was also able to repair 3 mm diameter circular wounds in the cornea and 4 mm diameter wounds in the corneoscleral and scleral regions. By adding the CV membrane to the adhesive, we were able to repair the wounds of approximately double that diameter: 6 mm in the cornea and corneoscleral regions and 8 mm in the scleral region (Figure 3.3B).

3. 3. 2. Release and potency of CS-PEG adhesive encapsulated antibiotics

Release kinetics of two vancomycin forms (V-FB and V-HCl) in the CS-PEG adhesives were investigated (Figure 3.4A and B). In the cumulative release, the encapsulated V-HCl had a burst release where almost 60% of the total amount was

released. On the other hand, the amount of released V-FB (about 40%) was less than that of V-HCl after the first 5 hours. By the end of three days (72 hours), V-HCl and V-FB had released approximately 93% and 88% of their total loading amount, respectively. Although both forms started with the same amount of antibiotics, the V-FB release showed lower burst and more sustained release compared to V-HCl in the whole release period (Figure 3.4A). The daily amount of vancomycin released during the first nine days was above the minimum inhibitory concentration (MIC) in both the encapsulated V-FB and V-HCl forms. The encapsulated V-FB form released more than that of V-HCl during the experiments (Figure 3.4B).

The activity of antibiotics released from the adhesives was evaluated using the KBBI test. Due to the effect of burst release, V-HCl (8.6 mm) loaded CS-PEG adhesive significantly inhibited a larger area of bacteria than that of V-FB (7.6 mm) loaded adhesive. However, the size of ZOI turned around at 3 day time point; the radius of ZOI by V-FB capsulated adhesive was significantly larger than that of V-HCl capsulated CS-PEG at the 4 day time point. Even though the radius of ZOI was getting smaller, it could still get up to 3~4 mm by the final day of experiment (Figure 3.4C).

3. 3. 3. Applicability of cornea shaped collagen vitrigel patches

Using novel methods, a new CV was created with a controlled three-dimensional curvature relevant to the eye (Figure 3.5A). Compared to a flat CV, the curved CV improved the applicability. The curved CV showed a self-supporting capability (Figure 3. 5A) which facilitated the membrane handling compared to the flat CV when implanting in cadaveric eyes (Figures 3.5B-D). The three-dimensional shape of the curved CV

matched the corneal contour precisely, allowing extensive host-graft integration over a large area without any wrinkle formation due to unmatched curvature which had been observed with the flat CV. As shown in Figures 3.5E and F, the histological results further confirmed the integration of the curved CV in the lamellar corneal pocket. The applicability of curved CV was also confirmed *in vivo* (Figure 3.5G). Due to the matched curvature to the eye by the curved CV, the CS-PEG adhesive was able to be applied to the eye more uniformly and showed an enhanced attachment of the collagen membrane to the eye surface, compared to the flat CV which usually experiences large wrinkles.

3. 4. Discussion

In this study, we demonstrated that the combination of CS-PEG and CV has the potential to repair the types of open globe injuries which threat to vision on the battlefield. In previous retrospective studies, corneal abrasion and laceration were the most common injuries, accounting for more than one fourth of total eye injuries [92]. During OIF/OEF, the length distribution of reported corneal lacerations was from 0.5 mm to 12 mm, with a mean value of 3.7 mm [93]. Although the CS-PEG alone method has limitations in repairing the largest-sized wounds, it could potentially seal the majority of corneal laceration wounds on the battlefield as it can successfully repair wounds of up to 5~6 mm in length in the corneal and corneoscleral regions. In addition, the adhesive could help to prevent secondary injuries by additional applied force from outside since it can support the cornea by sealing the leakage of linear wounds. In the corneoscleral repair, CS-PEG alone is not adequate to repair the larger corneoscleral wounds (mean length 8.7 mm)

encountered in the Iraqi conflicts [93]. As results shown, the limitations of using CS-PEG alone for the large linear wounds found in war could be overcome by using it in combination with CV. The CS-PEG + CV method, as tested in our model, can successfully repair the maximum-sized injury in both corneal and corneoscleral regions. Since the sharp linear wounds created in the sclera were self-sealing, repair of linear scleral lacerations was not investigated. Yet, the performance of the CV and adhesive in the treatment of round scleral wounds and linear corneoscleral wounds suggests that CS-PEG + CV should be capable of adequately sealing the majority of scleral wounds encountered on the battlefield.

Approximately 30% of lacerations are not linear but are either stellate or round and accompanied by tissue loss. Although CS-PEG alone could not seal the large wounds adequately [94], the addition of the CV membrane contributed substantially to a more robust repair. After adding CV membrane, the reparable defect size was markedly greater than that of CS-PEG alone. When repairing wounds with adhesive alone, it was necessary to use enough adhesive to create a hydrogel "cap" over the wound to provide sufficient strength for the repair. The protruding cap could irritate the palpebral conjunctiva and wear down with friction. The CV membranes provided a structural rigidity to the repair and reduced the amount of adhesive needed to seal the wound. By reducing the amount of adhesive, the CV membrane could minimize the potential interference of the CS-PEG hydrogel bump with the eyelid.

Clinically, penetrating wounds have to be treated in a timely manner because such injuries increase the risk of endophthalmitis, tissue necrosis and deformation of eye [95]. Due to the specific limiting conditions of the battlefield, those types of wounds were

associated with very poor outcomes [93]. Conventional suturing is the gold standard for repairing penetrated ocular injuries, except where the amount of tissue loss prevents adequate apposition or where too much irregular astigmatism would be generated. Tissue adhesives could be an alternative method to seal defects in the ocular surface. However, this method has so far been limited to relatively small diameter wounds ($\leq$ 2 mm) [94]. Penetrating keratoplasty, conjunctival flap or patch graft is recommended for relatively large penetrating wounds [95]. However, including suture closure, these methods are only useful under trained ophthalmologists and surgical team with ophthalmic instruments and an equipped operating room. Recently proposed methods with adhesive and various patches such as amniotic membrane, absorbable fibrin sealant patch, and tectonic drapes have been developed to treat larger penetrating wounds. However, those materials only can treat wounds less than 5 mm in diameter [96-100]. The CS-PEG and CV are promising materials in the battlefield since the combination of these two materials could potentially be used to treat larger size wounds without reliance on a fully equipped microsurgical operating room. In addition, another benefit of these materials is their transparency that allows subsequent care providers to examine the injuries without removing materials.

The severe wounds encountered with military injuries have high rates of contamination and subsequent infection. Incorporating antibiotic with the CS-PEG adhesive has the potential to reduce the incidence of infection through the application of a controlled release of bioactive antibiotics for several days. Vancomycin is a widely used antibiotic for treating injuries of eye [95]. Based on the results, CS adhesive with V-FB is superior to the V-HCl form considering the sustainability of the releasing kinetics and

inhibition of bacteria. By converting V-HCl into V-FB, we profoundly decreased the water solubility (from 200 mg/ml to 20 mg/ml) of vancomycin and increased its hydrophobicity [91], which is essential for controlled release in a hydrophilic environment such as CS-PEG tissue adhesive. Consequently, V-HCl embedded adhesive had a high burst release initially, while the V-FB form released a significantly reduced amount followed by a more controlled release. Moreover, both forms were able to release higher than MIC which could inhibit the growth of bacteria for nine days. We believe that the release time of vancomycin is enough to cover the time for evacuation of the wounded solder to a hospital where definitive medical and surgical treatment can be offered.

CV is a biosynthesized acellular membrane with a distinctive advantage of being able to form customized three-dimensional shapes by modifying the processing method. While the flat CV membrane generally conforms well to the curvature of the eye occasionally some wrinkles form at its edges during application. We speculate that these wrinkles may weaken the seal and potentially impede epithelial healing. The performance of the CVs was improved by using curved CVs with a shape that conforms to the natural curvature of eye.

We have demonstrated, in a porcine cadaver model, the potential suitability of CS-PEG + CV to provide sufficient mechanical strength to treat most battlefield ocular injuries. However, additional challenges need to be overcome to create a viable product for use on the battlefield and in the clinic. These include the requirement for stable long-term storage of the adhesive in a usable form that would be ready on demand, and the availability of CVs in a variety of basic sizes and configurations.

Although we demonstrated that the combination of CS-PEG adhesive + CV as a promising method to treat severe ocular traumas, there are additional limitations to creating a viable product for use on the battlefield and in the clinic. The adhesive and patch require stable long term storage in a usable form that would be ready on demand and CVs are needed in a variety of basic sizes and configurations. Additionally, the gelation time of CS-PEG adhesive is significantly decreased in temperatures exceeding 35 °C16. Some operations in high temperature situations may decrease application time by approximately one minute after its preparation. If the CS-PEG + CV is to be used in a high temperature environment, reasonable cooling methods need to be developed.

3. 5. Conclusion

The combination of CS-PEG adhesive and CV membrane demonstrated potential for repairing penetrating ocular injuries on the battlefield. In addition, incorporation of antibiotic release functionality and modification of the curvature of the collagen membranes were accomplished to further improve the applicability of those materials for the special demands of battlefields.

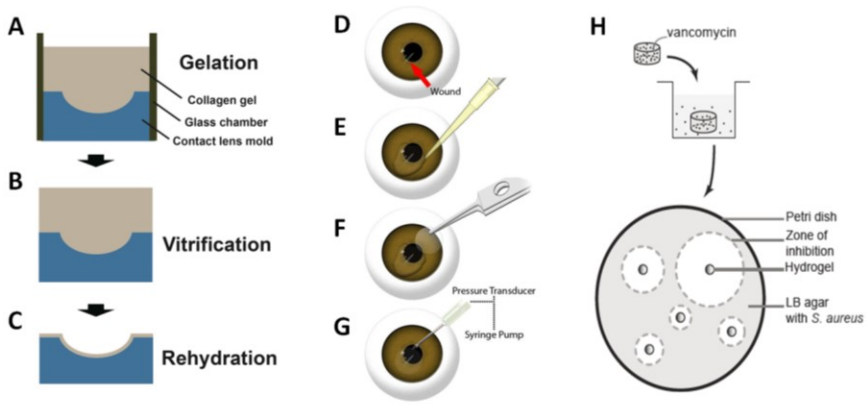

Figure 3. 1. **Curved vitrigel preparation procedures, wound repair model and burst test, and KBBI test**. After mixing the collagen solution with the proper media, the process of gelation (A) and fast vitrification (B) were followed in the curved mold. Rehydration using PBS buffer was performed prior to application to the eye (C). A defect was made in enucleated porcine eyes via scalpel or trephine (D), followed by application of CS-PEG adhesive to the wound and surrounding tissue using a conventional pipette (E). In the case of CV and CS-PEG adhesive repairs, the CV was applied to the wound area with forceps after adhesive application (F). After allowing the CS-PEG to firm up for approximately 15 minutes, a needle was inserted through the limbus into the anterior chamber and the intraocular pressure was increased through use of a syringe pump until the intraocular pressure reached 35 mmHg. If there was no leakage, the corneal wound was considered to be repaired (G). After creating vancomycin encapsulated in CS-PEG columns and soaking them in PBS buffer, the columns were placed on a Petri-dish uniformly covered with *Staphylococcus aureus* (*S. aureus*, MicroBiologics, St. Cloud, MN). At each time point, the zone of inhibition (ZOI) was measured (H).

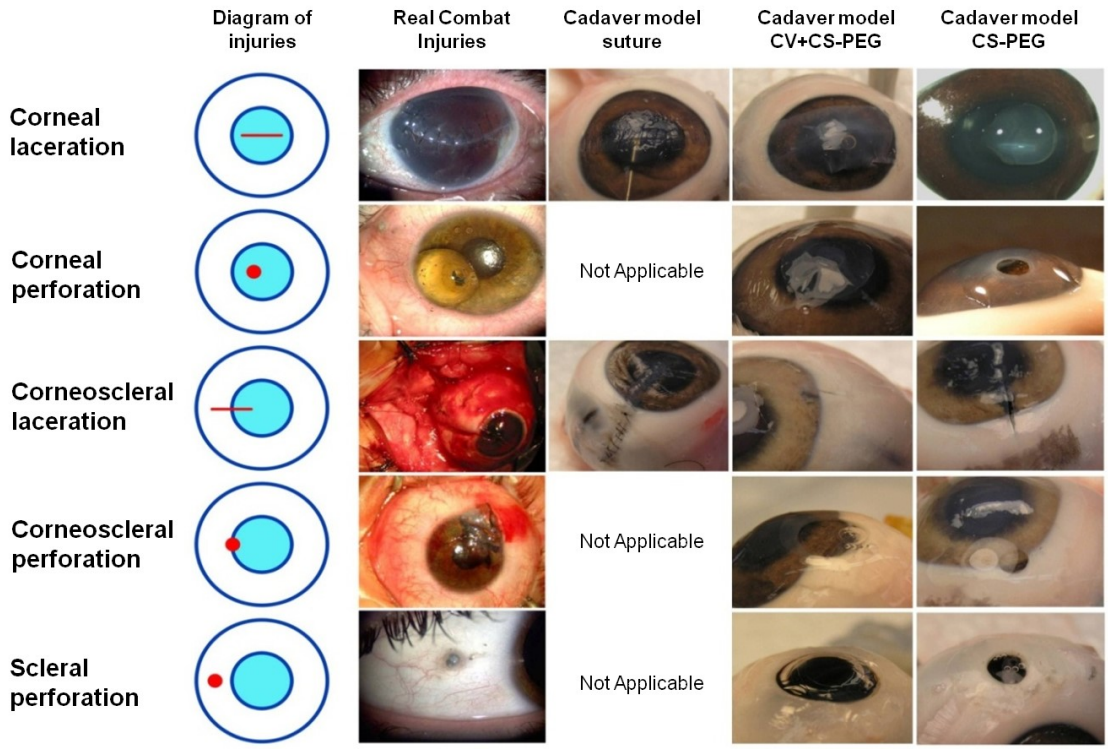

Figure 3. 2. The representative combat injuries on the ocular surface and their repair by suture, CS-PEG + CV and CS-PEG adhesive in a porcine eye model. CS-PEG adhesive + CV can effectively repair the various types of wounds without deformation of the eye. In addition, they can be applied to large, circular wounds that can be difficult to treat using only conventional sutures or adhesives.

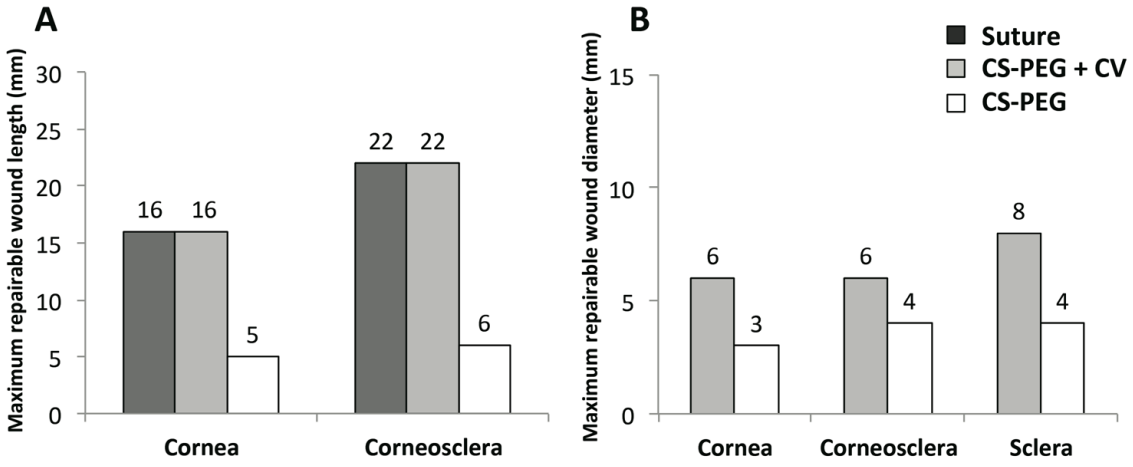

Figure 3. 3. Maximum reparable wound size depended on the method of treatment and characteristics of the wound: in linear and round types of defects. Conventional suture and CS-PEG + CV treatment can repair the same maximum size of wounds in linear types of defects on both corneal and corneoscleral surfaces **(**A). The addition of the CV membrane enabled the repair of larger wounds than CS-PEG adhesive alone. The reparable defect size using CS-PEG + CV was markedly greater than that of CS-PEG alone (B). The maximum repairable size of ocular wounds was indicated by each bar.

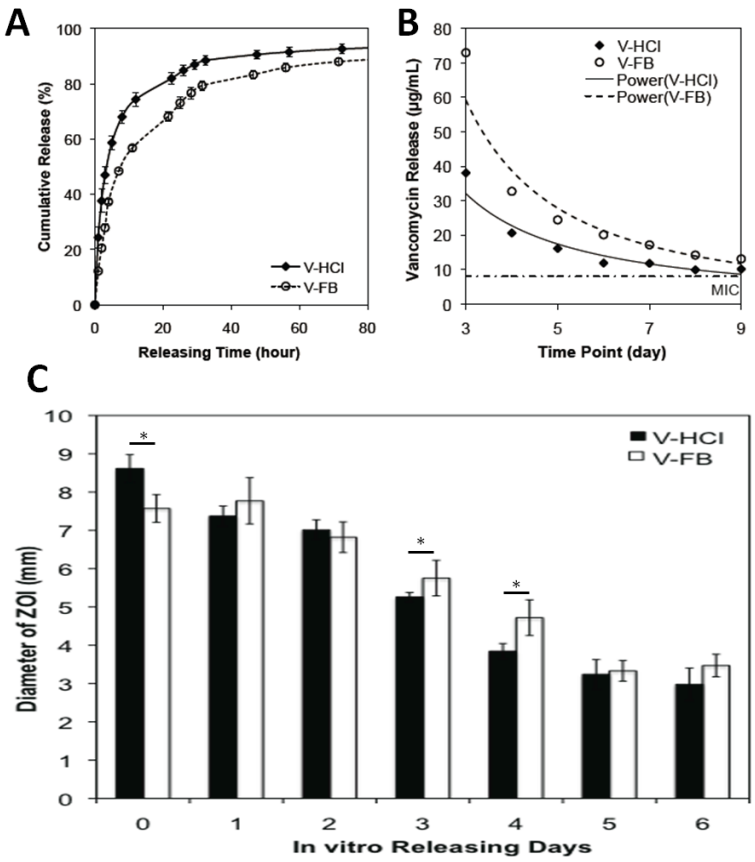

Figure 3. 4. Vancomycin release kinetics and zones of inhibition measured for vancomycin released with encapsulated vancomycin hydrochloride (V-HCl) and vancomycin free base (V-FB). Cumulative release of vancomycin in CS-PEG adhesive showed V-FB had a more sustained release than V-HCl (A). The daily release amounts of the two forms of vancomycin in CS-PEG adhesive demonstrated both forms of vancomycin could be released above the MIC for up to nine days (B). A KBBI test of the antibiotics released confirmed the released antibiotics efficiently inhibit the growth of bacteria up to seven days and that encapsulated V-FB are more efficiently controlled than encapsulated V-HCl (C). *: Statistical significance was established by Mann-Whiney test at $p < 0.05$.

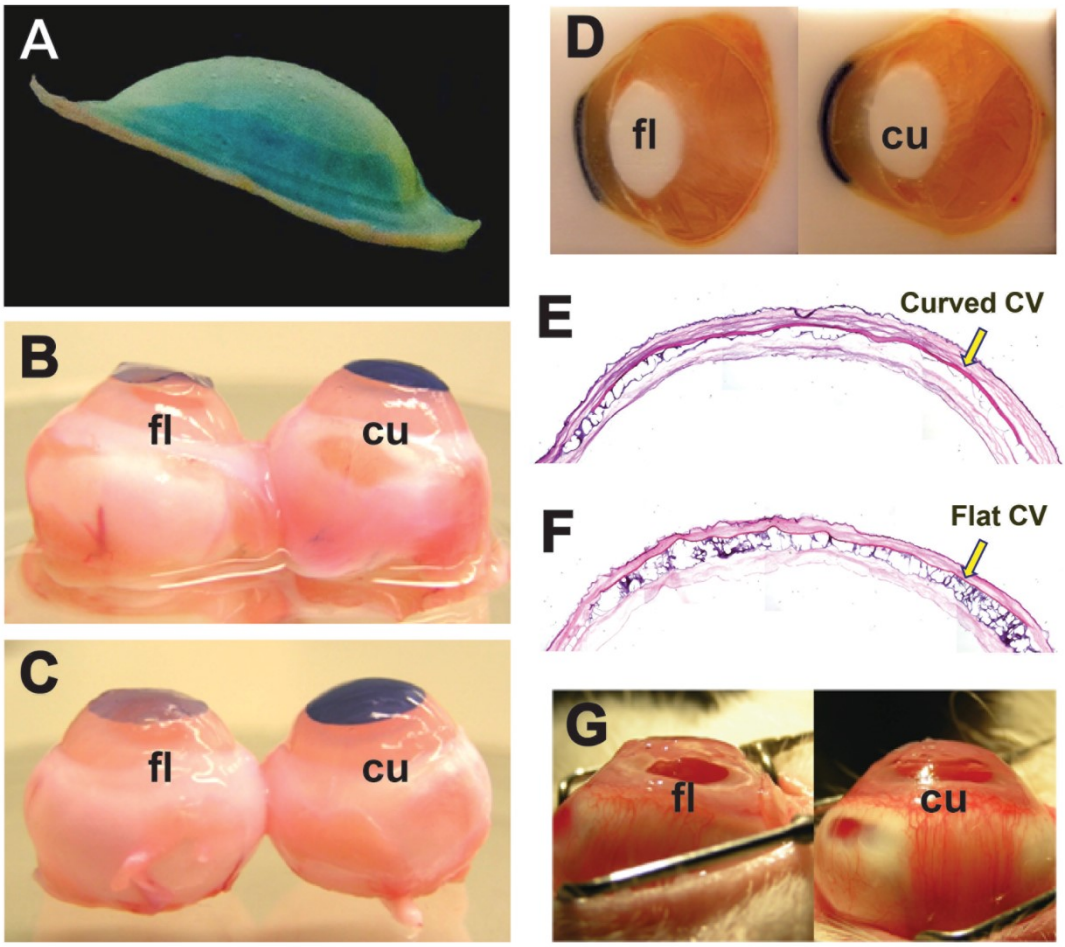

Figure 3. 5. An external view of curved collagen vitrigel (CV) with blue dye, and a comparison between curved and flat collagen vitrigels on rabbit eyes. A representative photograph of the curved CV stored in PBS buffer (A). Flat and curved CV applied to the rabbit cornea: on the cornea (B) and in the lamellar corneal pocket (C). The images of CVs on the ocular cross-section (D), in the lamellar corneal pocket with H&E staining (E-F) and on live rabbit corneas affixing by CS-PEG bioadhesive (G) showed the superior attachment of the curved CV which did not cause wrinkles on the corneal surface. **fl**: Flat CV and **cu**: Curved CV. Scale bar: 1 mm

4. Physical and biological characterization of the gamma-irradiated human cornea[3]

4. 1. Introduction

Corneal disease is the fourth leading cause of blindness worldwide [101]. Many of these cases could be cured by allogeneic corneal transplantation, one of the most common and successful tissue transplantation procedures [63]. However, there are obstacles to corneal transplantation, including insufficient quality and quantity of donors, a short viable timeframe between donation and transplantation, contamination by bacteria and fungi during donor preparation, and the possibility of disease transmission [63, 102, 103]. In addition, conventional corneal transplantation has a high failure rate in high-risk populations due to immune rejection or mechanical graft failure [102].

The gamma-irradiated human cornea (VisionGraft®, Tissue Banks International, Baltimore, MD) may help to alleviate such problems. Donor corneas unsuitable for transplantation, typically due to low endothelium quality, become commercial gamma-irradiated corneas though cryogenic treatment and approximately 17-23 kGy of gamma irradiation from a cobalt-60 source. Those processes extend shelf life, expanding the pool of potential donor corneas. Another benefit to using the gamma-irradiated cornea is the

[3] Part of this chapter was previously published as a paper here: Chae JJ, Choi JS, Lee JD, Lu Q, Stark WJ, Kuo IC, Elisseeff JH. (2015). "Physical and Biological Characterization of the Gamma-Irradiated Human Cornea" **Cornea** 34 (10): 1287-1294

reduction of disease transmission risk and microbial contamination during donor preparation. Third, the gamma-irradiated cornea can potentially be transplanted in populations at high risk of immune rejection when using conventional human corneas [63, 104, 105]. Despite the fact that the gamma-irradiated cornea cannot be used for full-thickness corneal transplantation, it can be used for lamellar keratoplasty (which does not require viable endothelial cells) and for corneal patch grafts [105]. In addition to applications in corneal surgery, this tissue can be used to cover glaucoma tube shunts and act as the skirt of the keratoprosthesis [63]. To accommodate the surgeon's preferences, these corneas can also be provided in various shapes and sizes with full- or partial-thickness stromas.

Gamma irradiation of donor corneas, however, may alter the structure of corneal extracellular matrix (ECM) and change its physical and biological properties, which would in turn affect cornea physiology and limit its surgical utility. The effect of gamma irradiation has been studied on various tissues. Although there were no significant changes after applying a low dose (2-10 kGy) of gamma irradiation in the Achilles tendon [106], most studies have indicated that gamma irradiation induces substantial physical and/or biological alterations with structural changes [107-111]. The structural alterations include inter- and intra-collagen crosslinking, collagen molecular fragmentation or degradation by polypeptide chain scission, and collagen fibril reorganization [111-114]. Because collagen is the main component of corneal proteins [115], gamma irradiation could be expected to biologically and physically alter the corneal ECM. In addition, altered physical and biological properties influence the

reconstruction process of the cornea and surgical manipulation such as handling and suturing the donor tissue.

Although the gamma-irradiated cornea has been used successfully in clinical situations and its popularity is rising, there is limited information about its optical properties and structure, especially compared with fresh donor corneas [116, 117]. Therefore, the purpose of this study was to characterize physical and biological properties of the commercial gamma-irradiated cornea, to determine if it is a viable surgical material.

4. 2. Materials & Methods

4. 2. 1. Corneas

Gamma-irradiated human corneas were donated by Tissue Banks International (Baltimore, MD). Human corneas were handled according to the Declaration of Helsinki, and the study was approved by Johns Hopkins Medicine Institutional Review Boards. A total of 28 fresh and 25 gamma-irradiated corneas (within expiration date) were used in this experiment. The average age of donor, average days in storage, and average preservation time were 52.9 ± 15.8 years (range, 18~74 years), 8.8 ± 4.4 days (range, 1 ~ 13 days), and 12.5 ± 5.1 hours (range, 3 ~ 22.7 hours), respectively. As a negative control, to emulate a degrading tissue matrix, six gamma-irradiated corneas that were more than two years past the manufacturer's expiration date ("outdate gamma-irradiated corneas") were evaluated for the characteristics of light transmittance, compressive modulus, and hydration. The term 'gamma-irradiated cornea' indicates a cornea within its expiration date. Fresh corneas were preserved in Optisol GS (Bausch & Lomb, Rochester, NY) at 2–

8 °C and gamma-irradiated corneas were stored in hyperosmolar albumin-based media at room temperature. All samples were prepared by removing the scleral rim and epithelium using conventional ophthalmic scissors and a #15 blade before performing experiments.

4. 2. 2. Light transmittance

Five full-sized, fresh and gamma-irradiated corneas, and three full-sized outdated gamma-irradiated corneas were cut with a 10-mm trephine. Each cornea was washed 3 times using balanced buffer solution (BSS) and placed on a 48-well microplate. Using a multimode microplate reader (Synergy 2, Biotek, Seattle, WA), the blank-corrected light absorbance of each cornea was measured in 10-nm increments over the full visible spectrum (400 to 700 nm). The light transmittance was derived by the Beer-Lambert law with the equation, transmittance (%) = e-absorbance x 100.

4. 2. 3. Compressive modulus

Immediately after measuring light transmittance, the same corneas were used for measuring compressive modulus. Compression was applied to the full-sized sample from 0% to 10% thickness of the cornea using an Electroforce 3200 testing instrument (Bose, Eden Prairie, MN) with a 250-g load cell at room temperature. The modulus was calculated using a computer program (MATLAB, MathWorks, Natick, MA) to find the slope of the best fit curve with a linear region of stress versus strain plot, as performed previously [86].

4. 2. 4. Hydration

Swelling ratio (wet mass / dry mass) was determined as follows: five half-sized, fresh and gamma-irradiated corneas and three half-sized, outdated gamma-irradiated corneas were immersed in a sealed conical tube containing 10 mL of BSS and incubated at 37°C for 24 h. After 24 h, the swollen corneas were weighed after removing excess BSS using filter paper and a digital balance (XS 105, Mettler toledo, Columbus, OH). The samples were then lyophilized for 72 hours and weighed to obtain the dry mass.

4. 2. 5. Thermal properties

The thermal properties of each cornea, collected from both the central and peripheral areas, were characterized using differential scanning calorimetry [DSC (DSC 8000, PerkinElmer, Norwalk, CT)] as described previously [88]. Using a 4-mm trephine, samples approximately 20-mg in mass were collected from five full-sized, fresh and gamma-irradiated corneas. One sample was taken from the central cornea and 4 buttons were excised from the peripheral region. The specimens were sealed in a 30-μL aluminum pan to prevent evaporation of the water content; an empty sealed pan was used as a reference. At a rate of 5°C/min, the samples were cooled from room temperature to -30°C under nitrogen flow, and then heated to 90°C. A set of cooling and heating was repeated. The thermograms were analyzed and the denaturation temperature was determined using the Pyris series software (PerkinElmer, Norwalk, CT). Denaturation temperatures of each cornea were analyzed regardless of location to determine whether there were any differences between fresh and gamma-irradiated corneas. The geometric effect on denaturation temperature was then evaluated by comparing the central and peripheral regions of each cornea.

4. 2. 6. Structural assessment

Five half-sized, fresh and gamma-irradiated corneas were used to access corneal structure. After removing central and peripheral portions of the cornea using 1.5- and 4-mm trephines, each specimen was collected for microstructural assessment using a 3-mm trephine. Other portions of the cornea were used for evaluating corneal macrostructure. Both fresh and gamma-irradiated corneas were dehydrated, embedded in paraffin and stained with hematoxylin and eosin (H&E) using standard techniques. For transmission electron microscopy (TEM), the central part of corneas was fixed using a solution of 3% paraformaldehyde, 1.5% glutaraldehyde, 5 mM $MgCl_2$, 5 mM $CaCl_2$, 2.5% sucrose, and 0.1% tannic acid in 0.1 M sodium cacodylate buffer at pH 7.2 overnight in a cold room. After a PBS buffer rinse, the samples were stained with 1% osmium tetroxide on ice for 1 hour, rinsed in deionized water, and stained *en block* overnight in Kellenberger uranyl acetate. Following dehydration with a graded series (75%, 95%, and 100%) of chilled ethanol solutions, the samples were embedded in EPON resin (Eponate 12, Ted Pella, Redding, CA) at 60°C for 60 to 96 hours. The embedded samples were sectioned using an ultramicrotome (Ultracut UCT, Leica, Wien, Austria), collected on grids, and stained with uranyl acetate. The samples were examined and electronic digital pictures were taken using a TEM (Philips 420, FEI Co., Hillsboro, OR) system at 80 kV. Images were taken at depths between 20 and 80% of full corneal thickness. After pictures were converted to TIF files, ten TEM images in each cornea were magnified approximately 100,000-fold. Five areas were randomly chosen in each picture, and areas were defined as 1×1 μm^2. The collagen fibrils within the square were manually counted by masked

observers, and the numbers of collagen fibrils were presented per μm^2, as demonstrated previously [118].

4. 2. 7. DNA content

The DNA content of each cornea was determined using Hoechst 33258 dye (Molecular Probes, Eugene, OR) as described previously [119]. Briefly, lyophilized corneas for the hydration test were digested in a 125-µg/mL papain solution (Worthington, Lakewood, NJ) for 16 hours at 60 °C, and the fluorescent intensity of a mixture of 30-µL papain digestion and 1 µg/mL of Hoechst dye in TNE buffer was measured using a fluorometer (DyNA Quant 200, Hoefer, Holliston, MA). The DNA content was calculated from a standard curve generated using calf thymus DNA.

4. 2. 8. Human corneal epithelial cell proliferation test

Fresh human corneas not used in the characterization were treated with 1.2 U/ml of dispase II (Roche Diagnostics, Mannheim, Germany) in the Epilife® medium (Invitrogen / Life Technologies, Grand Island, NY) at 4°C for 16 hours. Under a dissection microscope, epithelial sheets were collected and incubated in the 0.05% trypsin-EDTA solution at 37°C for 30 minutes. After vigorous pipetting and neutralizing trypsin-EDTA, primary cells were cryopreserved at -120°C for preparation for the proliferation assay. To evaluate the proliferation of human corneal epithelial cells (hCECs) on corneas and tissue culture plates (TCPs), a 48-well microplate was prepared. Each of 16 TCP wells was either covered by approximately 100-µm thick fresh or gamma-irradiated cornea or left untreated. hCECs were thawed in a 37°C water bath and subcultured in the Epilife medium with the Human cornea growth supplement (HCGS, Invitrogen/Life

Technologies, Grand Island, NY) and 2.5 ng/ml epithelial growth factor (EGF, Upstate Biotechnology, Lake Placid, NY) at a density of 5×10^4 cells/cm^2 until confluent. After detaching confluent hCECs using 0.05% trypsin-EDTA, the cells were seeded on the microplate with a density of 1.0×10^4 per well. At 0, 5, 14, and 21 days after seeding cells, the number of hCECs was measured in 4 wells of each of the three groups using the cell counting kit-8 CCK-8 (Dojindo Molecular Technology, Inc., Rockville, MD) following manufacturer instructions. The absorbance, correlated with the number of cells, was measured using a multimode microplate reader (Synergy 2, Biotek, Seattle, WA) at 450 nm.

4. 2. 9. Statistical analysis

Data are displayed as means ± standard deviation (S.D.). Results were analyzed by the Mann-Whitney test, Student's t-test or Spearman's rank correlation, depending on the size and character of samples. Statistical analyses were performed using SPSS 15.0 for Windows (SPSS Inc., Chicago, IL). Statistical significance was established at $p < 0.05$.

4. 3. Results

4. 3. 1. Light transmittance, compressive modulus and hydration

Transparency—the main characteristic of a cornea—elasticity (compressive modulus), and crosslinking density (swelling) were measured in three different corneas: fresh, gamma-irradiated, and outdated gamma-irradiated. There was no significant

difference between gamma-irradiated corneas and fresh corneas in transparency, elastic modulus, or crosslinking density (Figure 4.1).

To quantify transparency, we measured the transmittance of visible wavelength. Although the transmittance of visible light through gamma-irradiated cornea was slightly greater than that of the fresh corneas, the difference was not statistically significant. However, the light transmittance of the gamma-irradiated cornea was significantly greater than that of the outdated gamma-irradiated cornea from 400 to 540 nm (Figure 4.1A). The compressive modulus was measured by indentation. There was no difference in the elasticity between fresh corneas (24.4 ± 6.4 kPa) and gamma-irradiated corneas (25.1 ± 5.8 kPa, $p = 0.452$). However, the elastic modulus of outdated gamma-irradiated corneas (7.5 ± 2.5 kPa) was significantly lower than that of gamma-irradiated corneas ($p = 0.036$, Figure 4.1B).

Hydration (swelling ratio; wet weight/dry weight) was measured to assess the crosslinking density of the corneas. Wet masses of fresh, gamma-irradiated and outdated gamma-irradiated corneas were 97.58 ± 6.59, 96.18 ± 10.91 and 108.67 ± 3.60 mg, respectively. After lyophilization, the dry masses of fresh, gamma-irradiated and outdated gamma-irradiated corneas were measured as 13.98 ± 1.17, 14.3 ± 1.79, and 14.4 ± 0.72 mg, respectively. The dry masses between the different corneas were statistically similar ($p > 0.750$). There was no difference in swelling ratio between gamma-irradiated corneas (6.98 ± 0.16) and fresh corneas (6.73 ± 0.17, $p = 0.096$, Figure 4.1C). Outdated gamma-irradiated corneas, however, had a significantly larger swelling ratio (7.56 ± 0.40) compared to that of gamma-irradiated corneas (Figure 4.1C), indicating less crosslinking density ($p = 0.036$).

4. 3. 2. Thermal properties

The thermal properties, which represent matrix organization, differed between the gamma-irradiated and the fresh corneas. The denaturation temperature of whole gamma-irradiated corneas (61.8 ± 1.1 ^{0}C) was significantly lower than that of fresh corneas (66.1 ± 1.9 ^{0}C, p = 0.004, Figure 4.2A and C). This difference varied based on region, with similar denaturation temperatures in central regions (p = 0.413), but significantly lower in the peripheral region of gamma-irradiated corneas (p = 0.029, Figure 4.2B). Within gamma-irradiated corneas, the denaturation temperature of the central region of (64.2 ± 1.3 ^{0}C) was significantly higher (p = 0.010) than the peripheral regions (61.3 ± 1.5 ^{0}C). The denaturation temperatures of central (66.5 ± 3.0 ^{0}C) and peripheral (64.7 ± 2.8 ^{0}C) regions of fresh corneas were similar (p = 0.149, Figure 4.2B).

4. 3. 3. Macro- and microstructures of corneas

H&E staining and transmission electron microscopy (TEM) of the mid-peripheral region were used to measure the structure of gamma-irradiated corneas. Many keratocytes were found in the stromal layer of fresh corneas, whereas minimal cellular debris was observed in the stromal layer of gamma-irradiated corneas (Figure 4.3). In the TEM images, the gamma-irradiated cornea demonstrated lower collagen fibril density than did the fresh cornea (Figure 4.4A). Although intact cellular structures could not be detected, some cellular fragments were observed in the gamma-irradiated cornea stromal sample (Figure 4.4B). In a defined 1-μm^2 area, the density of collagen fibrils in the gamma-irradiated cornea stromal sample (160.6 ± 33.2 fibrils/μm^2) was significantly lower than that in the fresh cornea stromal sample (310.0 ± 44.7 fibrils/μm^2, p = 0.001,

Figure 4.4C). Qualitatively, we observed thinner collagen fibrils in the gamma-irradiated corneas compared with fresh corneas. Additionally, the density of collagen fibrils in gamma-irradiated cornea stromal samples ranged from 80 to 240 fibrils/μm^2 whereas fibril density in the fresh cornea stromal samples ranged from 260 to 400 fibrils/μm^2 (Figure 4.4D).

4. 3. 4. DNA content of the corneas and human corneal epithelial cell proliferation test

Regarding biological properties, the residual cell content (amount of DNA) was decreased after gamma-irradiation, with gamma-irradiated corneas (1.04 ± 0.11 μg DNA/mg- dry tissue) containing significantly (p = 0.004) less DNA than fresh corneas (1.90 ± 0.22 μg/mg) as shown in the morphological evaluation (Figure 4.5A). However, seeded cells did not respond differently to the gamma-irradiated and fresh corneas. There were no significant differences between proliferation of hCECs on the fresh and gamma-irradiated cornea at any time point over the course of 21 days (Figure 4.5B). In general, cell proliferation increased over the course of 14 days, and was more abundant when compared with TCP. Between 14 and 21 days, the proliferation of hCECs in both corneas decreased whereas proliferation did not change on TCP (Figure 4.5B).

4. 4. Discussion

Characterization of a biological material is important in establishing suitability for clinical application. Despite the availability of the gamma-irradiated donor human corneas to ophthalmic surgeons, many fundamental properties have not been carefully evaluated. In this study, we characterized several physical and biological properties,

including swelling ratio, light transmittance, elastic modulus, denaturation temperature, collagen fibril density, DNA content, and corneal epithelial cell proliferation.

Corneal ECM is an optically clear hydrogel compromised of primarily collagen and proteoglycans [46]. It is well known that the amount of crosslinking (crosslinking density) governs the physical properties of a hydrogel [120] and many riboflavin-UVA crosslinking studies demonstrated this with corneal tissue. When the crosslinking density of corneal ECM is increased, light transmittance, one of the main properties of the cornea, increases [121], as do the degree of material stiffness [122, 123] and brittleness [124], which limit surgical handling while decreasing the swelling ratio [121]. Thus, the crosslinking density, which affects the physical properties of corneal ECM, must be balanced to ensure optimal qualities for a corneal replacement tissue. We demonstrated that the gamma-irradiated cornea shared similar hydration, light transmittance, and elastic modulus as the fresh cornea, indicating that gamma-irradiated corneas have the ideal crosslinking density. In addition, these shared properties suggest that 17-23 kGy irradiation does not affect certain functional qualities of human cornea. Therefore, they could potentially share functional aspects of the fresh cornea, including surgical handling of the tissue and quality of vision. An example is lamellar keratoplasty where stromal and epithelial (but not endothelial) corneal tissue can be replaced by gamma-irradiated cornea.

Nevertheless, the denaturation temperature and collagen fibril density were significantly lower in the gamma-irradiated corneas than in fresh corneas. Thermal analysis provides information about the hierarchical organization of tissue [109], including corneal tissue [125] and its substitutable biomaterial [88]. The difference in denaturation temperature in our study indicates that matrix organization of the cornea was

altered by 17-23 kGy gamma-irradiation. Although there is little information as to how thermal properties of ECM affects corneal function, the matrix alteration by this amount of irradiation may not be great enough to change the crosslinking density of the cornea. Thermal analysis also showed the denaturation temperature in the peripheral cornea is lower than that in the central cornea. This finding may be related to the fact that the structure of corneal ECM differs depending on location within the cornea. For example, the central cornea has a thinner stromal layer [126], a higher collagen density [127], a thinner collagen diameter [128], and a higher hydration [129] than the peripheral cornea. These regional differences in ECM may influence the regional effect of gamma irradiation. Future studies could examine how irradiation may be performed to account for these localized differences.

Collagen density of corneas varies depending on the region and depth of the cornea, tending to be higher in the central and posterior regions than in the peripheral and mid-cornea [127, 130]. Owing to this variation, we performed micro-structural assessments in a specific area of cornea: the mid-peripheral region at mid-stromal depth. In our study, the human mid-peripheral and mid-stromal cornea density (310.0 ± 44.7 fibrils/μm^2) was lower than what has been reported for the rabbit central and posterior-stromal cornea (396 ± 21 fibrils/μm^2) [118], although others reported the human cornea to have higher collagen fibril density than that of rabbit [130]. Furthermore, collagen fibril density of the irradiated cornea was significantly lower than that of the fresh cornea. However, a previous study reported collagen density was decreased in the superficial area but not significantly different in the other area of gamma-irradiated human corneas[17]Owing to the irradiation dose-dependent structural changes in the various

studies mentioned above, we suggest that the low fibril density of irradiated corneas is caused by the application of 17-23 kGy gamma irradiation, which may be different from other studies.

We demonstrated that light transmittance of gamma-irradiated cornea was not significantly different from that of fresh cornea. However, a recent study indicated that transmission was improved in irradiated versus fresh corneas at certain wavelengths [117]. We believe that this discrepancy is due to differences in the sample size, the methods for transmittance measurement, and statistical analysis between present and previous studies. However, both studies clearly demonstrated similar light transmission properties of fresh and gamma-irradiated corneas. Corneal transparency increases with small-diameter collagen fibrils and low interfibrillar spacing [116]. Because the collagen fibril density of gamma-irradiated corneas was lower than that of fresh corneas in our study, but transparency was unchanged, we posit that the small diameter of collagen fibril in the gamma-irradiated cornea increases transparency, which compensates for decreased corneal transparency by increased interfibrillar spacing.

Because the ECM strongly influences cell physiology, cell-based studies are essential to characterize the biological properties of the gamma-irradiated cornea [131]. Corneal epithelialization is the first step of corneal healing [132]. By measuring the rate of CEC proliferation, one can estimate the potential of a biomaterial for corneal reconstruction. In our study, the proliferation rate of hCECs was not significantly changed between fresh and irradiated corneas, indicating that the materials are equally compatible, although in vivo studies would be necessary to confirm. However, a previous study reported that the proliferation of rabbit CECs correlated with increased collagen

coating density on a synthetic material [131]. The discrepancy in proliferation between these two studies may be attributed to differences in supporting materials and cell sources. Our study was conducted using fresh and gamma-irradiated human corneas and human CECs, which we believe to be clinically relevant.

Although hCEC proliferation was similar in fresh and irradiated corneas, gamma-irradiation appeared to reduce the number of keratocytes in the stroma as well as DNA content. A previous mouse penetrating keratoplasty study similarly showed the potential of gamma irradiation to decrease the risk of immune rejection by damaging donor keratocytes [104]. DNA content of both donor tissue and contaminating pathogens are known to activate immune response [133], and allogeneic DNA may contribute to immune rejection by activating the major histocompatibility-I (MHC-I) class molecule [134, 135]. Thus, by damaging both keratocytes and DNA, irradiating transplant material could reduce immune rejection.

Fresh human cornea tissue prepared for tissue donation should be used within 14 days when kept in a preserved solution between 2-8ºC in a refrigerator [136]. One of the advantages of gamma-irradiation is that the procedure extends shelf life up to 2 years without complex storage requirements. Nevertheless, outdated gamma-irradiated corneas had a lower swelling ratio (lower crosslinking density) than normal gamma-irradiated corneas, suggesting a finite shelf life for gamma-irradiated corneas as they undergo structural alterations with time. The decrease in light transmittance and elastic modulus over time support this theory. Strategies to maintain crosslinking density in the gamma-irradiated cornea should be investigated to maximize the shelf life.

In conclusion, we have characterized the mechanical and biological properties of gamma-irradiated corneas and compare them with the properties of fresh human corneas. Gamma-irradiated corneas and fresh corneas have similar physical and biological properties, which imply the 17-23 kGy of gamma irradiation does not affect surgical handling, the healing process by epithelial cells, and the tissue clarity. However, it is notable that the density of fibrils and the thermal stability of gamma-irradiated cornea are less than those of fresh cornea. Because of the similar biological and mechanical properties between irradiated and fresh corneas, longer shelf-life of gamma-irradiated corneas compared to fresh donor tissue, and decreased risk of rejection, gamma-irradiated corneas may be a suitable tissue substitute in various types of ophthalmic surgeries.

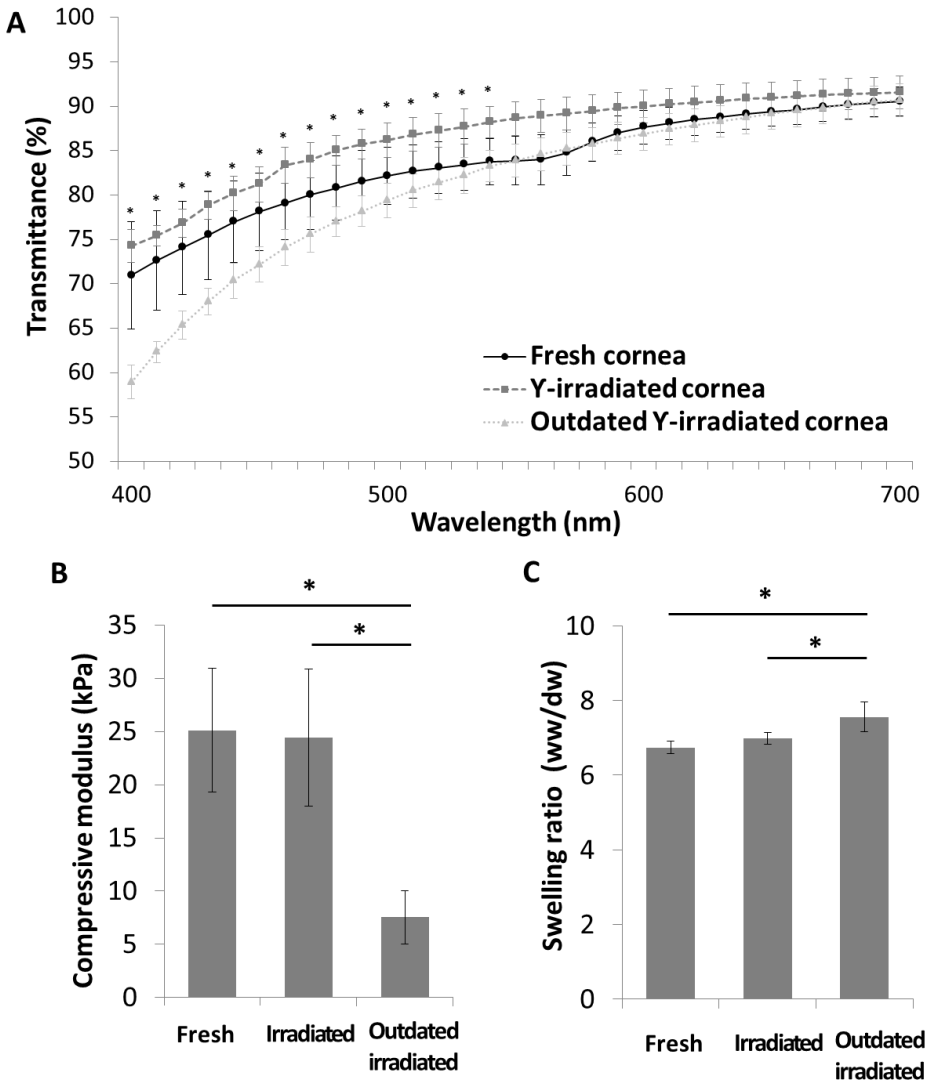

Figure 4. 1. Light transmission, compressive modulus, and hydration of fresh gamma-irradiated corneas, and outdated gamma-irradiated corneas. (A) Transmittance of visible wavelengths every 10 nm from 400 to 700 nm, (B) elastic modulus, and (C) swelling ratio [ratio of wet weight (ww) to dry weight (dw)] were determined for fresh (n = 5), gamma-irradiated (n = 5) and outdated gamma-irradiated (n = 3) corneas. * $p < 0.05$ versus outdated corneas unless otherwise noted, Mann-Whitney test. Data in (A to C) are means ± SD.

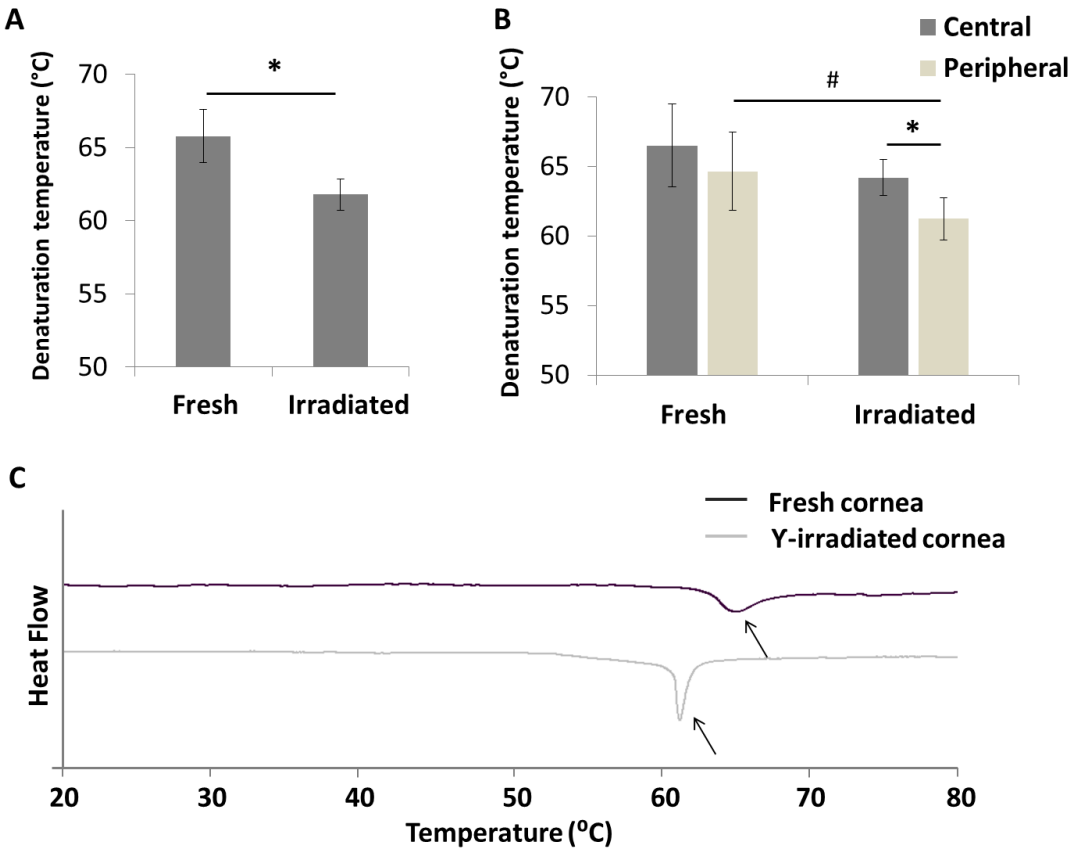

Figure 4. 2. Thermal properties of fresh and gamma-irradiated corneas. Denaturation temperature across the whole area (A) and in the central and peripheral areas of corneas (B). Data in (A and B) are means ± SD (n = 5). (C) Representative DSC thermograms for fresh and gamma-irradiated corneas. Black arrows indicate denaturation curves in the thermogram. Statistical significance was established by one-tailed Student's t-test (*) or Spearman's rank correlation (#) at $p < 0.05$.

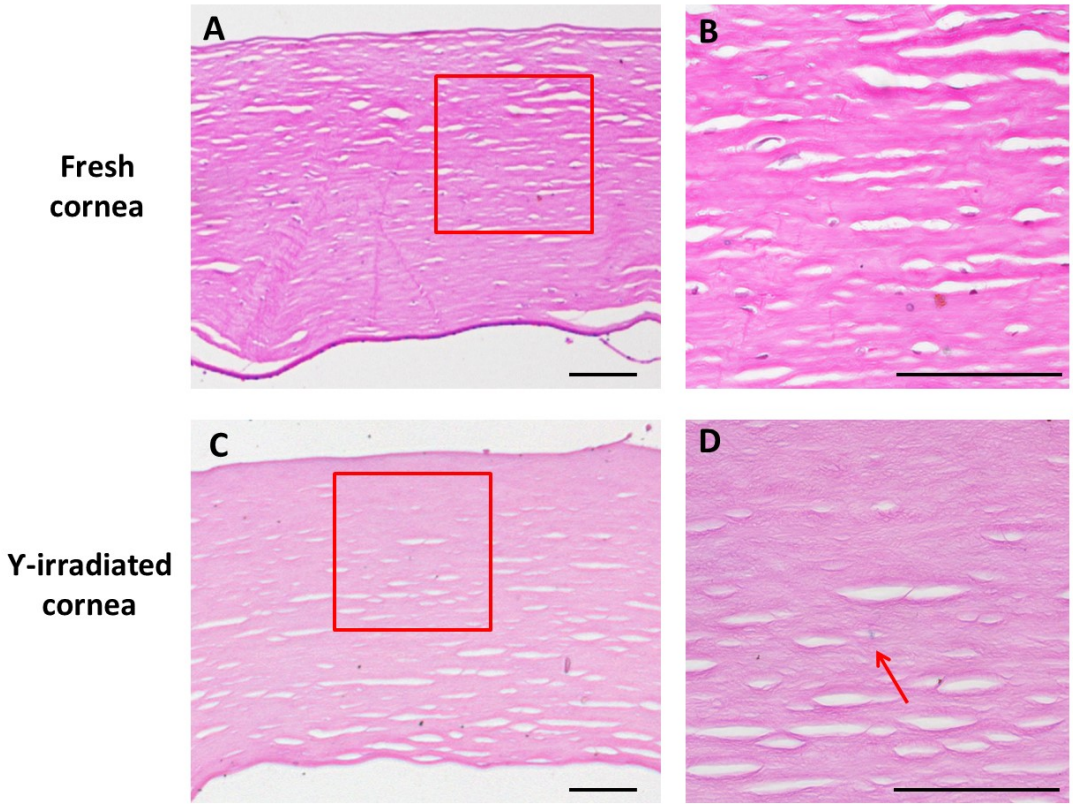

Figure 4. 3. Histology of fresh and gamma-irradiated corneas. H&E staining of the mid-peripheral region revealed structure, keratocytes, and debris in gamma-irradiated corneas. Keratocytes are seen in blue in the fresh cornea. Cell-like debris (red arrow) was found in the gamma-irradiated cornea. Scale bars, 100 μm.

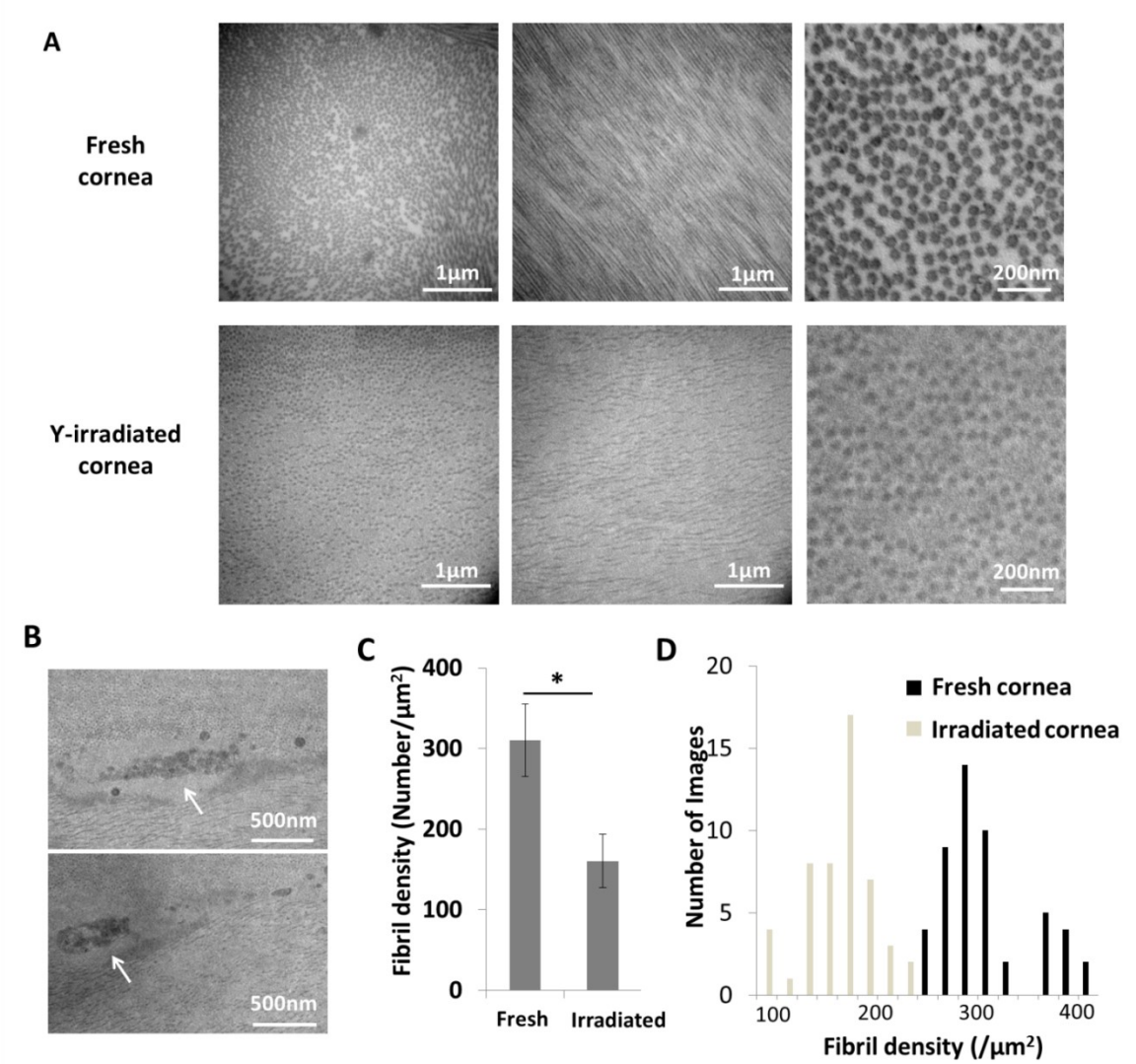

Figure 4. 4. Transmission electron micrographs of fresh and gamma-irradiated human corneas in the mid-peripheral region. (A) TEM images of fresh and gamma-irradiated corneas, (B) Cell fragments (indicated by white arrows) in gamma-irradiated corneas. (C and D) Collagen fibrils and fibril density quantified in 50 randomly chosen 1-µm^2 areas. *$p < 0.05$ by one-tailed Student's t test. Data are means ± SD ($n = 50$).

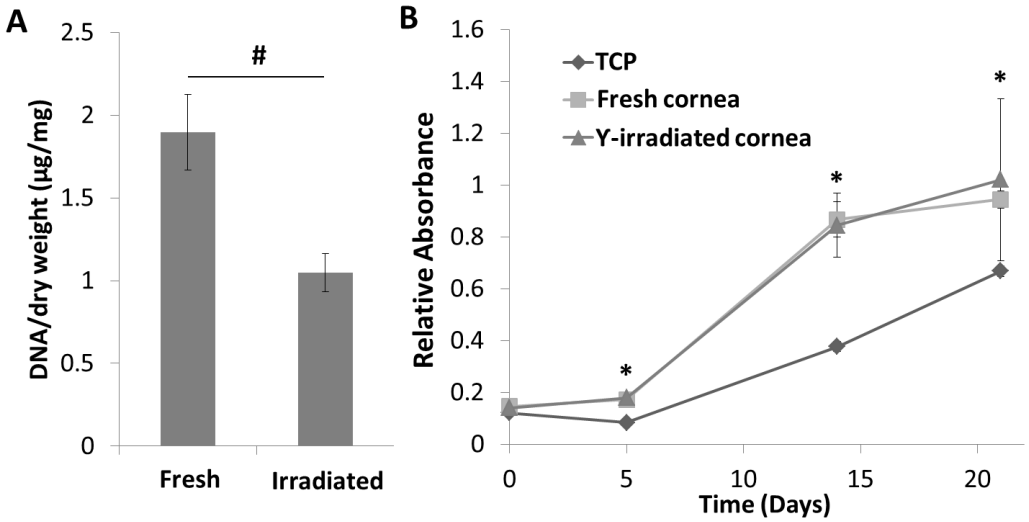

Figure 4. 5. Biological characterization of fresh and gamma-irradiated corneas. (A) DNA content in fresh and gamma-irradiated corneas relative to dry weight. (B) Proliferation rate of hCECs over 21 days after seeding on fresh and gamma-irradiated corneas and on tissue culture plate (TCP). * $P<0.05$ compared to TCP unless otherwise noted, Mann-Whiney test. Data are means ± SD ($n = 5$).

5. Reconstructed decellularized tissue for corneal regeneration

5. 1. Introduction

Corneal blindness, resulting from corneal diseases or injuries, is the fourth leading cause of blindness worldwide [24]. Although allogenic corneal transplantation is the only effective method for restoring vision from corneal blindness and its success rate is relatively high, global donor shortages limit the application of this excellent treatment [30, 137]. To address this issue, many researchers have attempted to develop corneal substitutes, widely categorized within two types: synthetic keratoprostheses and tissue-engineered corneal substitutes [60]. Among tissue-engineered corneal equivalents, both bottom-up and top-down approaches have been used.

Several keratoprostheses, such as AlphaCore^{TM}, have been used clinically [138]. However, they could still be inappropriate for long-term use due to their severe complications including poor integration with host tissue, progressive stromal melting, epithelial defects, glaucoma and endophthalmitis [139, 140]. The bottom-up approach also has produced various corneal equivalents from components of corneal extracellular matrix (ECM), such as collagen [132, 141] and glycosaminoglycans (GAGs) [142] as well as other proteins such as silk fibrin [143]. Despite their potential, all engineered corneas to date have been unable to attain the ideal characteristics of successful corneal application including transparency, proper curvature, non-toxicity, non-immunogenicity, and proper mechanical and biological properties. For example, the recombinant human

collagen-based implant may be limited by its poor mechanical properties and inability to withstand conventional suture techniques in clinical trials [47]. Top-down approaches including tissue-based corneal substitutes have recently remerged as an alternative strategy. The gamma-irradiated human cornea has shown great characteristics in a previous study and is clinically available [64]. However, the irradiated human may alleviate the donor shortage issue but not completely address it.

Decellularization of xeno-originated corneas is an attractive top-down approach. The animal cornea is relatively inexpensive, easily obtained and has similar protein compositions when compared to the human cornea [62]. In addition, decellularized xeno-originated tissue generally contains most native tissue composition including various functional proteins such as integrins that improve biological properties [144]. To ensure successful corneal xenotransplantation, the efficient removal of the main animal antigen, cell components, is required [145]. Although decellularization methods have been applied to animal corneas in many studies, their effects have not clearly quantified and a standardized protocol has not been developed [58]. Another significant problem of this approach is that most decellularization processes causes structural damage to the corneal ECM [60, 146, 147]. Damaged corneal ECM loses its unique transparency and curvature and as a result, two of its critical functions: allowing light penetration and generating refractive power, are also lost. A gentle decellularization method is available to maintain the corneal structure to some extent. However, the method leaves cell components in corneal ECM which would induce immune rejection after transplantation [57, 62]. For this reason, specific strategies are needed to create an optimal animal decellularized cornea

Recently, our group has developed technologies to manipulate structures of collagen ECM with the ultimate goal of producing optimal corneal substitutes. Vitrification is a process to control the fibril structure of collagen biomaterials [50, 88]. By controlled evaporation of water under the specific temperature and humidity, the vitrification process allows self-organization of collagen fibrils which has an impact on the optical, mechanical, and thermal properties of the collagen biomaterial as well as keratocyte behavior [50, 88]. Another significant method is the process of customizing the three dimensional shape of the collagen material using a single mold. We previously reported that the shaped collagen material (collagen vitrigel: CV) was successfully constructed and that the material improved the applicability for implanting to cadaveric eyes [72]. Due to sharing the main composition of native cornea [8], type I collagen, these technologies may be able to manipulate the ECM structure of the cornea similarly to CV. In addition, these methods have the potential to reconstruct the damage decellularized cornea after decellularization processes.

The present study was performed to produce an optimal xenotransplantable corneal substitute based on the decellularization approach used with structural reconstruction methods. To achieve this goal, we investigated various decellularization methods to develop a protocol for the porcine cornea first. After, the decellularized cornea produced from the optimized protocol was reconstructed with our novel technologies with modified methods. In addition, corneas were characterized to evaluate the properties of corneal ECM as well as the validity of these technologies. Finally, the optimized corneal substitute was applied to two animal models to assess biocompatibility and potential as a xenotransplantable corneal substitute.

5. 2. Materials and Methods

5. 2. 1. Animals

Eight New Zealand white rabbits, 2 to 3.5 kg in weight, were used for two animal models according to the Association for Research in Vision and Ophthalmology (ARVO) Statement for the Use of Animals in Ophthalmic and Visual Research. In addition, all experimental procedures were approved by the Institutional Animal Care and Use Committee at Johns Hopkins University.

5. 2. 2. Preparation of porcine corneas with conventional decellularization methods

Whole porcine eyes were obtained from a local butchery within 24 hours post-mortem. The full thickness cornea buttons were prepared using a 12 mm-diameter biopsy punch and then washed in a sterile balanced buffer solution (BBS) with 5% antibiotic / antimycotic solution (Anti-anti, Gibco, 15240) three times. The corneas were then divided into eight groups: 1) The native cornea as a control group; three physically treated groups including 2) freezing-thawing, 3) hyperosmolar dextran and 4) hypertonic sodium chloride (NaCl) groups; two chemically treated groups including 5) sodium dodecyl sulfate (SDS) and 6) Triton-X groups; and two enzymatically treated groups including 7) fetal bovine serum (FBS) and 8) DNase treated groups. Corneas were treated with one of the following methods: 1) Fresh cornea without any treatment 2) corneas treated five times with liquid nitrogen freezing for 30 minutes, and thawing at room temperature for 3 hours. 3) Corneas immersed in 20% (w/w) of hyperosmolar dextran (Fisher 1004-00-60) solution at 4°C for 3 days, 4) corneas in the 2.0 mol hypertonic NaCl (Fisher 7647-14-5) solution at 37°C for 3 days, 5) corneas in the 1% (v/v) SDS

(Sigma 71727) solution at room temperature for 3 days 6) corneas in the 1% (v/v) Triton-X (Sigma 9234) solution at room temperature for 3 days 7) corneas in the 10% FBS (Thermo Fisher Scientific, USA) with Dulbecco's Modified Eagle Medium (DMEM, Gibco 31053) at 37°C for 3 days and 8) corneas in the 600U/ml DNase I (Roche, Germany) solution with PBS at 37°C for 3 days. Corneas in group 3) to group 6) were treated on a conventional magnetic stirrer at 150rpm and those in group 7) and 8) were done on a gyrator rocker at 70rpm. After treatment, each cornea was irrigated using sterile PBS three times.

5. 2. 3. Decellularization process

Selected decellularization methods were combined to maximize cell removal. After washing corneal buttons with 5% antibiotic solution as described before, the fresh porcine corneas were treated with 1% SDS followed by 1% Triton-X for 3 days at room temperature respectively . The corneas were aseptically washed in sterile PBS on a conventional magnetic stirrer at 180 rpm for 7 days at room temperature to remove remnant chemical agents. Next, the corneas were placed in 10% fetal bovine serum in DMEM for 3 days at 37^0C and were then washed with PBS containing 1% antibiotic/antimycotic for 24 hours. The cornea treated by those 3 decellularization methods will be called the decellularized cornea (DC) in this study. Each decellularization process was agitated as described above.

5. 2. 4. Microscopic structural reconstruction

To reconstruct the microstructure of DC, two processes, vitrification and riboflavin crosslinking (the reconstruction process), were conducted. The vitrification

process was performed with a modified method from a previous study [148]. After tearing the Descemet's membrane, DC was placed in a conventional tissue culture plate (TCP) and incubated at 4°C in 40% relative humidity for 3 days followed with a 1 hour PBS wash. Afterwards, the cornea was vitrified by drying at 37°C for a week in 40%relative humidity within a vitrification chamber. Riboflavin crosslinking was used to increase material stability. After rinsing with PBS, the vitrified DC was immersed in a 20% dextrose solution with 0.1% Riboflavin (Sigma, R7649) overnight at 4°C. The cornea was washed with 20% dextrose solution and was cross-linked using UV radiation (370nm, 3.0mW/cm^2) for 1.5 hours on both sides. The DC with the applied reconstruction process will be called the reconstructed cornea (RC) in this study. If it is not specified, RC was made on a flat TCP.

5. 2. 5. Histology

Corneas (n=5) were dehydrated and imbedded in paraffin. Sections (5 μm thick) were stained with either hematoxylin and eosin (H&E) or Alcian blue, using standard techniques. The stained slides were observed under a light microscopy (Observer A2, Carl Zeiss, Germany).

5. 2. 6. Light transmittance assay

After each process, five corneas were cut with a 10-mm trephine for each group and washed 3 times using BSS. With a multimode microplate reader (Synergy 2, Biotek, Seattle, WA), the light transmittance of the corneas on a 48-well microplate was measured in the full visible spectrum. Using obtained absorbance data, the light transmittance was calculated by the Beer-Lambert law with the equation, transmittance (%) = $e^{-absorbance}$ x 100 as a previous study [64].

5. 2. 7. Biochemical analysis – DNA contents, GAG and Collagen

Corneas (n=5) were lyophilized for 48 hours and the dry masses were taken. The lyophilized cornea was digested in a 125-μg/mL papain solution (Worthington, Lakewood, NJ) for 16 hours at 60 °C. Quantification of DNA content was performed using a Hoescht Dye 33342 DNA assay as a previous study [64]. The fluorescent intensity of the mixture composed of the papain digestion and Hoechst dye in TNE buffer was measure using a fluorometer (DyNA Quant 200, Hoefer, Holliston, MA). The DNA content was calculated using the standard curve generated by calf thymus DNA. The amount of sulfated GAG (sGAG) were measured using a 1,9-dimethylmethylene blue (DMMB) dye assay [149]. Papain-digested samples were mixed with a DMMB dye solution and the mixture was quantified using a spectrophotometer at 525nm. The quantified data were calculated by the standard curve made from chondroitin sulfate standards. Collagen was quantified with a hydroxyproline content assay [149]. The papain digestion was incubated in 6 N hydrogen chloride overnight at 125°C, neutralized and oxidized with chloramine-T. After, *p*-dimethylaminobenzaldehyde was added to the solution and its absorbance at a wavelength of 550 nm was measured. Hydroxyproline was used for generating a standard curve.

5. 2. 8. Western Blot

To evaluate the amount of remnant cell debris, fresh porcine, SDS and Triton-X treated and decellularized corneas (n=5) were homogenized using a pestle and a mortar in liquid nitrogen. Confluent porcine keratocyte-induced fibroblasts were harvested (n=5 well) in a 6-well plate to serve as a control group. After washing samples twice using ice-cold PBS, each sample was lysed with RIPA buffer (ThermoFisher Scientific) containing

protease inhibitor mixture (Sigma) according to the manufacturer's instructions. Protein concentration was quantified using the BCA assay kit (Pierce). Using 10% SDS-PAGE, proteins were separated and transferred onto a polyvinylidene difluoride (PVDF) membrane. The membrane was blocked for 2 hours using 5% non-fat dry milk in Tris-buffered saline containing 0.1% tween-20 (TBS-T). Primary β-actin (1:300, Sigma, USA) antibody was applied overnight at 4°C, followed by horseradish peroxidase conjugated secondary antibodies (1:5000, Bio-Rad) for 1 hour at room temperature. Finally, β-actin was detected by chemiluminescence (Thermo Scientific).

5. 2. 9. Transmission electron microscopy and Quantities collagen fibers

Corneas (n=5) were fixed using a mixture of 3% paraformaldehyde, 1.5% glutaraldehyde, 5 mM MgCl2, 5 mM CaCl2, 2.5% sucrose, and 0.1% tannic acid in 0.1 M sodium cacodylate buffer at pH 7.2 overnight in a cold room. The samples were rinsed in PBS buffer and post-fixed with 1% osmium tetroxide on ice for 1 hour. After a deionized water rinse, the sample was *en bloc* stained in Kellenberger uranyl acetate overnight. Following dehydration with a graded series (75%, 95%, and 100%) of chilled ethanol solutions, the sample was infiltrated with Eponate 12 resin (Ted Pella, Redding, CA) at 60^0C for 60 to 96 hours. The resin embedded samples were cut using an ultra-microtome (Ultracut UCT, Leica, Wien, Austria), collected on grids, and stained with uranyl acetate. The samples were examined and electronic digital pictures were taken using a TEM (Philips 420, FEI Co., Hillsboro, OR) system at 80 kV. After images were taken, ten TEM images in each cornea were magnified approximately 100,000-fold. Five areas were randomly chosen in each picture, and areas were defined as $1 \times 1\ \mu m^2$. The collagen fibers were manually counted by two masked observers. A collagen fiber in the

center of each picture was selected and its diameter was measured using computer software (Axiovision, Zeiss, Germany).

5. 2. 10. Thickness and Hydration

The thickness of five corneas was measured using a Starrett thickness gage after each process. To estimate crosslinking density, hydration was measured. After removing excess corneal fluids corneas (n=5) with a filter paper, wet weight (Ww) of each cornea was measured with a standard scale and the corneas were lyophilized for 48 hours to calculate dry weight (Wd). Hydration (H) was calculated using the following equation: H = Ww / Wd as a previous study [64]

5. 2. 11. Compressive modulus

Compressive modulus was measured to evaluate stiffness of corneas after each procedure as a previous study [64]. Briefly, compression was applied to the corneas (n=5) from 0% to 10% thickness using an Electroforce 3200 testing instrument (Bose, Eden Prairie, MN) with a 250-g load cell. To calculate compressive modulus, a computer program (MATLAB, MathWorks, Natick, MA) was used.

5. 2. 12. Thermal properties

Thermal properties of each cornea (n=5) were characterized using differential scanning calorimetry [DSC (DSC 8000, PerkinElmer, Norwalk, CT)] as described previously [64]. Samples were collected in the central cornea using a 5-mm biopsy punch. The collected samples were weighted and sealed in a 30-μL aluminum pan. An empty sealed pan was served as a reference. The specimens were cooled from room temperature to -30°C under nitrogen flow, and then heated to 90°C at a rate of 5°C/min. The produced

thermograms were evaluated and the denaturation temperature was automatically calculated using the Pyris series software (PerkinElmer, Norwalk, CT).

5. 2. 13. Collagenase degradation test

To evaluate the collagenase resistance of each cornea, collagenase degradation tests were performed. After rinsing 3 times with PBS and removing excess water content with a filter paper, corneas (n=5) in each group were immersed in 5 mg/mL type I collagenase (Worthington Biochemical Corp., Lakewood, NJ) with DMEM. At every hour, the corneas were weighted after gently removing the water contents on the surface. The ratio of initial mass to the mass at each time point was calculated to present the percentage of residual corneal mass.

5. 2. 14. Macroscopic structural reconstruction

To generate curvature of RC, macrostructural reconstruction was performed (Figure 5.1). Pairs of Polymethyl methacrylate (PMMA) molds (Figure 5.1A) following curvature of the rabbit cornea (7.5mm) were kindly donated from eyegenix LLC (Honolulu, HI). After removing the posterior layer, DC was placed on a curved mold (Figure 5.1B) and gentle pressure was applied to conjunct the bottom of DC to the surface of the mold (Figure 5.1C). After conducting the vitrification process (Figure 5.1D) as mentioned above, 100µl of 0.1% riboflavin with 20% dextran solution was applied (Figure 5.1E). Using conventional sealing paper, a pair of molds was combined each other and tightly sealed. The mold including DC was kept overnight at 4°C. After UV radiation, as mentioned above, was applied within the mold for 2 hours on both sides

(Figure 5.1F). After opening the mold (Figure 5.1G) and applying a few drops of PBS, the shape reconstructed cornea was carefully detached from the mold (Figure 5.1H).

5. 2. 15. Optical coherence tomography and curvature analysis

The optical setup of the Optical coherence tomography (OCT) imaging system is shown in Figure 5.2A The home-built OCT imaging system consists of a swept source OEM engine (AXSUN, central wavelength λ0: 1060nm, sweeping rate: 100kHz, scan range: 3.7mm in air), a balanced photo-detector and a digitizer with a sampling rate of up to 500MSPS with 12-bit resolution, a Camera Link DAQ Board, and a Camera Link frame grabber (PCIe-1433, National Instruments). For the optical scanning head, 2D galvanometer mirrors (GVS002, Thorlabs) and OCT scan lens with 36mm effective focal length (LSM03-BB, Thorlabs) were used. The workstation (Precision T7500, Dell) with general-purpose computing on graphics processing units (GPGPU, GeForce GTX980, Nvidia) processed the sampled spectral data and reconstructed the 3D OCT image. The parallel processing (CUDA, Nvidia) of the GPGPU significantly reduced the signal processing time including FFT (Fast Fourier Transform). Finally, 512 x 512 x 1024 volumetric OCT images were reconstructed and 10 duplicated 3D images were averaged to increase SNR (Signal-to-Noise Ratio). Based on the reinforced 3D OCT images, canny edge detection algorithm was applied in order to extract the curvature information of the shaped reconstructed cornea as well as the mold. Then, the gray-scale image was converted into a binary image with a specific threshold value to extract the surface line of the cornea and the mold. The surface binary image was rescaled in accordance with the physical scanning size. Using this final image, the mean value of curvature was

calculated by measuring 6 (3 by 3) different positions of the cornea as shown in Figure 5.2B.

5. 2. 16. Cell Culture (Human epithelial cell, Human keratocyte and Bovine endothelial cell)

The human corneal epithelial cell, human keratocyte and bovine corneal endothelial cell were cultured to evaluate the cell response to DC and RC. Six human corneas were donated by Tissue Banks International (Baltimore, MD) and the study was approved by Johns Hopkins Institutional Review Boards. All human samples were handled following the Declaration of Helsinki. To culture the human corneal epithelial cells and keratocytes, the epithelium was separated from the stroma by treating with 1.2 U/ml of dispase II (Roche Diagnostics, Mannheim, Germany) in the Epilife® medium (Invitrogen / Life Technologies, Grand Island, NY) at 4°C for 16 hours. Under a conventional dissection microscope, epithelial sheets were aseptically collected and transferred into a conical tube containing 0.05% trypsin-EDTA solution. The epithelial sheet was incubated at 37°C for 30 minutes and then human corneal epithelial cells were collected using a cell strainer. After mechanical disruption with a pipette and neutralization of trypsin-EDTA solution, primary cells were sub-cultured in the Epilife® medium with the Human cornea growth supplement (HCGS, Invitrogen/Life Technologies, Grand Island, NY) at a density of 5×10^4 cells/cm^2 until confluent.

Human keratocytes were isolated using type I collagenase digestion. After collecting the epithelial sheet, the endothelium was removed and the remained stroma was cut into small pieces with a # 10 blade. The corneal pieces were incubated in 3 mg/mL collagenase in DMEM/F-12 for 1 hour. The remaining corneal pieces were

collected and transferred to a fresh collagenase solution for 4 hours. After repeating the process for a third 4 hour digestion, primary keratocytes were collected from the second and third digestion solutions using a cell strainer. After obtaining cell pellets with a conventional method, keratocytes were subcultured in a DMEM solution containing 1% RPMI vitamin mix (Sigma), 100 μm non-essential amino acids (Gibco), 100 μg/ml ascorbic acid (Sigma) and 1% antibiotic / antimycotic solution (Gibco) at 37°C and 5% CO2 with a density of 5 × 104 cells/cm^2 for a week.

Bovine endothelial cells were harvested from six bovine eyes within 24 hours after slaughter. The corneas were placed on a Petri dish with the endothelial side facing up. Under a dissection microscope, Descemet membranes with intact endothelium were peeled and incubated in 0.02% Tripson-EDTA for 1 hour at 37°C. After vigorous pipetting, bovine corneal endothelial cells were collected after passing through a cell strainer. The cells were seeded in a 6-well TCP te precoated using FNC Coating Mix (AthenaES , Baltimore, MD) with DMEM media including 10% FBS (Thermo Fisher Scientific), 50 μg/ml pituitary extract (Sigma) and 1% antibiotic / antimycotic solution (Gibco) at 37°C and 5% CO2 with a density of 5 × 10^4 cells/cm^2 until confluent.

5. 2. 17. Live/Dead cell analysis, immunocytochemistry and proliferation test

To evaluate the cell behavior within corneas, 48-well plates were covered with the fresh porcine corneas: either the decellularized or reconstructed cornea. Some of them were left untreated to serve as a control group. For the bovine endothelial cell study, pre-coated TCPs with FNC Coating Mix were used as the control group. After subculturing as described above, corneal cells were detached using 0.05% trypsin-EDTA and seeded on either cornea covered or control TCPs.

In order to evaluate the cytotoxicity of the cornea, keratocytes were seeded on corneas or TCPs (n=4) with a density of 1 X 10^4 cells/cm^2 for a week. The keratocytes were differentiated from fibroblasts with serum-based medium contained DMEM/F-12, 10% FBS 1% antibiotic / antimycotic solution (Gibco) at 37°C and 5% CO2. The live and dead cells were observed with a kit (LIVE/DEAD® Viability/Cytotoxicity Kit, Life Technologies) according to the manual.

For Immunocytochemical staining, corneal cells were seeded onto the corneas or TCP (n=4) as above. If it is not specified, the procedures were performed at room temperature. At 7 days after seeding cells, the cells were rinsed twice with PBS and fixed with 4% paraformaldehyde in PBS for 15 minutes. After washing twice with PBS, cells were permeabilized with 0.25% Triton® X-100 (Sigma, St. Louis, MO) for 10 minutes and then washed three times in PBS for 5 minutes. Using 5% Bovine serum albumin (BSA, Sigma), non-specific antibodies were blocked for 30 minutes. Primary antibodies were applied for overnight at 4°C and then incubated with respective secondary antibodies for 1 hour in the dark room as shown in Table 5.1. Using the Hoechst 33342 solution (1μg/ml), all nuclei in the cells were stained for 1 minute and then, PBS washings were carried out twice. The cells were observed and photographed under a microscope system (Observer A2, Carl Zeiss, Germany).

Proliferation tests were performed using the cell counting kit-8 (CCK-8, Dojindo Molecular Technology, Inc., Rockville, MD) following manufacturer instruction. The absorbance, corresponding to the number of cells, was measured with a multimode microplate reader (Synergy 2, Biotek, Seattle, WA) at 450 nm. After seeding the three types of cells with a 5×10^3 cells/cm^2 density on corneas and TCP, the measurements

were performed until the corneal cells were confluent in the TCP. The endothelial cells, which rapidly proliferate, were measured every day whereas other cells were done at 0, 1 and every other day after seeding cells. Due to quiescence, the test was not performed for the keratocyte.

5. 2. 18. Surgical procedures for interlamellar and anterior lamellar keratoplasty

The procedures were performed under general anesthesia by intramuscular administration of ketamine (35 mg/kg of body weight) and xylazine (5 mg/kg of body weight). After inducing general anesthesia, two drops of topical anesthesia (Proparacaine, Akorn, Lake Forest, IL) were administered just prior to performing the surgical procedure. Two procedures were performed in this study: interlamellar keratoplasty and anterior lamellar keratoplasty.

To evaluate the biocompatibility of RC, interlamellar keratoplasty was performed using four rabbits. An incision was created using 8 mm Hessburg-Barron vacuum trephine to about a half thickness depth of the full cornea. With a crescent knife, lamellar dissection was performed to produce an intrastromal pocket (Figure 5.3A). A flat RC, with a 6mm diameter and approximately 100 μm thickness, was inserted into the intrastromal pocket (Figure 5.3B and 5.3C). The incision was closed with two interrupt 10-0 nylon sutures. A gentamycin and prednisolone combined ophthalmic ointment (Pred-G, Allergan, Irvine, CA) was applied once a day for 3 days. General ophthalmic examinations was performed at 3, 7, 14 days and 1, 2, 3, 6 months after surgery. At 1 and 6 months post-surgery, two rabbits were sacrificed respectively for further pathological examination with H&E stating.

To evaluate the clinical potency of RC as a corneal substitute, a pilot study was carried out using the anterior lamellar keratectomy model with 4 rabbits. Rabbits were randomly divided two groups: 3 rabbits for the RC group and 1 animal for the untreated negative control. Using 6mm Hessburg-Barron vacuum trephine (Barron Precision Instruments LLC, Grand Blanc, MI) and a crescent knife (LaserEdge, Bausch&Lomb, Rochester, NY), approximately 125 μm of anterior corneal tissue was removed from a randomly chosen eye of each rabbit. After inducing injuries, rabbits in RC cornea group received a shaped RC (approximately 125 μm thickness, 6.25mm diameter and 7.5mm curvature) affixed using 12-14 interrupted 10-0 nylon sutures. The negative control groupwas similarly operated on, but did not receive any material and rather, was allowed to heal naturally. A mixture of steroid and antibiotic ointment (Pred-G, Allergan, Irvine, CA) was applied for 14 days as a post-operative treatment. Gross observations, including ophthalmomicroscopy and fluorescein staining were performed at day 3, 7, 14 and 1 month after surgery. In addition, *In vivo* pachymetry were carried out to calculate the thickness of the animal cornea before sacrificing using a pachymeter (Corneo-Gage plus^{TM}, Sonogage, Cleveland, OH). Corneas were harvested after 30 days post-surgery for pathological examinations.

5. 2. 19. Statistical analysis

Data are presented as means ± standard deviation (S.D.) and were analyzed by either the Mann-Whitney test or ANOVA test with the Bonferroni Post-hoc depending on the size and character of samples. Statistical analyses were carried out with SPSS 15.0 for Windows (SPSS Inc., Chicago, IL). Statistical significance was established at $p < 0.05$.

5. 3. Results

5. 3. 1. Evaluation of decellularization methods

To establish a valid decellularization protocol for the porcine cornea, conventional decellularizing methods were carried out and their effects were evaluated. Chemical and enzymatic treatments presented efficient methods to reduce cellular constituents. Histological examination revealed only cell debris remained in chemically and enzymatically treated porcine corneas (Figure 5.4A). In addition, the DNA content analysis supported this finding; the DNA contents were significantly decreased (p = 0.004) after applying chemical and enzymatic decellularizing processes (Figure 5.4B). However, the mechanical methods left many visible keratocytes as well as their debris (Figure 5.4A), and could not significantly reduce DNA contents in the porcine cornea (Figure 5.4B). On gross observation, all decellularization methods reduced clarity of porcine corneas (Figure 5.5A). The finding on gross observation was confirmed by the quantitative light transmittance test: light transmittance at a representative visible wave length (550 nm) of all treated corneas was significantly (p = 0.008) decreased after a single decellularization process (Figure 5.5B).

5. 3. 2. Characterization of the decellularized cornea with an optimized decellularization protocol

Although chemical and enzymatic decellularization methods presented their efficiency, the degree cellular component removal of a single method was limited. To maximize the decellularizing efficiency, a decellularization protocol, including applications of two chemical methods (SDS, Triton-X treatment) and one enzymatic

method (FBS), was performed to porcine corneas. The decellularization efficiency was demonstrated with the DNA assay. The assay revealed that the DNA content of the porcine corneas was significantly reduced (p=0.008, all treatment) following each treatment. In addition, approximately 97% of porcine DNA (3.30 ± 0.10 μg /mg to 0.14 ± 0.03 μg /mg) was removed in the cornea after the protocol (Figure 5.6A). To analyze the removal of cell contents, the western bolt using a cell content marker, β-actin, was performed. The produced decellularized cornea (DC) was depleted of β-actin implying the cell contents were removed after the protocol (Figure 5.6B). However, the light transmittance test presented transparency of the porcine cornea was significantly decreased (p = 0.08) after chemical treatments in representing visible wave lengths (450, 550 and 650 nm, Figure 5.6C). In addition, quantitative collagen and GAG assays revealed ECM collagen and GAG were significantly decreased (p = 0.032 in collagen and p = 0.008 in GAGs contents) after the decellularization protocol (92.5% of collagen; and 41.5% of GAG remains in the decellularized cornea, Figure 5.7).

5. 3. 3. Characterization of the decellularized and the reconstructed cornea

To improve the physical properties of DC, vitrification and riboflavin crosslinking (reconstruction process) were conducted. On gross observation, clarity of DC was increased after the reconstruction process. However, yellowish color from riboflavin was observed in the RC (Figure 5.8A). The light transmittance test was confirmed those finding. Light transmittance was significantly increased (p = 0.08) after the reconstruction process in all visible wave length (400 nm to 700 nm). However, transparency of the reconstructed cornea was significantly lower (p = 0.08) than that of the native cornea. In addition, between 430 nm to 480 nm of wave length, the graph of

light transmittance was bulged indicating the cornea was stained with yellow color with riboflavin (Figure 5.8B).

Histological assessment for evaluation of the macrostructure with H&E and Alcian blue staining revealed neither visible cells nor cellular elements were found in DC as well as RC (Figure 5.9). The collagen structure of DC was severely distorted as shown by its opacity during gross observation and the light transmittance test. The distorted collagen structure of DC was reconstructed to a compact structure after the reconstruction process (Figure 5.9). In the Alcian blue staining, DC was palely stained by blue color indicating depletion of GAG contents. However, the intensity of staining was increased after the reconstruction process in RC (Figure 5.9).

The ultrastructural evaluation with TEM presented severe structural alteration in DC which was reorganized in the reconstructed cornea (Figure 5.10). Although the orientation of corneal ECM was disassembled, no cell remnants were visible in the DC. As shown in the macrostructural assessment, the reconstruction process demonstrated its role by rebuilding unorganized collagen structure. The cornea reconstruction processing produced a layer-by-layer structure, similar with that of the fresh porcine cornea (Figure 5.10A). Quantitative analysis of TEM images presented decreased collagen fibril density after the decellularization procedure, compatible with translucent appearance of the decellularized cornea. However, the density was significantly increased ($p = 0.08$) after the reconstruction procedure and light transmittance of the reconstructed cornea was improved (Figure 5.10B). However, the diameter of collagen fibrils showed a different trend. The diameter did not increase after the reconstructed procedure, but gradually decreased during the processing (Figure 5.10C).

The decellularization process also altered many properties including thickness, hydration and denaturation temperature. The decellularization procedure significantly increased thickness of the corneas (1.03 ± 0.14 mm to 8.88 ± 1.21 mm, $p = 0.008$, Figure 5.11A) and hydration (10.04 ± 0.84 to 25.83 ± 3.24, $p = 0.008$, Figure 5.11B), and decreased the denaturation temperature (65.85 ± 0.52 °C to 53.58 ± 2.06 °C, $p = 0.008$, Figure 5.12). After reconstruction, the properties were repaired but some were not fully restored. Thickness of RC (0.85 ± 0.06) was significantly ($p = 0.032$) decreased when compared to that of the native porcine cornea (Figure 5.11A). In addition, the hydration of the reconstructed cornea (8.1 ± 0.95) also followed the result of the corneal thickness ($p = 0.008$, Figure 5.11B). However, the denature temperature of the reconstructed cornea (65.26 ± 1.37 °C) was not significantly different ($p = 0.421$) from that of the native porcine cornea and the reduced height of the peak was also restored after the reconstruction process (Figure 5.12).

On the other hand, the compressive modulus of corneas showed a different trend. There was no significant difference of elasticity between fresh (16.90 ± 5.30 kPa) and decellularized corneas (12.63 ± 4.09 kPa, $p = 0.310$). However, the reconstruction process significantly increased stiffness of RC (33.80 ± 6.93 kPa, $p = 0.008$, Figure 5.13A).

To evaluate the collagenase resistance of corneas, the collagenase degradation test was performed. The decellularization process decreased whereas reconstruction increased the collagenase resistance of corneas. To be fully degraded in in 5 mg/mL type I collagenase, the native and the decellularized cornea took 7 and 6 hours respectively. During 6 hours period, the percentage of the remaining DC was significantly lower ($p =$

0.008) than that of the remaining native cornea in each time point. The reconstruction process extended the full degradation time up to 9 hours. Except 5 hours after starting the test, the percentage of residual RC is significantly higher than that of the residual native cornea for 8 hours (Figure 5.13B).

5. 3. 4. Cell behavior test

The live/dead cell analysis was performed to check the cytotoxicity of corneas using keratocyte-induced fibroblasts. None of the corneas showed cytotoxicity. Only a few numbers of dead cells with red color were found, but the majority of cells were stained green implying that they lived well on corneas and TCP (Figure 5.14).

The cell proliferation test was performed to evaluate the ability of corneal cells to repopulate the corneas. All corneas and TCP allowed for the rapid proliferation of keratocyte-induced fibroblasts. There were no significant differences of proliferate rates among the groups and time points (Figure 5.15A). Corneal epithelial and endothelial cells shared a similar proliferation pattern on corneas and TCP. Although the cells on TCP present the highest proliferation rates, RC allowed more rapid growth for both types of cells than DC and the native cornea. However, the native cornea barely allowed proliferation of both cell types until cells were confluent on TCP (Figure 5.15B and C).

The capacity of the corneas to support corneal cells was evaluated with immunocyotochemistry with cell specific markers. The human corneal epithelial cells with cytokeratine 3 (K3) antibody staining revealed the cells on DC and RC formed many clusters expressing the K3 protein similarly to those on TCP. However, the size of cells on DC and RC was smaller than those on TCP. The cells on the native cornea could not

make a cluster form but only a few cells were scattered on the cornea. The human keratocyte was well distributed on all corneas and TCP and all cells presented a strong a keratocyte-specific protein, keratocan,-positive regions. Seeded bovine corneal endothelial cells mostly covered RC and DC as well as TCP. In addition, the cells showed expression of a tight-junction associate protein (ZO-1) on both the RC and DC as on TCP. However, the bovine endothelial cells on the native cornea covered only limited area and barely expressed the ZO-1 protein (Figure 5.16).

5. 3. 5. Evaluation of Macroscopic structural reconstruction

Using an OCT system, the regenerated concave shape of RC regarding curvature of the rabbit cornea was evaluated. The 3D OCT image revealed the shaped RC had a similar architecture with the mold. In addition, RC presented a smooth surface in 2D OCT image (Figure 5.17). In the curvature analysis, the curvature of the reconstructed cornea (7.613 ± 0.136 mm) was identical with that of the mold (7.615 ± 0.138 mm).

5. 3. 6. Interlamellar corneal transplantation

To evaluate the biocompatibility of RC, a pilot interlamellar keratoplasty was performed with a rabbit model. The rabbit cornea kept the transparency and any significant lesions, including immune rejection, were not found during the 6 month period. In addition, the yellowish color of the reconstructed cornea was gone within a month after implantation (Figure 5.18A). During pathological examination, the biocompatibility of RC was confirmed. Any significant immune response presented by immune related cells was not found at 1 month and 6 month post-surgery. At 1 month post-surgery, some keratocytes were found in the surrounding animal tissue and collagen fibrils connected the implanted RC to host rabbit tissue. However, the gap between the

host tissue and the reconstructed cornea remained. Integration between host tissue and the reconstructed cornea was completed before the 6 month time point post-surgery. However, no cells migrated into the reconstructed cornea until 6 months post-surgery (Figure 5.18B).

5. 3. 7. Anterior lamellar keratoplasty model

To evaluate the potency of the shaped RC as a corneal substitute, a rabbit partial keratectomy model was conducted. The re-epithelialization in the RC implanted cornea was completed before 14 days post-surgery whereas that on the control cornea was done before 7 days post-surgery. Corneal neovascularization, graft degradation, immune rejection and other complications were not observed during the study. The initial thickness of corneas that received RC and the control cornea was 353.7 ± 10.3 μm and 360μm respectively. A month later, RC treated corneas kept their thickness (360.8 ± 9.5) with RC. However, the control cornea was limited in its ability to regenerate its thickness (275 μm). Although slight corneal haze was found in the RC implanted group during 30-day period, corneal haze in the experimental group was not as serious as the control cornea (Figure 5.19). The pathological examination with H&E staining presented that the RC implanted cornea allowed cornea epithelial cells as well as keratocytes migration on and into RC respectively (Figure 5.20A). In addition, the migrated keratocytes remodeled the collagen structure of the RC (Figure 5.20B). In ultrastructural evaluation, the RC treated cornea had not fully integrated with host tissue until 1 month post-surgery. Some gaps between RC and host cornea were found in the interface. In addition, some keratocytes were found in the implanted RC. The collagen density of implanted RC was higher than that of the reconstructed control cornea (Figure 5.20C).

5. 4. Discussion

An ideal xeno-originated corneal substitute for patients must have a similar composition and structure with the human cornea without containing animal immunogenic antigens. To address these requirements, the decellularized animal cornea aims to achieve two critical goals, maintaining composition and structure of the animal cornea while reducing animal cellular components. However, these goals are difficult to achieve together only using a decellularization procedure and a special strategy is needed. In the present study, we proposed an alternative strategy: to reconstruct the damaged corneal structure after harsh decellularization processes with our two novel procedures.

To establish an optimal decellularization process, we evaluated three categories of decellularization methods: mechanical, chemical and enzymatic treatments in the present study. Chemical and enzymatic methods efficiently removed visible cells and their debris. However, mechanical methods could not efficiently reduce cellular contents. Chemical decellularization methods with SDS and Triton-X are well known to efficiently remove cells by solubilizing the cellular membrane [55, 147, 150-152]. However, these methods have several challenges including remnants of toxic agents and structural deformations of proteins after treatment [152]. Since vigorous washing steps and our novel reconstruction process address these problems, both processes were adopted in our combined decellularization protocol. Both enzymatic methods fully removed visible cells in the porcine cornea as previous studies [58, 153]. The mechanism of enzymatic decellularization is not clear yet. In addition, ironically, FBS has been widely used in conventional cell culture and does not damage the cells in this setting. However, the

enzymatic methods have already demonstrated their efficacy in destroying immunogenic DNA content after other decellularization processes [154, 155]. Although DNase treatment proved its potency, we selected FBS due to the efficiency considerations in our decellularization protocol after the optimization process. The mechanical treatments, except the high-hydrostatic pressure method, preserved the collagen structure of the cornea relatively well. However, the decellularization effect would be dependent on only mechanical changes of intracellular components and would not be enough to fully remove cells [58, 60, 152]. The results in the present study confirmed this. Although hypertonic solution may reduce a certain number of cells, the weak potency of mechanical methods was unable to efficiently reduce not only the cell number but also the amount of cell contents. Despite the great preservation of the corneal structure, the methods could not be selected in the present study due to the possibility of immune rejection after transplantation [62].

Transparency is a critical role of cornea as it is the window of eye. It is well known that a highly organized corneal structure maintains the transparency of the cornea [1] and hydration could be a good indicator of structural integrity [60]. In this study, we confirm that all decellularization methods significantly decreased corneal transparency. The decellularization process could also affect the structural integrity of cornea by destroying the function of the corneal endothelium. When the endothelium loses its function, the water flux is not controlled which leads to structural alteration of the cornea represented by swelling and decreased transparency [1, 60]. The degree of structural alteration would be different depending on each decellularization method. However, all decellularization methods allowing flux of solution would not avoid the loss of

transparency. Application of dextran solution or glycerol could reduce the water content of cornea that may somewhat increase transparency of cornea [60]. However, without the reconstruction of corneal structure, it would be expected to rehydrate and be translucent after applying hypo to isotonic solution [156].

To address this issue, we applied our novel vitrification and riboflavin crosslinking procedures; the reconstruction process. Through self-organization of collagen structure during evaporation, the layer-by-layer structure was restored and confirmed through microscopic evaluation and the process reinforced structural stability represented by decreased hydration. The hydration, which represents material stability and crosslinking density, is positively correlated with thickness [157] while negatively correlated with light transmittance [121], stiffness [122, 123] and enzyme resistance [158]. After the decellularization process, hydration of the porcine cornea was significantly increased and decreased after the reconstruction process. Other corneal properties were also a function of destruction and restoration of material stability.

Transparency of the cornea was increased after the reconstruction process not only by restored material stability but also structural reconstruction. Light transmittance of the cornea increased with small-diameter collagen fibrils and low interfibrillar spacing which negatively correlated with fibril density [64, 116]. The restored layer-by-layer lamellar structure would explain how the reconstruction process increases transparency of cornea by structural restoration. However, increased fibril density and decreased collagen diameter in RC would also contribute to increased transparency of RC with alteration of collagen fibril structure. The light transmittance test and gross observation revealed a yellowish color from riboflavin was stained in RC which could be problematic. However,

the color was gone within 1 month after implantation in both animal models and we believe it would not cause significant visual problems after transplantation.

The reconstruction process reorganized the corneal structure by reinforcing the strength of molecular bonding. Thermal stability represented by denaturation temperature indicates the amount of the molecular bonding interaction and inherent strength of the material which correlates with hierarchical tissue organization [159]. In this study, the denaturation temperature of RC cornea is significantly increased after the reconstruction process and comparable with that of the native cornea. It implies the material organization and inherent strength is restored after the reconstruction process which would benefit the microstructural stability.

However, compressive modulus of RC was significantly higher than those of the native cornea and DC. This would result from increased crosslinking density, represented by decreased hydration, after the reconstruction process. The increased modulus indicates increased degree of material stiffness and brittleness that limits surgical handing, especially suture technique and handling the material with surgical forceps. However, in this study, we successfully applied interrupt sutures on RC without significant problems and there were no marks of indentation in the material from forceps during either surgical procedure. In addition, modulus of RC was not significantly different with that of human cornea in the previous study which was performed in the same conditions [64]. Thus, although compressive modulus was increased after the reconstruction process, the mechanical properties of RC could be acceptable as a corneal substitute for transplantation to patients.

After corneal transplantation, collagenase activity is essential to remodel tissue and promote wound healing [160, 161]. Collagenase resistance of materials is critical to maintain tissue stability after implantation [158]. However, if the material does not respond to collagenase, integration with host tissue could be impeded [161]. Thus, the material needs to have an appropriate response to collagenase to ensure successful implantation. The reconstruction process extended collagenase resistance time from the low collagen resistant DC by increasing material stability [162]. The extended but similar resistance time of RC compared to that of the native cornea may indicate the potential for good integration with host tissue.

One of significant weaknesses of chemical decellularization is residual agent which is strongly cyototoxic and harmful in the implantation. In the present study, both RC and DC did not show cytotocitiy and allowed good proliferation of keratocyte-induced fibroblasts. As shown in other studies [55, 147, 151], vigorous washing could remove enough detergent to ensure safety. In addition, DC and RC supported three types of cells when compared to the native cornea. Favorable biological properties of DC and RC indicate potential as cell carriers with customizable 3D shapes in various applications such as endothelial transplantation [163].

Another important function of cornea is generating refractive index through its novel concave shape. After structural deformation, the curvature of DC is altered which may not guarantee visual acuity after transplantation. Previously, we generated controlled 3D shapes in CV [72] using a single mold. However, the portion of the implant which was not in contact with the mold had an uneven rough surface. The uneven surface may impede the epithelial migration after implantation which would lead to a delayed healing

process. Our double molding method successfully generated a desirable concave shape with smooth surface on both side. In addition, the customizable 3D shape of RC could improve applicability compared to the flat cornea in the surgical room. In addition, our technique could generate patient-catered RC in the near future by generating various accurate curvature of RC through modifications of mold curvature.

Implantation of the reconstructed cornea in two rabbit models showed good integration with host tissue and the implants remained transparent without any remarkable problems. In addition, the shaped RC allowed functional regeneration of epithelium in the anterior lamellar keratoplasty model. However, surprisingly, between the two animals, keratocyte behavior was different. The interlamellar implantation model did not allow keratocyte infiltration within the implant whereas anterior lamellar keratoplasty model supported cell migration within a month. The migrated keratocytes into the implant may allow stromal remodeling by secreting various components including collagen GAGs [60, 164] that would be helpful during reconstruction of the wounded patient cornea. When remodeling the stromal layer, an important factor to activate keratocytes is a cytokine-mediated interaction between epithelial cells and keratocytes [60, 161]. The anterior lamellar keratoplasty induced epithelial cell damage whereas interlamellar keratoplasty did not. The lack of stimulating epithelial cell-induced cytokines may limit activation of keratocytes which may have resulted in the different behaviors of keratocytes between two animal models.

In conclusion, we have successfully developed a xenotransplantable corneal substitute with micro and macroscopic reconstruction processes. The reconstruction process restored properties to the decellularized cornea and regenerated the corneal

concave shape. The shaped RC was implanted into two rabbit models and presented the great potency of this material as a corneal substitute. In addition, the reconstruction methods may be able to contribute to the production of other corneal substitutes in the field of tissue engineering.

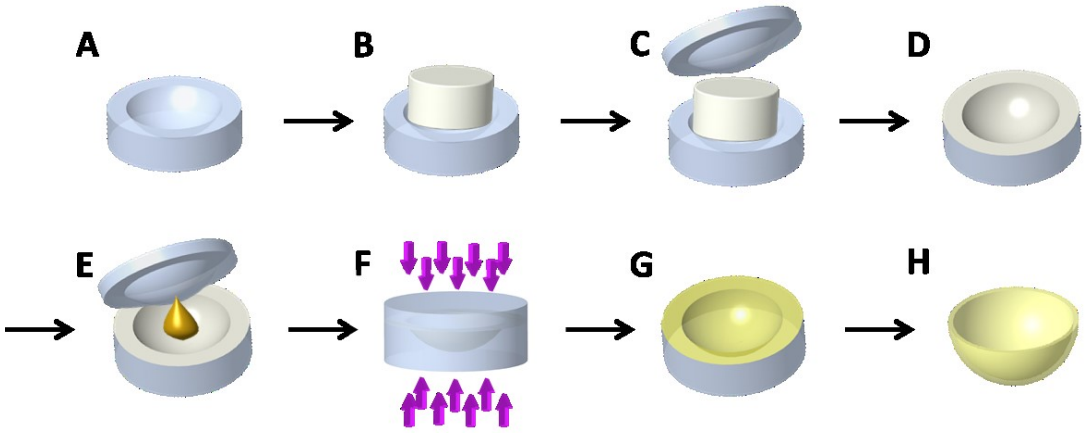

Figure 5. 1. **Schema for generating the concave shape of the reconstructed cornea.** The concave mold following the contour of the rabbit cornea was made by PMMA (A). A decellularized cornea was place on the mold (B) and gentle pressure was applied to make the cornea conjunct with the surface of the mold (C). Vitrification was carried out for 2 weeks (D) and then a few drops of 0.1% of riboflavin solution were applied within the mold (E). After incubating the cornea overnight in a cold room, UV light was applied for 90 minutes each side (F). The mold was opened (G) and the shape reconstructed cornea was gently removed from the mold after applying a few drops of PBS (H).

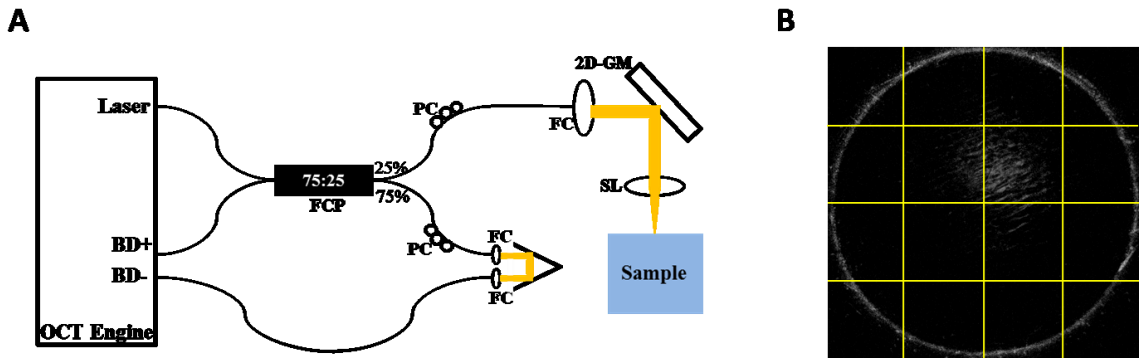

Figure 5. 2. **The method to evaluate curvature of the shaped reconstructed cornea using an optical coherence tomography (OCT) imaging system.** The system was set up with a swept source OEM engine, a balanced photo-detector (BD), a fiber coupler (FCP), polarization controllers (PCs), a fiber collimator (FC), a galvo-mirror (GM), a scanning lens (SL) and other components (A). Curvature of the reconstructed cornea and the mold was measured at two central, and four mid-central regions (indicating with yellow line) using 2D OCT images (B).

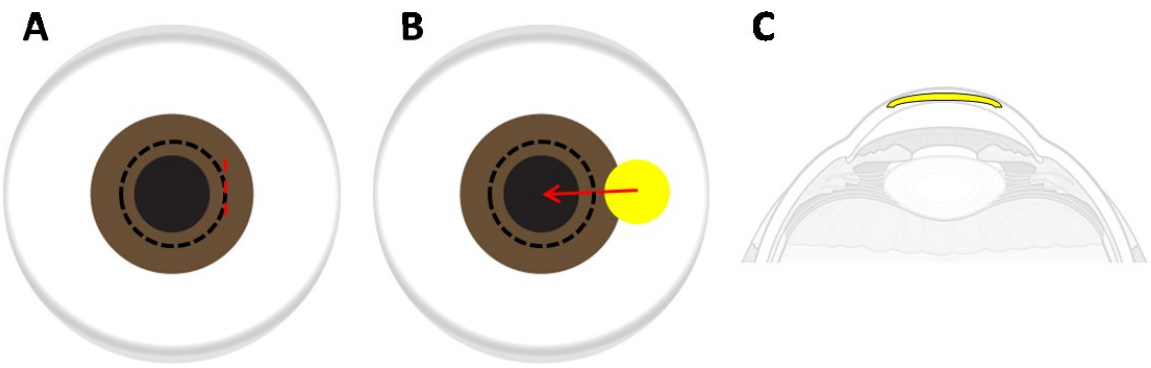

Figure 5. 3. **Schematic feature of the procedure of interlamellar keratoplasty.** After making an incision using 8mm Hessburg-Barron vacuum trephine about half the thickness of full cornea, lamellar dissection was performed to produce an intrastromal pocket with a crescent knife (A). After, a plat reconstructed cornea was inserted into the intrastromal pocket (B). The reconstructed cornea was placed in the middle of the stromal layer of the rabbit cornea (C).

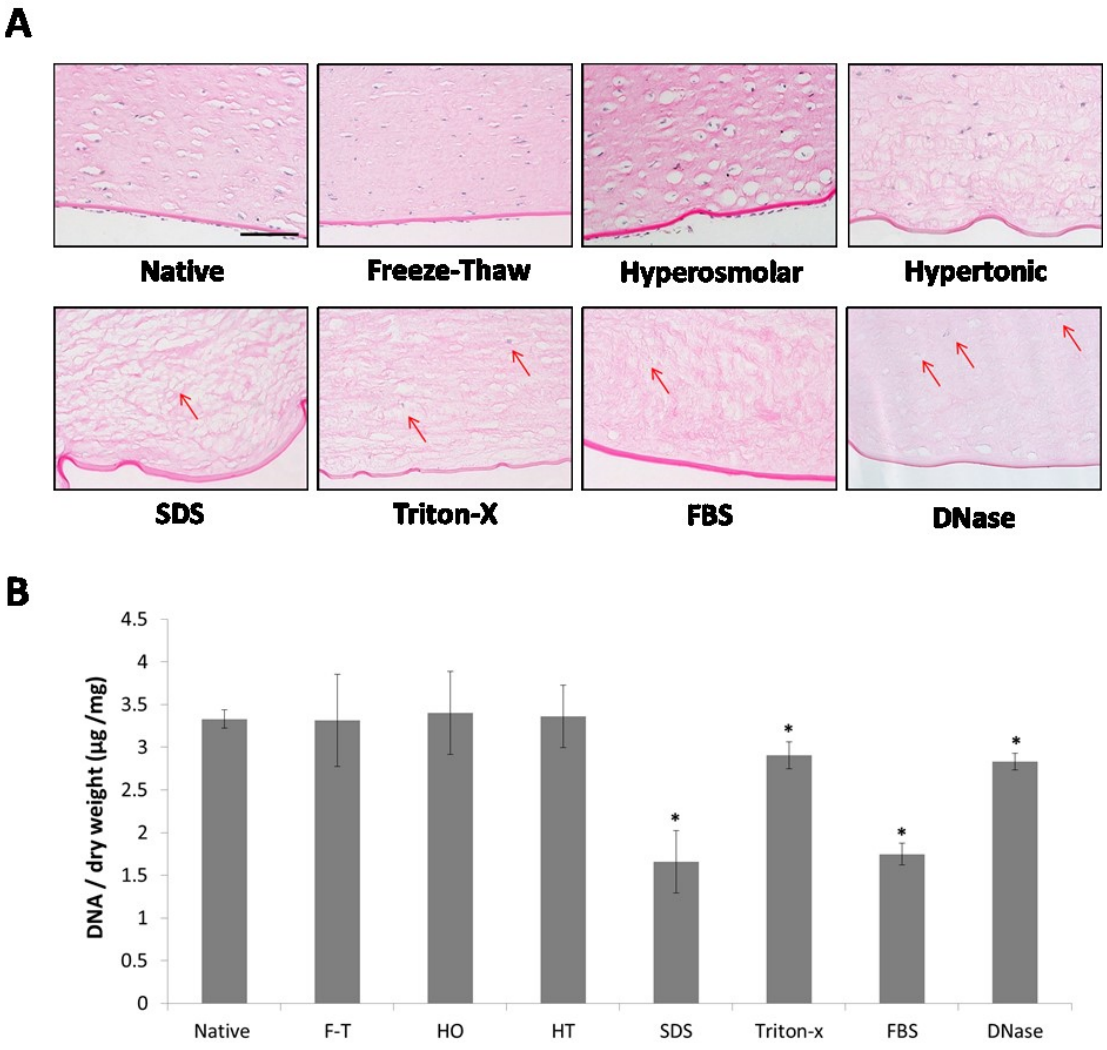

Figure 5. 4. Evaluation of the efficiency of conventional decellularized methods for porcine corneas. Representative H&E staining of cornea (A, n=5) and Quantification analysis of the amount of residual DAN in porcine corneas (B) after treating by each decellularization process. * indicates $p < 0.05$ for difference versus the native cornea with Mann-Whitney test. Data in (B) are means ± SD (n=5). Red allows indicates residual cell debris in the corneal stroma. Scale bar, 100 µm. SDS: Sodium dodecyl sulfate, FBS: Fetal bovine serum.

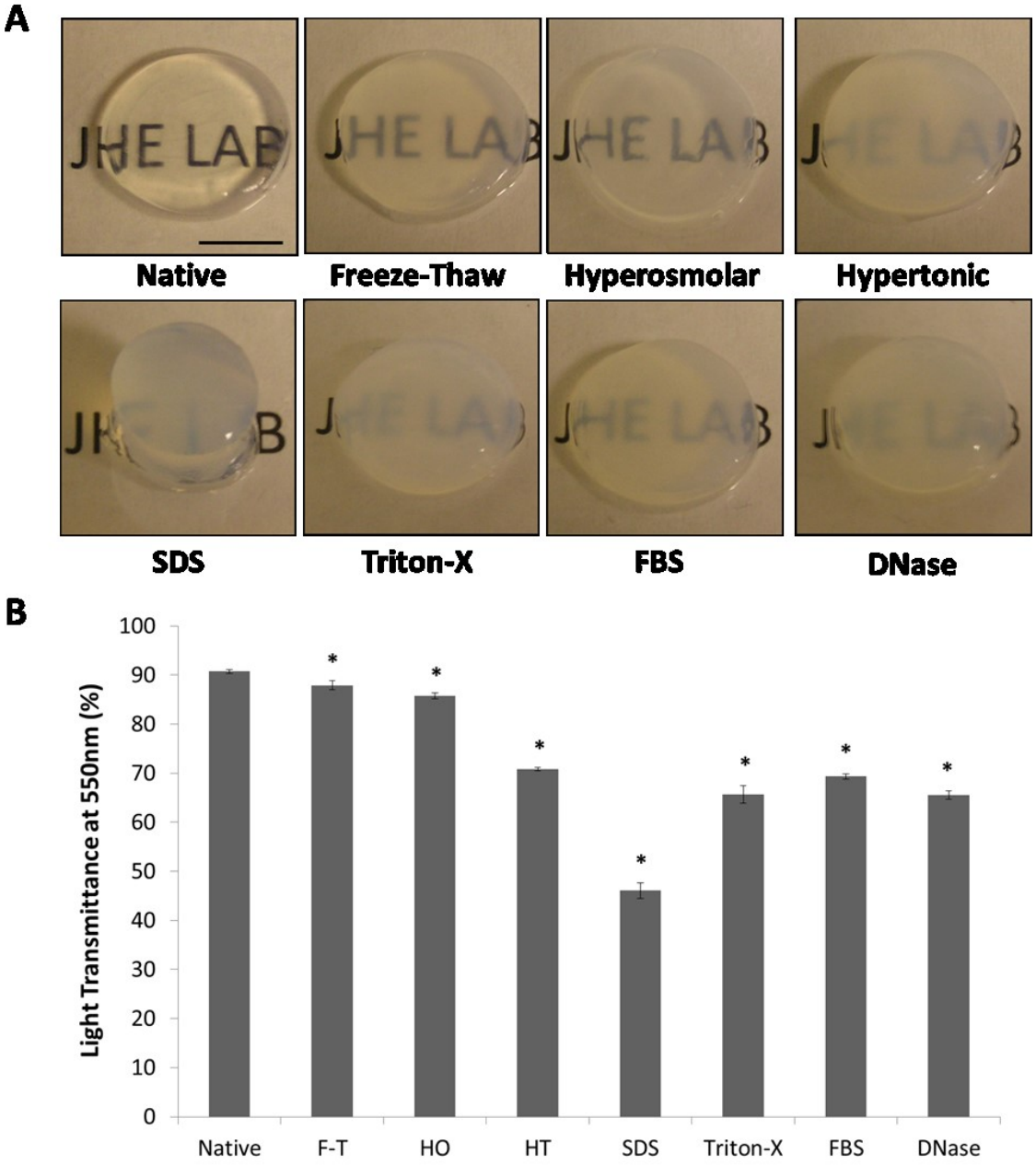

Figure 5. 5. Alteration of transparency of porcine corneas after each decellularization process. Gross images (A) and quantitative light transmittance of porcine corneas (B) after treating with each decellularization process. * indicates $p < 0.05$ for difference versus the native cornea with Mann-Whitney test. Data in (B) are means ± SD (n=5). Scale bar, 5mm. SDS: Sodium dodecyl sulfate, FBS: Fetal bovine serum.

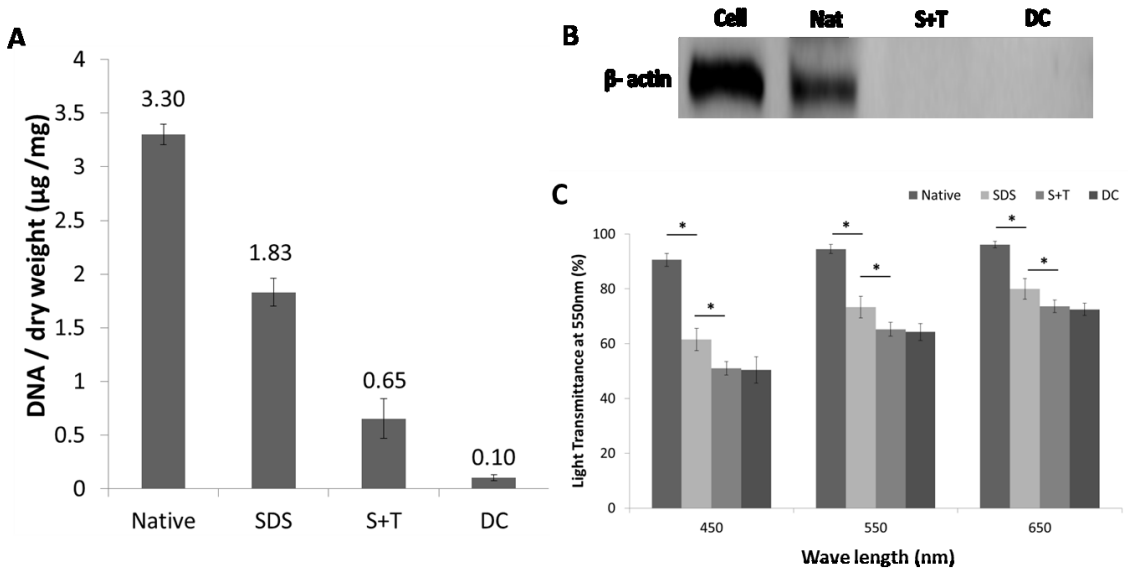

Figure 5. 6. **Effects of the combine decellularization protocol (I).** Quantification of the amount of residual DNA (A), Immunoblot for β-actin (B) and light transmittance of representative wave lengths (C) in corneas. The sample from keratocyte extraction was used a control in the β-actin immunoblot. * indicates $p < 0.05$ for difference versus the native cornea with Mann-Whitney test. Data in (A) and (C) are means ± SD (n=5). Nat: Native cornea, Cell: Keratocyte extraction, SDS: Sodium dodecyl sulfate treated cornea, S+T: SDS and Triton-X treated cornea, DC: Decelluarized cornea treated by SDS, Triton-X and fetal bovine serum.

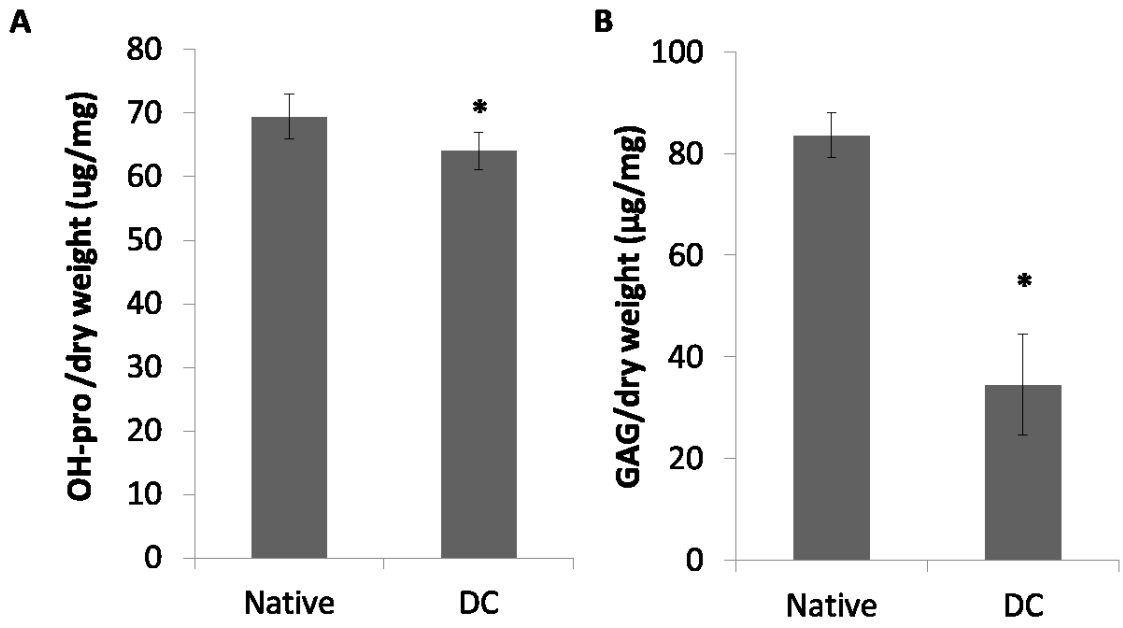

Figure 5. 7. **Effect of the combined decellularization protocol (II).** Collagen (A) and glycosaminoglycan (GAG) contents of the native cornea and the decellularized cornea (DC). * indicates $p < 0.05$ for differences versus the native cornea with Mann-Whitney test. Data in (A) and (B) are means ± SD (n=5). OH-pro: hydroxyproline.

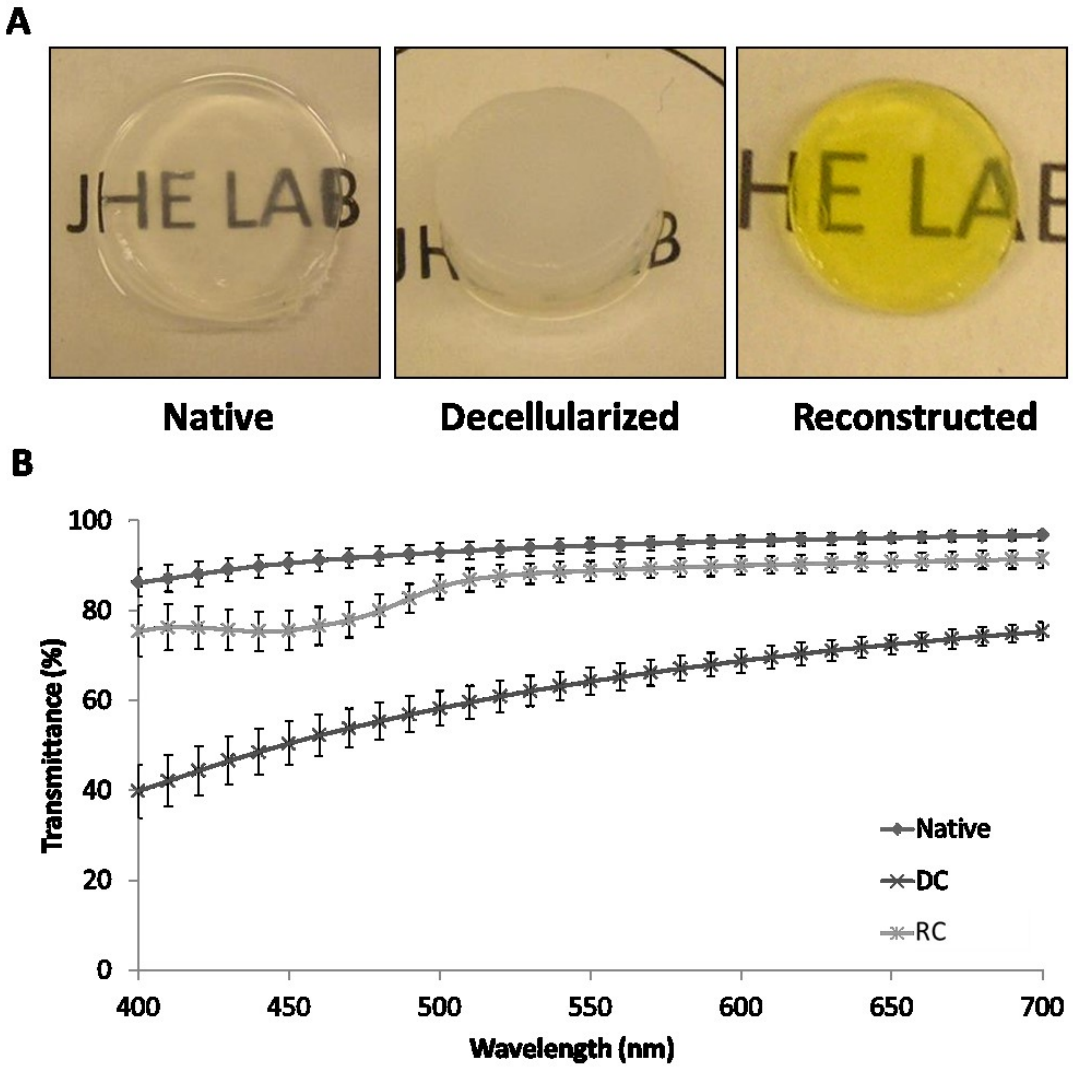

Figure 5. 8. Effect of the reconstruction process for transparency of corneas. Representative images (A, n=5) and light transmittance in all visible wave length (B) of native, decellularized (DC) and reconstructed cornea (RC). In all wave lengths, light transmittance of the reconstructed cornea is significantly ($p < 0.05$ by Mann-Whitney test)higher and lower than that of the decellularized and the native cornea respectively. Data in (B) are means ± SD (n=5).

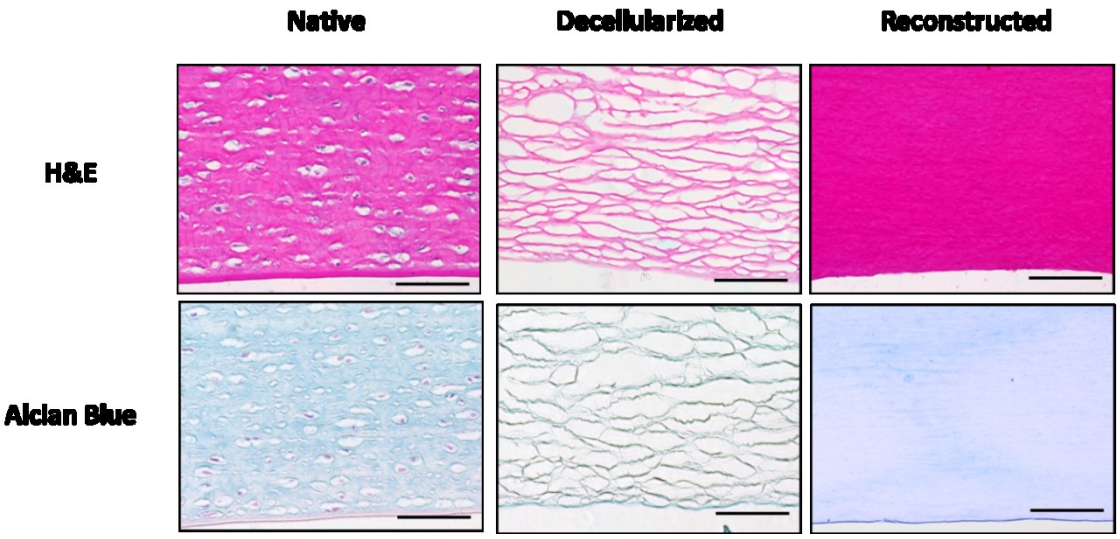

Figure 5. 9. Macrostructural evaluation for native, decellularized and reconstructed corneas with H&E and Alcian blue staining.

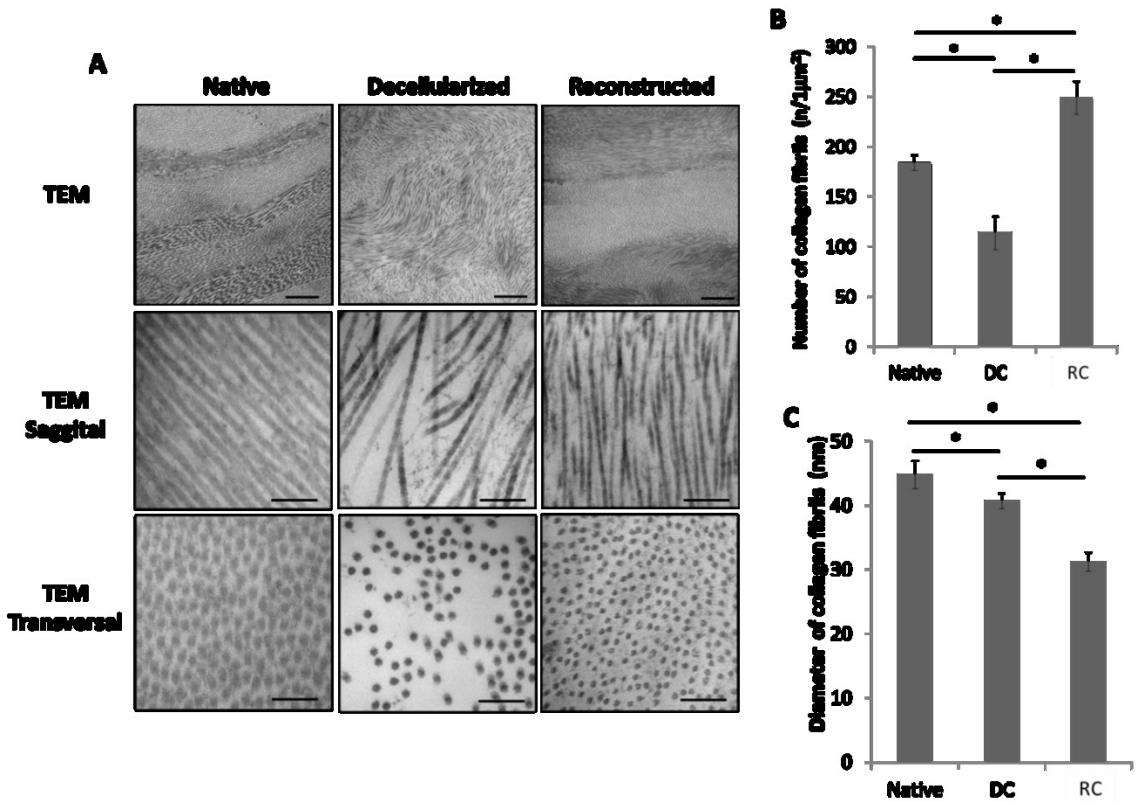

Figure 5. 10. Ultrastructural evaluation for native, decellularized (DC) and reconstructed corneas (RC). Representative transmission electron microscopy images (A, n=5), quantitative analysis of collagen fibril number in the defined area (B) and collagen fibril diameter (C) for corneas. * indicates $p < 0.05$ for difference between corneas with ANOVA and Boneferroni post-hoc. Data in (B) and (C) are means ± SD (n=50).

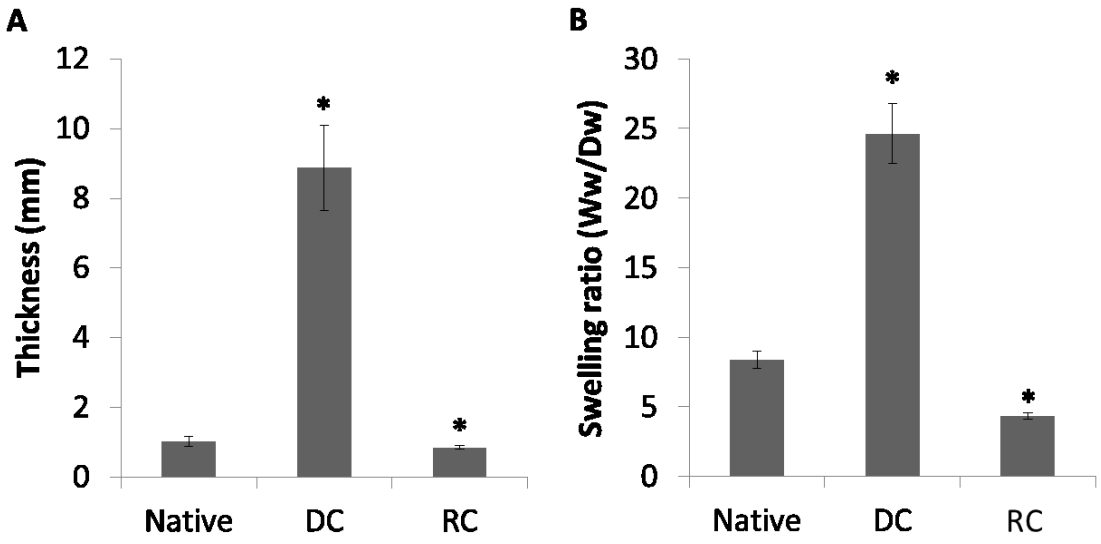

Figure 5. 11. Characterization of corneas. Measurement of thickness (A) and hydration (B) of the native, the decellularized (DC) and the reconstructed cornea (RC). * indicates $p < 0.05$ for difference versus the native cornea with Mann-Whitney test. Data in (A) and (B) are means ± SD (n=5).

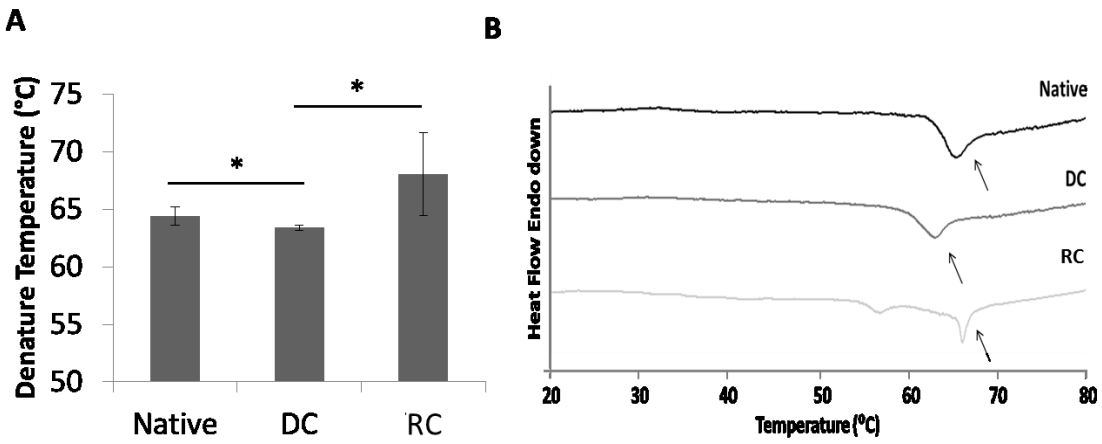

Figure 5. 12. Thermal properties of corneas. Denature temperature (A) and representative thermogram (B, n=5) of differential scanning calorimetry for native, decellularized (DC) and reconstructed corneas (RC). * indicates $p < 0.05$ for difference between corneas with with Mann-Whitney test. Data in (A) are means ± SD (n=5).

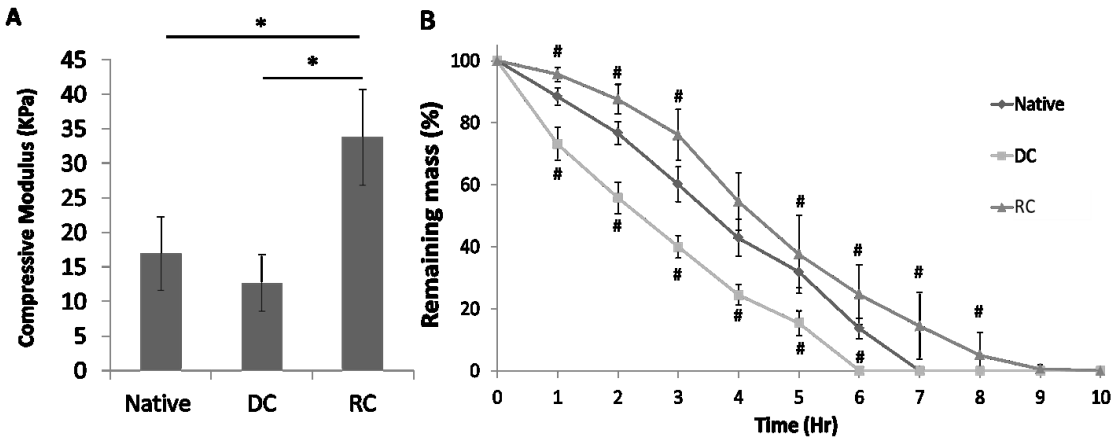

Figure 5. 13. Mechanical characterization and degradation profile of corneas. Compressive modulus (A) and collagenase degradation rate (B) of native, decellularized (DC) and reconstructed corneas (RC). * indicates $p < 0.05$ for differences between corneas with Mann-Whitney test. # means significant differences versus the native cornea with Mann-Whitney test at $p < 0.05$. Data in (A) and (B) are means ± SD (n=5).

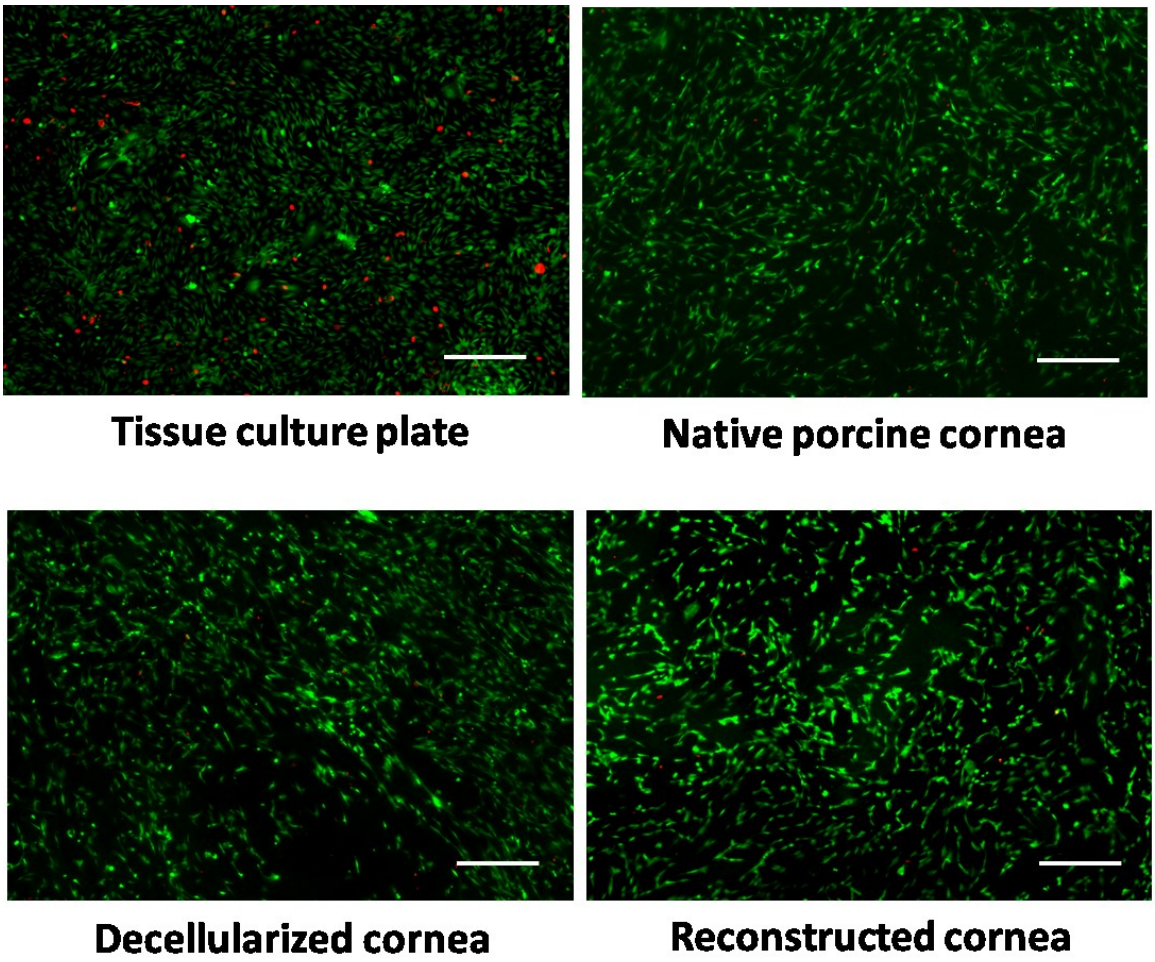

Figure 5. 14. Cytotoxicity analysis with Live/Dead cell staining for tissue culture plate, native, decellularized and reconstructed corneas.

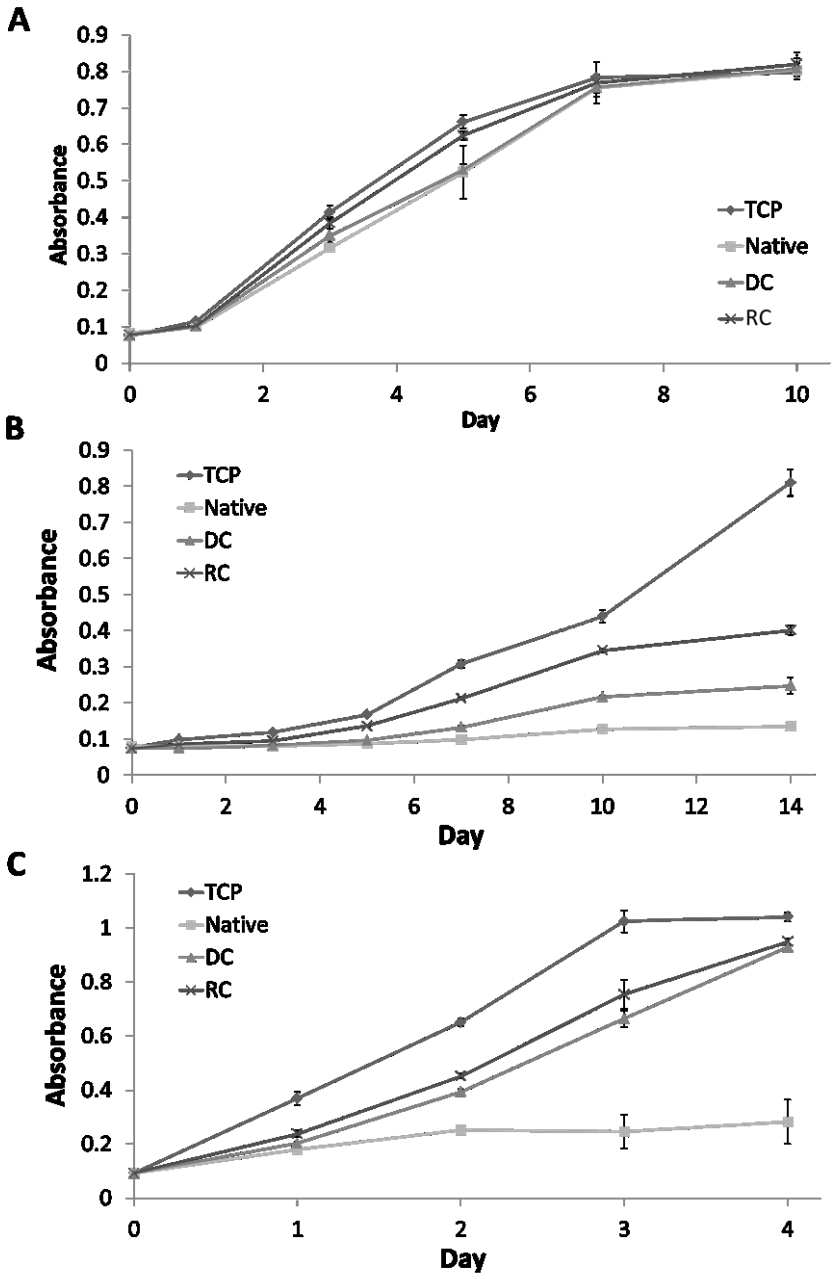

Figure 5. 15. Proliferation prolife of three corneal cell types on corneas. Proliferation rate of human corneal epithelial cells (A), human keratocyte-induced fibroblasts (B) and bovine corneal endothelial cells (C) on tissue culture plate (TCP), native, decellularized (DC) and reconstructed corneas (RC).

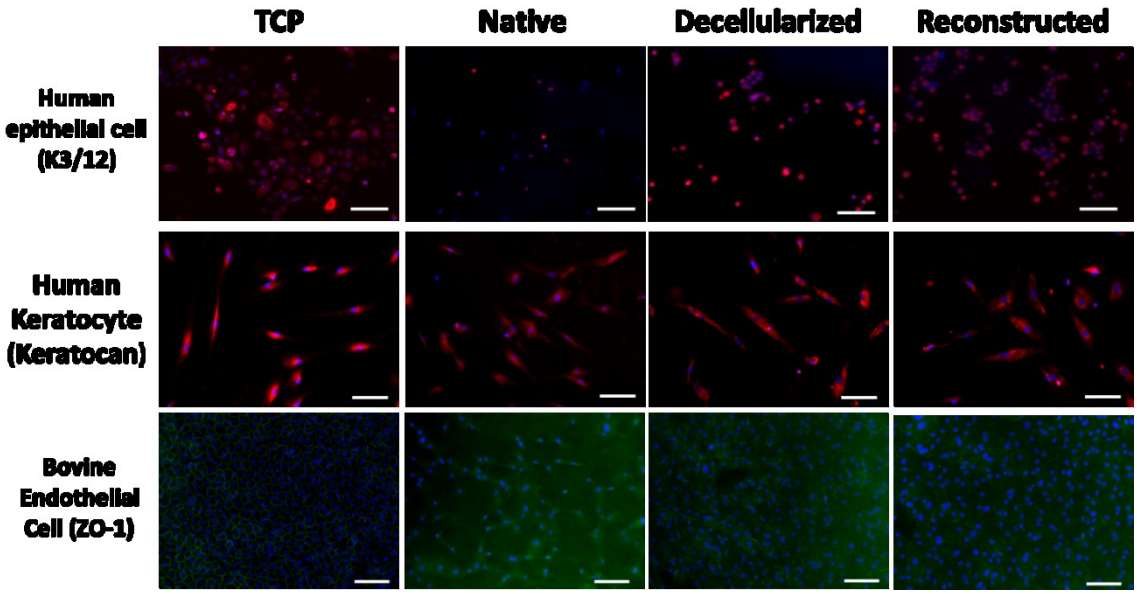

Figure 5. 16. Immunocytochemistry for human epithelial cells, human keratocyte and bovine endothelial cells on tissue culture plate (TCP), native, decellularized and reconstructed corneas.

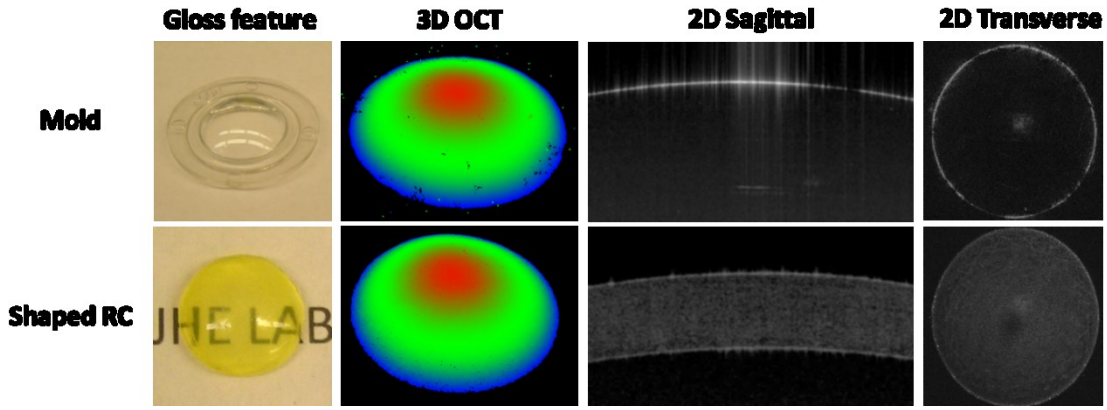

Figure 5. 17. Representative gloss feature, 3D and 2D optical coherence tomography (OCT) images for the mold and the shaped reconstructed cornea (RC).

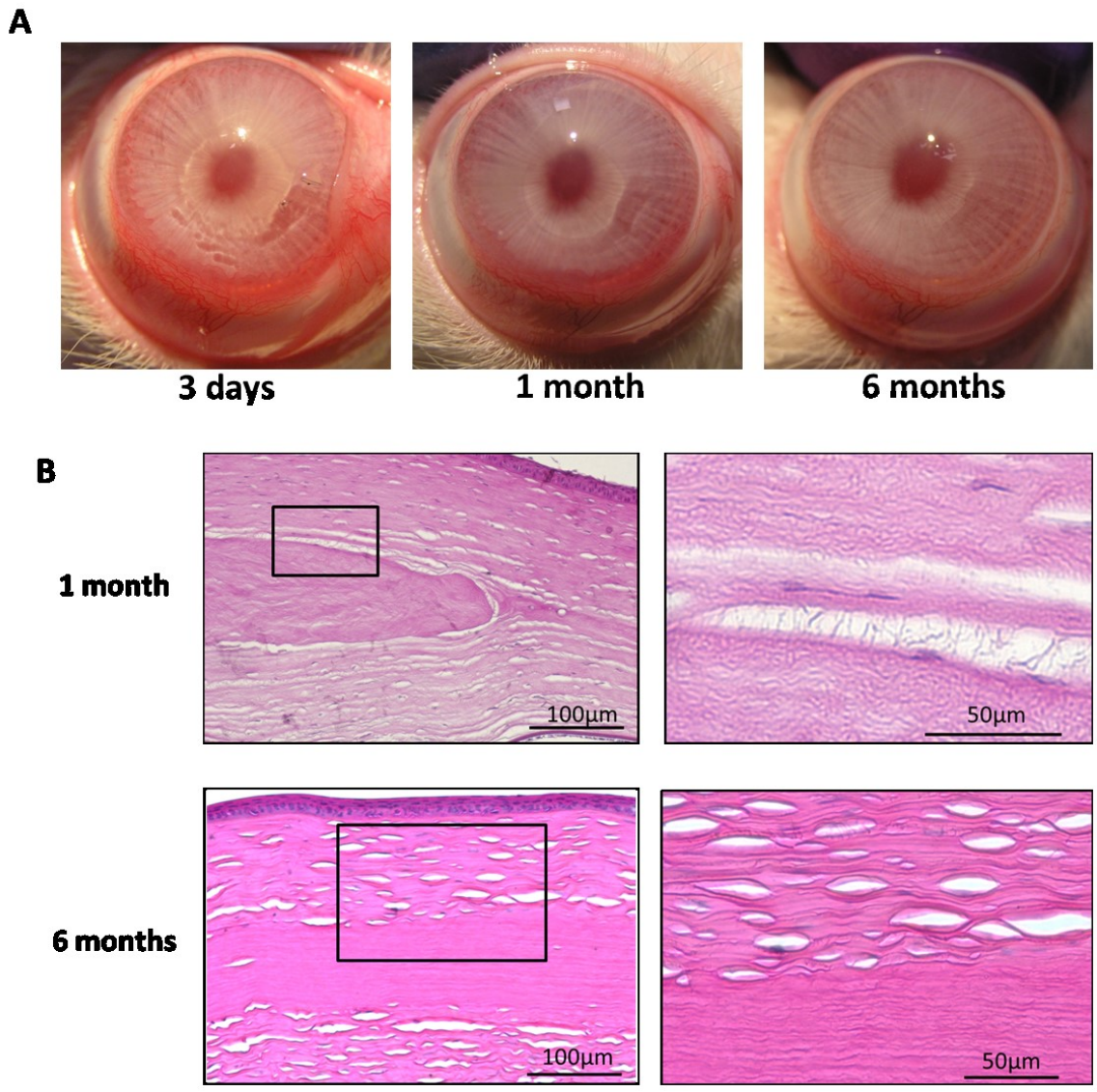

Figure 5. 18. Intrastromal implantation of the reconstructed cornea (RC) for rabbits. Post-operative observation (A) and H&E stating (B) of the rabbit interlamellar keratoplasty model.

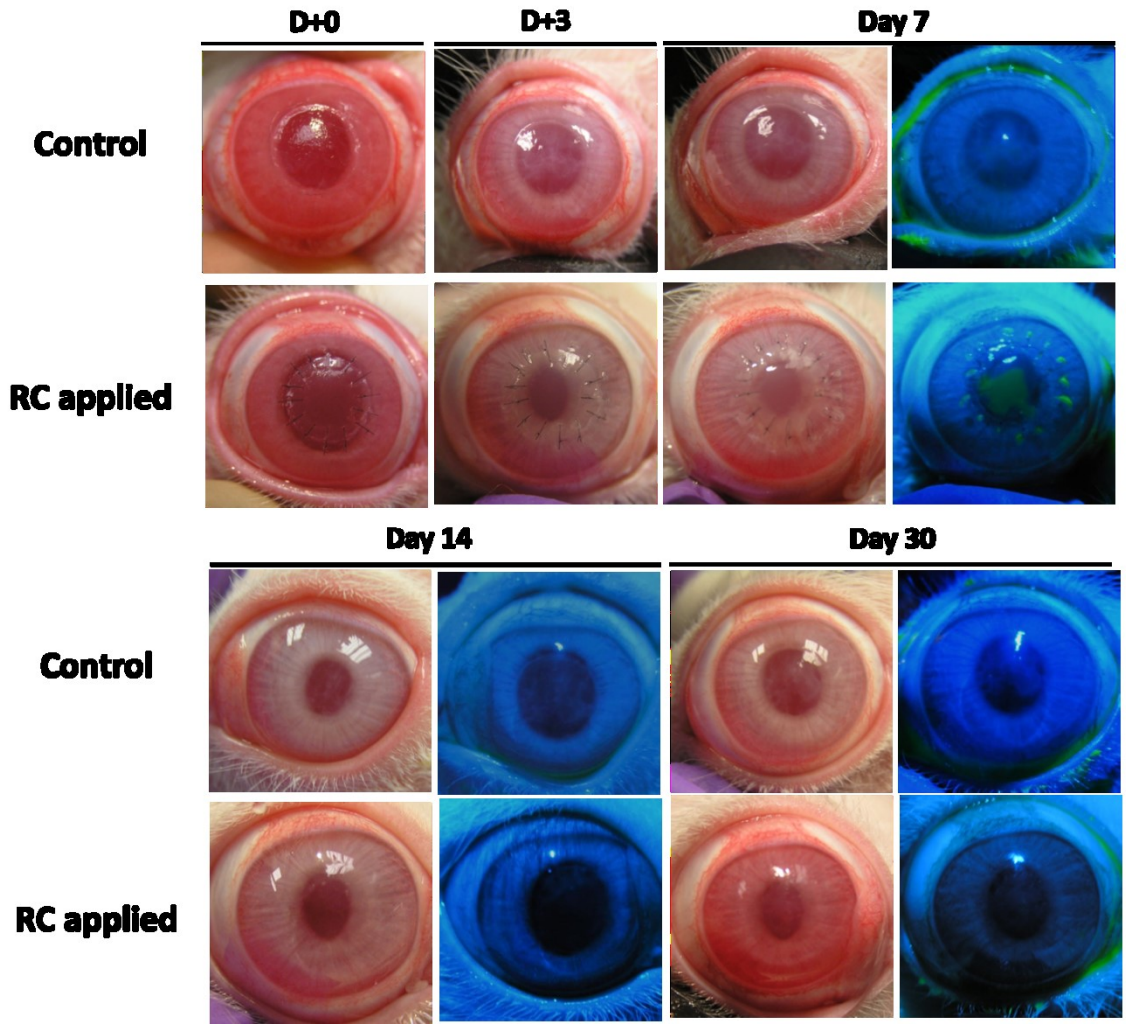

Figure 5. 19. Implantation of the reconstructed cornea (RC) into rabbits with anterior lamellar keratoplasty. External features and the re-epithelial process of the control (n=1) and the RC applied rabbit corneas (n=3) after the lamellar keratoplasty during 1-month period.

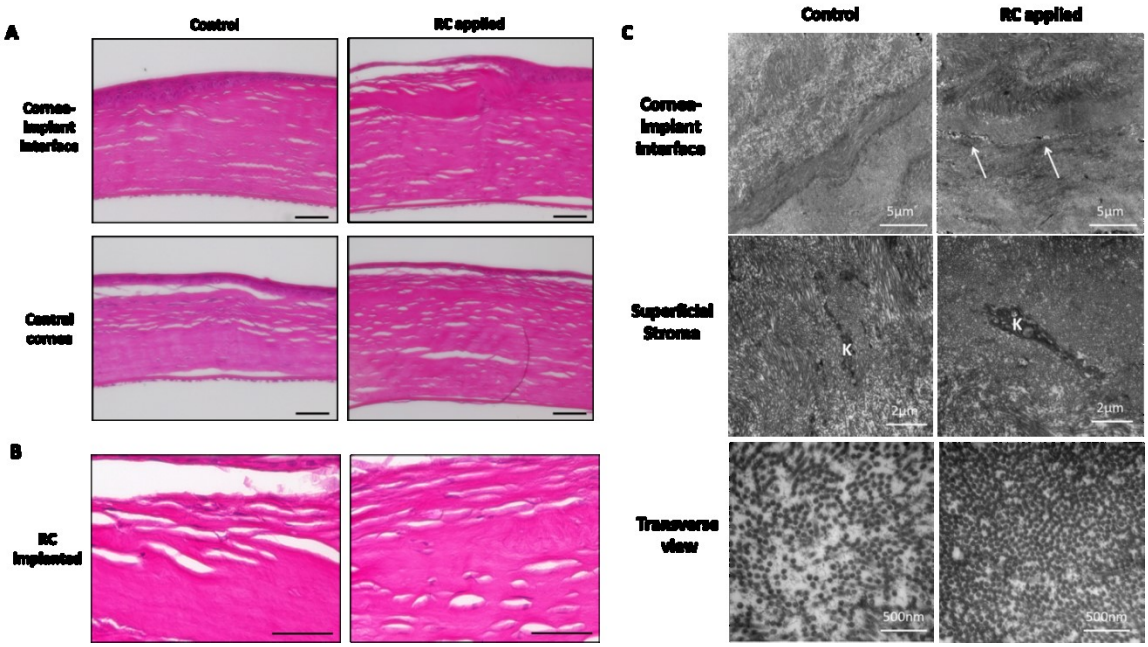

Figure 5. 20. Pathological examination for the rabbit cornea implanted the reconstructed cornea (RC) with anterior lamellar keratoplasty. Images of H&E staining (A and B) and transmission electron microscopy (C) for the control (n=1) and the reconstructed cornea (RC) applied rabbit corneas (n=3) after the lamellar keratoplasty. Scale bar for (A) and (B): 100 μm. White arrow: A gap between the native cornea and RC, K: Keratocyte

Table 5. 1. Information about antibodies.

Cell type	Antibody		Source	Antibody Concentration
Epithelial cell	Primary	Cytokeratine 3	Millipore	1:100
	Secondary	Alexa Fluor 546 Donkey anti-mouse	Molecular Probes	1:200
Keratocyte	Primary	Keratocan	Santa Cruz	1:200
	Secondary	Alexa Fluor 578 Donkey anti-goat	Molecular Probes	1:200
Endothelial cell	Primary	ZO-1	Zymed	1:50
	Secondary	FITC Goat Anti-rabbit	Jackson Lab	1:100

6. Nictitating membrane fixation improves stability of the contact lens on the animal corneal surface

6. 1. Introduction

Animal models are the primary tool to evaluate comprehensive physiological responses to biomaterials in the ophthalmic research. A proper animal model study is considered an essential procedure to ensure a successful translational application of an ophthalmic biomaterial to clinical use. However, the anatomical and physiological differences between humans and animals can preclude accurately capturing the anatomy and physiology of the human eye [165]. The nictitating membrane (NM), also termed the third eyelid, exemplifies species-specific differences of the eye. Anatomically, most animals have this accessory eyelid around the medial canthus, whereas human and anthropoids keep a vestigial remnant of this organ, *plica semilunaris* [166]. Physiologically, the function of the *plica semilunaris* in human is insignificant, but the NM in animals contributes to a healthy animal eye by producing and distributing tears, removing ocular debris, secreting immune proteins, and acting as a mechanical barrier [2]. The NM can limit animal studies of a new biomaterial, as a soft or a vulnerable material applied on the ocular surface can be easily damaged by movement of NM. Additionally, if the material weakly binds to the ocular surface, it could be displaced and consequently removed from the animal by NM.

Contact lens application can be hindered by both limitations. Although the NM could help keep a contact lens hydrated, it also reduces stability of the contact lens, preventing further preclinical study [167]. To increase stability, nictitating membranectomy and tarsorrhaphy have been used to remove the membrane or limit movement, respectively. However, excision of NM is an invasive procedure, and could cause mild to moderate dry eye syndrome [168] which leads to pathological cascades on the ocular surface [169] in some species. Closure of the palpebral aperture by suturing both eyelids decreases oxygen levels [170, 171], alters tear fluid osmolality [172] and swells the corneal epithelium [167]. Thus, these surgical procedures cause undesired secondary effects resulting in distortion of data from the animal study.

To improve upon existing models for preclinical biomaterials, especially contact lens research, we have developed a method to stabilize the nictitating membrane. By fixing the NM to the upper eyelid, the movement of the membrane can be limited which may lead to increased material stability on the ocular surface of animals. We evaluated the feasibility of NM fixation to improve material stability.

6. 2. Materials & Methods

6. 2. 1. Animals

Twelve New Zealand white male rabbits, 2.0 to 3.5 kg in weight, were used in this study. All experimental procedures in this study accord to the Association for Research in Vision and Ophthalmology (ARVO) Statement for the Use of Animals in Ophthalmic and Visual Research, and were approved by the Institutional Animal Care and Use Committee at Johns Hopkins University. Ten animals were used for tear and

contact lens stability tests, and two animals served for gross observation and pathological examination.

6. 2. 2. Nictitating membrane fixation

Membrane fixation was performed under general anesthesia with ketamine (15 mg/kg of body weight) and xylazine (2 mg/kg of body weight) delivered intramuscularly. NM fixation was applied to a randomly chosen eye and the other eye was untreated to serve as a control. After administering one or two drops of topical anesthesia (proparacaine 0.5%), a horizontal mattress suture using a 4-0 polyglactin 910 (Vicryl, Ethicon, Somerville, NJ) was placed between the free edges of the nictitating membrane and the upper eyelid. The suture needle first penetrated an ophthalmic spear cut 5 (length) x 10 (width) mm in size. Next, the suture was passed the upper eyelid through the palpebral conjunctiva in the medial canthus area (Figure 6.1A). The last suture was placed about 4-6 mm in length along the lateral margin of nictitating membrane, approximately 2 mm apart (Figure 6.1B). The following suture bite was backed out the palpebral conjunctival and passed through the upper eyelid (Figure 6.1C) and the ophthalmic spear (Figure 6.1D). The suture knot was made on the spear (Figure 6.1E), and the spear was trimmed to stay within the margin of the eyelid.

6. 2. 3. Schirmer tear test and tear break-up time

To assess the change of quantity and quality of tear production after the NM fixation procedure, Schimer tear test-1 (STT-1) and tear break-up time (TBUT) measurements were performed for both eyes (n = 10 rabbits) 6 hours after the surgery, and at days 1, 2 and 3. After bending the notch of a STT strip (Alchon®, Fort Worth, TX),

the folded end was placed within the inferolateral one-third of the lower conjunctival fornix for 3 minutes. The level of tear migration was marked and measured from the fold, immediately at removal. TBUT was assessed under blue light in a dark room. Each eyelid was closed manually to distribute the tear film. Then, the eye was held open and two drops of sodium fluorescein dye (Fluoresoft -0.35%®, Alden optical, Lancaster, NY) were added onto the corneal surface. The time for observing distortion of the reflected image was recorded.

6. 2. 4. Contact lens stability test

After the tear tests, rabbits underwent contact lens stability tests. Each contact lens (Hydrokone®, Visionary Optics, Front Royal, VA) was confirmed to fit each eye with the conventional contact lens fitting method using florescent dye and a slit lamp microscope. The base curvature and the diameter of lens were 8.4-8.6 and 14.00 mm, respectively. We measured stability of the contact lens by calculating the rate of "successful retention", which was defined in this study as the contact lens remaining on the corneal surface for more than four hours after application. The contact lens was applied four times per an animal.

6. 2. 5. Gross observation and pathological examination

Two rabbits not used for either tear or contact lens tests were observed for one month after NM fixation. At 1 and 2 weeks and 1 month after the procedure, each eye was examined with a conventional slit lamp microscope. After 1 month, the rabbits were sacrificed for pathological examination. The tissue was collected from the eye that underwent the procedure and the collateral eye served as a control. Dehydrated and

paraffin-embedded sections were stained with hematoxylin and eosin (H&E) using standard techniques.

6. 2. 6. Statistical analysis

Data from tear tests (STT values and TBUT) were presented as means ± standard deviation (S.D.). Results were analyzed by Mann-Whitney test to evaluate the differences between two eyes at each time point using SPSS 15.0 for Windows (SPSS Inc., Chicago, IL). Statistical significance was established at $p < 0.05$.

6. 3. Results

6. 3. 1. Tear tests

To evaluate secondary effects for the secretary system after NM fixation, we tested tear production quantity and quality. No significant differences of STT values and TBUT measurements were found between the control and experimental eyes. In the fixed eyes, the average STT value was 10.1 ± 2.0 mm 6 hours after the procedure on day 0 (Figure 6.2A). The values for both eyes were consistent through the three-day experiment, ranging from 9.5 to 10.2 mm. The TBUT in both groups also did not fluctuate significantly over the course of 3 days after NM fixation, ranging from 31.5 to 33.9 seconds (Figure 6.2B). Thus, the NM fixation procedure did not change the quantity and quality of tear production.

6. 3. 2. Contact lens stability test

Both contact lens curvatures of 8.4 and 8.6mm fitted well on the all rabbit corneas. The stability of contact lens was increased after applying NM fixation, where the rate of contact lens retention—considered to be the lens remaining on corneal surface after 4 hours— in the rabbit eyes that had procedure was higher than untreated eyes (90% versus 42.5%, respectively).

6. 3. 3. Gross observation and pathological examination

During the course of 1 month after NM fixation, we observed no substantial lesions, including corneal haze, conjunctival hyperemia or chemosis, aqueous flare, or iris lesions in the both untreated and NM-fixed eyes (Figure 6.3). Normal Purkinje image was found in the both sets of eyes during this time period. Corneas from both untreated and fixed eyes did not show any remarkable pathological lesions upon H&E staining. Additionally, Mason's trichrome staining confirmed there was no scar tissue formation in either eye (Figure 6.4).

6. 4. Discussion

The nictitating membrane can destabilize contacts lens on the animal eye, and thus be problematic when using animal models to reliably study the effect of new biomaterials on the corneal surface. The nictitating membranectomy is considered an essential procedure for contact lens retention in animal models [173]. However, the procedure is invasive and requires a relatively long surgical time, approximately a week of recovery, and additional surgical procedures, such as a cauterization. In addition, the surgery causes excessive tissue damage and presents ethical issues. We therefore

explored a new safe, simple, and non-invasive surgical approach that "fixes" the NM, in rabbits. The procedure and recovery time for NM fixation was minimal, and only brief training would be needed to use basic surgical instruments. In addition, the buffer effect of the ophthalmic spear prevents laceration or necrosis of the upper eyelid by excessive tension of the suture knot, one of the most common complications during NM fixation to the upper eyelid [174].

Another issue of the nictitating membranectomy is the unavoidable excision of the accessory lacrimal gland. Although some animals can compensate for decreased tear production through other lacrimal glands and the harderian gland after removing the NM [175], animal models such as dogs and cats are susceptible to dry eye syndrome [176, 177]. In addition, decreased tear production may affect contact lens retention by reducing hydration of soft contact lenses [170, 178]. Loss of goblet cell clusters in the nictitating membrane could decrease the mucin portion of tears, detracting from tear quality [166]. NM fixation does not require functional tissue manipulation of the NM, including the accessory gland, and a suture could induce only minimal tissue damage on the margin of NM and upper eyelid. We confirmed through STT and TUBT that the NM fixation procedure did not affect the quality and quantity of tears in rabbits. Furthermore, the procedure did not cause any substantial secondary morphological or pathological side effects at 1 month resulting from decreased quality and quantity of tear production.

As shown in the rabbit model, we expect that NM fixation would increase retention of the contact lens on the cornea and be feasible for testing various contact lens–based technologies, such as the drug-releasing contacts for the glaucoma treatment [179]. In addition, this technique could be used in veterinary practice. For instance, the

loss of the bandage contact lens on the corneal surface can be an issue when treating animals with chronic corneal epithelial defects, such as dogs [180]. Because NM fixation was performed under the general anesthesia, some issues, such as the anesthetic risk, could be raised in the veterinary practice. However, the procedure could be done with auriculopalpebral nerve block, topical anesthesia of the eye, and infiltration anesthesia as being done in the NM flap [174] that could be reduce issues of the general anesthesia. Besides contact lenses, NM fixation could be used for the application of soft biomaterials, such as fibrin glue, to the animal cornea. The restricted movement of NM may reduce damage to and promote retention of the soft material.

In conclusion, we demonstrated that NM fixation could increase stability of the contact lens without reducing the quality and quantity of tear production in healthy rabbits. In addition, the technique is simple and did not cause any major pathological changes. We suggest NM fixation would be helpful to design animal studies for investigating new contact lens and has potential to apply to other biomaterial research at the ocular surface.

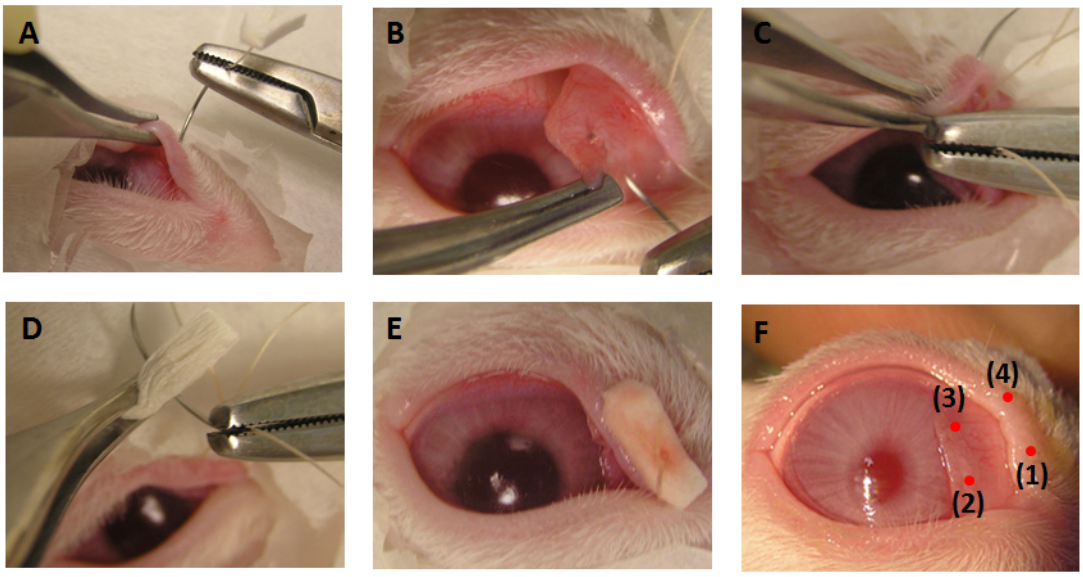

Figure 6. 1. Surgical procedure for nictitating membrane (NM) fixation. (A) After penetrating a tailored ophthalmic spear, the needle passed the upper eyelid through the palpebral conjunctiva. (B) A bite was made on the lateral part of the NM. (C) The followed bite was back out the palpebral conjunctival and passed through the upper eyelid. (D) Lastly, the needle penetrated the ophthalmic spear. (E) The suture was knotted. (F) Four bitten areas are shown in rabbit eyelid.

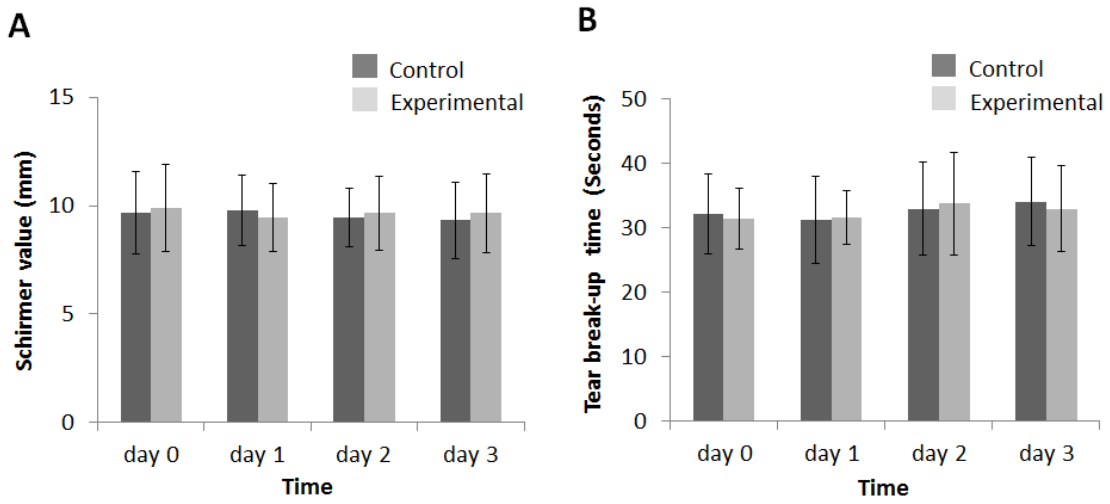

Figure 6. 2. Evaluation of tear quantity and quality. Rabbits underwent NM fixation in one eye, while the other was left untreated as a control on day 0. (A) Shimer tear test (STT). (B) Tear break-up time (TBUT) measurement. Data are averages ± SD (n = 10). No significant difference was found between both groups of STT values and TUBT measurements. Statistical significance was evaluated by Mann-Whitney test at $p < 0.05$.

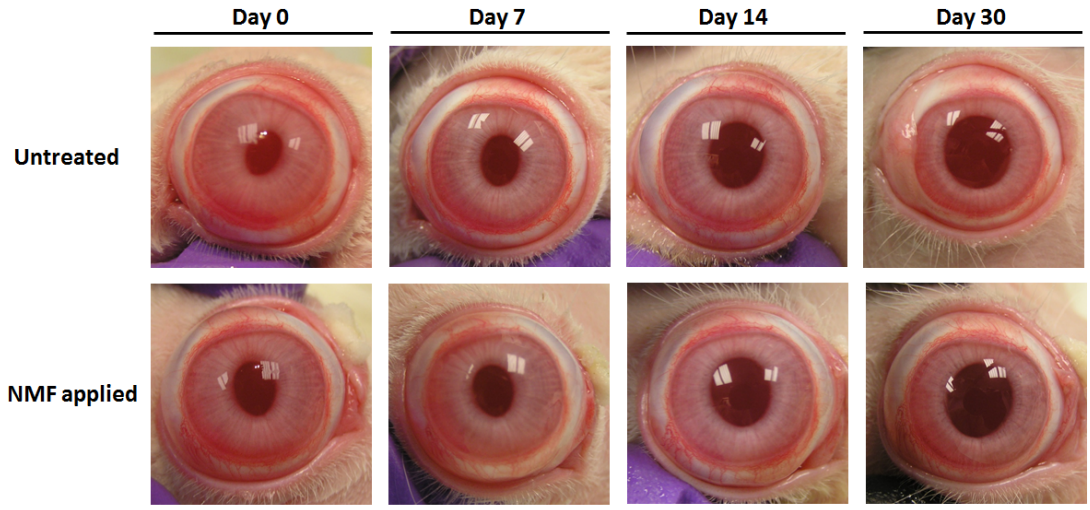

Figure 6. 3. Gross observation for untreated and NM-fixed eyes. Two rabbits were examined both eyes, looking for lesions such as corneal scar and conjunctival redness during 1-month period. There were no substantial lesions in both eyes. Images are representative of $n = 2$ rabbits.

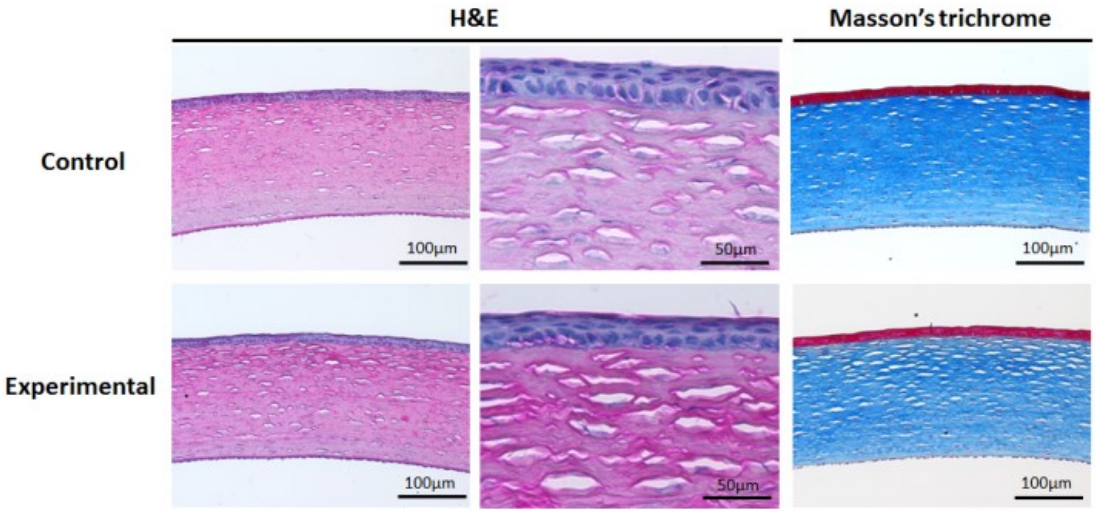

Figure 6. 4. Pathological examination for experimental and control corneas. Corneas were stained at 1 month with H&E and Masson's trichrome. Corneas from both untreated and fixed eyes did not show any remarkable pathological lesions. Images are representative of $n = 2$ animals.

7. Evaluation of the biocompatibility of regenerated cellulose hydrogels with high strength and transparency for ocular applications[4]

7. 1. Introduction

Ocular injury in the battlefield is considered to be more prevalent and more severe than in the civilian setting [181]. Prompt emergency treatment for ocular injury is essential to preserve vision, reduce pain and prevent secondary infection [72]. A bandage contact lens has the benefits of both treating and protecting the injured eye without compromising vision. Studies have shown the use of a bandage contact lens can relieve pain and photophobia in the mild to moderate ocular injury [182] and may promote healing of self-sealed perforations in more severe injuries [94]. Additional benefits of a bandage contact lens are the ease of application, particularly in a battlefield setting, and injury monitoring without removal.

Use of natural polymers for biomedical applications is increasing as these materials are thought to possess properties better tailored to living organisms than synthetic materials [183]. Cellulose, the most abundant natural polymer, produced not only by plants but also by bacteria (e.g., Acetobacter), algae, and fungi, has found

[4] Part of this chapter will be appear as a paper here: Patchan MW*, Chae JJ*, Lee JD, Calderon-Colon X, Maranchi JP, McCally RL, Schein OD, Elisseeff JH, Trexler MM. "Evaluation of the biocompatibility of regenerated cellulose hydrogels with high strength and transparency for ocular applications" **Journal of biomaterials applications**, 30(7): 1049–1059, *: co-first author

widespread use as a material for biomedical applications [184]. Plant cellulose has long been used in the form of cotton for wound dressings and sutures [183], and is also widely used as a binder in pharmaceutical tablets [185]. Additionally, contact lens conditioning solutions containing hydroxyethylcellulose have shown improved wetting of lenses and enhanced lens wearing comfort [186]. One drawback to plant-based cellulose is that it requires intensive processing to separate it from the lignin and other materials in the plant bulk before it can be used. Bacterial cellulose (BC), although identical to plant cellulose in chemical structure, is excreted as a biofilm [184] of pure cellulose, which requires little processing before use. BC is remarkable for its high water content and mechanical strength; however, large-scale production remains challenging [183].

Moisture management is critical to wound healing [187]. Poor moisture control of the wound environment impairs the healing process and increases the risk of infection [188]. Cellulose, both crystalline and BC, has unique moisture management characteristics [189] and several commercially available products take advantage of these characteristics. For example, Refresh Tears® an ophthalmic solution used to alleviate dry eye, contains carboxymethylcellulose (CMC) because it closely resembles the composition of natural tears [190]. Microbial cellulose marketed as Xcell® and used as a dressing for burn wounds, has been shown to effectively absorb exudate and hydrate dry areas of a wound, maintaining a moisture-balanced wound environment [191]. Given the above examples, cellulose-based materials seem ideal for ocular bandage applications, where adequate moisture on the ocular surface is critical for conjunctival and corneal wound healing.

Hydrogels are three-dimensional crosslinked polymeric networks with the capacity to hold water within the porous structure [192]. Developed and studied for use in a variety of biomedical applications, hydrogels from natural polymers, including cellulose, are of particular interest because of their hydrophilicity, biocompatibility, and biodegradability [193]. Hydrogels derived from plant cellulose and its derivatives show promise for many *in vivo* applications including drug delivery, wound healing, and cell transport [194-196]. Bacterial cellulose has been widely studied for use in wound healing and drug delivery, as well as tissue engineering, because of its high mechanical strength [191, 197-199]. In general, hydrogels are biocompatible because their hydrophilic surface has a low interfacial free energy when in contact with bodily fluids, which results in a low tendency for proteins and cells to adhere to these surfaces [200]. Plant-based and bacterial cellulose hydrogels have shown good biocompatibility [201, 202]. Thus, cellulose-based hydrogels have the potential to be used for therapeutic purposes for corneal injuries and diseases.

In our previous study [181], we demonstrated that the optical transparency and mechanical strength of hydrogels synthesized from different cellulose sources (plant, cotton, and bacterial) could be optimized within the range of contact lens material properties by tailoring synthesis parameters. The objective of this study was to evaluate the *in vivo* biocompatibility and related physical properties of the optimized cellulose-based hydrogels and to demonstrate that these hydrogels could be made with contact lens geometry for potential use for corneal applications.

7. 2. Materials & Methods

7. 2. 1. Material preparation

Regenerated cellulose hydrogels were prepared as reported previously [181]. Briefly, for the plant-based celluloses, Avicel PH 101 (denoted herein as Avicel 101, FNC Biopolymer) or Cellulose (denoted herein as MCC4, Sigma-Aldrich 435236), 5 g of as-received cellulose powder was activated in 100 mL *N*,*N*-dimethylacetamide (DMAc, Sigma-Aldrich) with stirring at 350 rpm for 24 hours. Following this, dissolution was initiated by addition of 8 g of lithium chloride (LiCl, Sigma-Aldrich) with continued stirring at 350 rpm and heating to 95 °C until the solution became clear. The resulting solution was then poured into the desired mold and allowed to gel; after which, the samples were gently washed in water to remove the excess LiCl/DMAc and stored in water prior to testing. For the bacterial cellulose, the as-received pellicle (prepared in-house [181]) was dried by heat pressing at 45 °C under 14 MPa pressure for 5 minutes using a Carver Press (Hydraulic Unit Model #3912) followed by an overnight dry in a 90 °C convection oven. Five hundred milligrams of the resulting dry sheet was placed in 100 mL of 8% LiCl/DMAc solution and stirred at 500 rpm until the cellulose dissolved (up to 10 days). The resulting BC/LiCl/DMAc solution was then poured into the desired mold, gelled, washed, and stored in the same manner as described for the plant-based cellulose varieties.

7. 2. 2. Oxygen permeability

A polarographic method was used to measure the oxygen permeability, Dk, of the hydrogels (Figure 7.1A). Polarography measures the oxygen permeation through a sample by measuring the current produced in a cell by reducing oxygen at a noble metal electrode [203-205]. Polarography is used to measure oxygen transmissibility, Dk/t, in units of Barrer/cm (Note: 1 Barrer = 10^{-11} (cm^3 O_2) cm cm^{-2} s^{-1} $mmHg^{-1}$). The oxygen

permeability can thus be calculated by multiplying the oxygen transmissibility by mean thickness of the material. A flat polarography cell was obtained from Rehder Development Corporation with a 4-mm outer diameter (O.D.), 24-karat gold cathode surrounded by a 5.75-mm inner diameter (I.D.), 12.50-mm O.D., pure silver anode. The polarography cell was calibrated using three rigid gas permeable reference materials with known oxygen permeability (Table 7.1) [206].

For each reference material, the sample thickness was measured with a thickness gage (Starrett model #1015MA) and then placed onto the surface of the electrode/cell and fixed in place by gently pressing toward the electrode. The system was held in a humidity chamber at 35 ˚C with high humidity (> 90 %RH). A saline solution (0.9 % NaCl, pH 7.4) was poured into the reservoir. A Keithley 2400 source-meter (source 0.75 V across the Au-Ag electrodes) was used to measure the electric current. Measurements were performed when the conditions described above were reached. The saline solution and the sample were then saturated with nitrogen to remove the oxygen. After the oxygen was removed and the current was nearly zero, air was bubbled through a glass frit into the solution. The increase in electric current was observed as the oxygen molecules reacted with the cathode. The current was recorded until it reached a stationary state. For each reference material, four different thicknesses were tested; thicker samples were achieved by stacking individual samples [204]. The determined offset between measured and reference values was utilized for the correction of the oxygen permeability of the hydrogels. The electric current was measured for several sets of hydrogels at various concentrations and the oxygen permeability was calculated from the slope of the linear regression plot of the edge-corrected resistance (t/Dk) versus the sample thickness (t)

[207] and corrected using the calibration equation developed from the standard materials (Figure 7.1B and C). The above process was followed for all hydrogels and a minimum of four different thicknesses were tested.

7. 2. 3. Endotoxin evaluation

In order to assess the pyrogenicity of the regenerated cellulose-based hydrogels, samples were sent to Lonza Walkersville, Inc. (Walkersville, MD) for Kinetic-QCL® (KQCL) testing. The assays were conducted in adherence to USP <85> Bacterial Endotoxin Test and Lonza's Quality System requirements and included a β-G-Blocker. Testing was performed according to Lonza standard operating procedures (SOPs) 162.6 and 162.16.

The KQCL assay is a quantitative, kinetic assay for the detection of Gram negative bacterial endotoxin and is intended as an *in vitro* end-product endotoxin test for human medical devices, drugs and other biological products. Briefly, a sample is mixed with the Limulus Amebocyte Lysate (LAL)-chromogenic substrate reagent, placed in an incubating microplate reader, and automatically monitored over time for the appearance of a yellow color. The reaction time is inversely proportional to the amount of endotoxin present and the concentration of endotoxin in unknown samples can be calculated from a standard curve [208]. The β-G-Blocker blocks the reactivity of LAL to β-1,3-Glucans, conferring increased endotoxin specificity to the LAL test and is intended as an adjunct for the KQCL assay [209].

7. 2. 4. Contact lens geometry

In order to test the hydrogels for ocular applications, a method of molding the hydrogels with contact lens geometry was developed [210]. A metal contact lens mold

was fabricated using measurements for the mean radius of curvature of the rabbit cornea found in the literature (7.26 ± 0.26mm) [211] and a sample plastic optical contact lens mold (Eyegenix™).

7. 2. 5. Animals

A total of four 6–week old female Sprague-Dawley rats and four male New Zealand white rabbits, approximately 3.5 kg in weight, were used in this study. All experimental procedures were approved by the Institutional Animal Care and Use Committee at Johns Hopkins University (JHU IACUC) and Animal Care and Use Review Office (ACURO) at the US Army.

7. 2. 6. Rat subcutaneous implantation model

The rat subcutaneous implantation is a reliable animal model used to evaluate the biocompatibility, including immunogenicity and cytotoxicity, of biomaterials [212, 213]. Three different types of cellulose-based hydrogels (Avicel 101, bacterial, and MCC4) and a conventional balafilcon A contact lens (PureVision plus®, Bausch & Lomb, Rochester, NY) were implanted to the rat subcutaneously. Under inhalation anesthesia with isoflurane (Forane, Baxter, Deerfield, IL), the hair on the back was clipped and the skin disinfected with a povidone-iodine swap stick and 70% alcohol by turns three times. After applying a surgical drape, two 1.5-mm incisions were made on the back of rats. Blunt dissection was performed to undermine the skin and each of the three hydrogel samples (8 mm diameters) was implanted under the skin pocket created. The incision was closed by a 4-0 nylon suture and the rat was placed on a hot pack until fully recovered. Two rats were sacrificed at both 3 and 7 days after surgery and the implanted hydrogel sample and its surrounding tissue were collected under aseptic techniques. Sections (5-

μm) of dehydrated, paraffin-embedded specimens were stained with hematoxylin and eosin (H&E) according to standard methods.

7. 2. 7. Rabbit ocular irritation study

Owing to the specificity of ocular environments, an additional ocular biocompatibility study based on the ISO 9394 (Ophthalmic optics- contact lens and contact lens care products- Determination of biocompatibility by ocular study with rabbit eyes) procedure [214] was conducted with a modified abrasion test. All procedures follow the Association for Research in Vision and Ophthalmology (ARVO) Statement for the Use of Animals in Ophthalmic and Visual Research.

To ensure each rabbit eye was free from ocular irritation, three days before starting the test an initial ophthalmic examination was performed using a slit lamp. In addition, to minimize the dislocation over the daily treatment period, nictitating membrane fixation and contact lens fitting were performed. The nictitating membrane was fixed on the upper eyelid under general anesthesia with ketamine (15 mg/kg–body weight) and xylazine (3 mg/kg–body weight) administered intramuscularly. The lens fitting was conducted with a fluorescent dye. After applying the experimental and control contact lenses (Hydrokone®, Visionary Optics, Front Royal, VA) respectively, a few drops of fluorescein dye were administered and the corneas examined under blue light to assess the staining pattern. In addition, to evaluate the possibility of corneal damage by the contact lens, an abrasion test was followed for each animal. After applying the contact lens, the contact lens was rubbed in a circular fashion about fifty times, and fluorescein dye was used to determine the presence of any resulting corneal abrasion.

After three days, the ISO 9394 procedure was performed. The ISO 9394 is a standard biocompatibility test for the evaluation of both novel contact lens material and contact lens care products. By applying a device to the rabbit eyes daily over 22 days, the degree of ocular irritation was evaluated. The experimental hydrogel and the control contact lens were applied to the left (cellulose hydrogel) and right (control) eyes of the each rabbit for 7 hours per day. After applying the lenses for 7 hours, the contact lenses were cleaned and kept in conventional lens solution. All animals were monitored hourly for dislocation of the lens and any evidence of stress by examining their behavior. If a lens displaced during the treatment period, it was rinsed with a conventional lens solution and reapplied. The rabbit eyes were examined using a Draize scoring system daily just prior to lens removal. On days 8, 15, and 22 days after lens removal, using a slit lamp biomicroscope, an eye examination, including florescent dye staining, was performed and scored with the McDonald-Shadduck system [214].

After the eye examination on day 22, rabbits were sacrificed for pathological examination. In addition, for the positive control, four native adult rabbit cadaver eyes were obtained from Pel-freez biological (Rogers, AR). Sections (5 μm) of dehydrated, paraffin-embedded specimens were stained with hematoxylin and eosin (H&E), Masson's trichrome, and Periodic acid–Schiff (PAS) according to a previous study [215].

7. 3. Results and Discussion

7. 3. 1. Oxygen permeability of cellulose-based hydrogels

The cornea is avascular and depends on external oxygen sources for cellular respiration [203]. For awake humans, the main source of oxygen to the cornea is from the

atmosphere, whereas during sleep it is from the palpebral conjunctiva or back of the upper eyelid [203]. Metabolic changes in the corneal epithelium are induced if the cornea does not receive adequate oxygen. Therefore, contact lenses, particularly those worn overnight, need to have sufficient oxygen permeability. Researchers have proposed widely varying minimum transmissibility values for contact lenses to prevent corneal hypoxia and limit corneal edema, ranging from 15 to 125 barrer/cm [204]. The oxygen permeability of commercial contact lenses depends on the component materials, but is generally in the range of 26-175 barrer/cm, which provides enough oxygen to the cornea to prevent problems, depending on the wear duration [216].

The oxygen permeability of cellulose hydrogels prepared from varying concentrations (2 to 5%) of Avicel 101 crystalline cellulose was characterized along with hydrogels from 5% MCC4 and 0.5% BC (Table 7.2). The results suggest that as cellulose concentration increases, the oxygen permeability decreases. This is expected as the oxygen permeability is impacted by the water content of the hydrogels [217] and we previously showed that the water content of the cellulose hydrogels decreases with increasing cellulose concentration [218]. All the hydrogel samples were found to have oxygen permeability in the range of that of commercially available contact lenses (~55-115 barrer). The 95% confidence limits were likely impacted by thickness asymmetries in the individual hydrogel samples, which would lead to less precise thickness measurements for the Dk/t calculations as well as amplify the boundary effects during stacking of the thicker samples. In addition, the wide 95% confidence limits around the BC oxygen permeability were likely due to small remnants of the BC pellicle left behind

by the incomplete dissolution of the pellicle, which would have yielded less uniform BC hydrogels; similar results were observed with a second lot of BC hydrogels.

7. 3. 2. Endotoxin in cellulose materials

Endotoxin, a component of the cell wall in Gram-negative bacteria, can cause adverse reactions in humans if present in drugs or medical devices. The general U.S. Food and Drug Administration (FDA)–recommended limit for endotoxin in medical devices is <0.5 endotoxin units (EU)/mL (based on a 40-mL rinse) [219]. Endotoxin tests performed on the as-received cellulose starting materials and their resulting hydrogels by an accredited laboratory, Lonza Walkersville, Inc., showed that the plant-based cellulose starting materials have an acceptable level of endotoxin for medical devices (<0.5 EU/mL) (Figure 7.2); however, the endotoxin level of the resulting hydrogels from these materials was above the acceptable limit, though within a reasonable range for *in vivo* testing [220].

It was hypothesized that handling of the hydrogels during synthesis was introducing endotoxins and that making small improvements to the synthesis procedures would reduce the endotoxin levels. Thus, important changes were made to the synthesis procedure: 1) use of depyrogenated glassware; 2) use of sterile, filtered deionized water (0.2-μm filter); and, 3) use of a laminar flow hood. These simple changes resulted in a 95% reduction in endotoxin level compared with the original hydrogel preparation. Further reduction to acceptable levels (Figure 7.2) was achieved by implementing aseptic cell culture techniques [221].

The hypothesis that unsterile handling of the hydrogels was causing increased endotoxin levels was tested after each modification to the synthesis procedure using hydrogels prepared from Avicel 101. Since the endotoxin levels decreased with each

synthesis modification, it was inferred that handling was the dependent variable and that the endotoxin level of the hydrogels was independent of cellulose type, so further endotoxin testing was not done for the other plant-based materials.

For the bacterial cellulose, the endotoxin level of the hydrogel (108 EU/mL) was lower than the level for the as-received pellicle (354 EU/mL). It was hypothesized that the incomplete removal of the cellulose generating bacteria was the cause. Additional washing procedures were implemented for the BC pellicle [222-224], which succeeded in lowering the endotoxin level of the starting material by 90% (34.6 EU/mL). Though not below the <0.5 EU/mL threshold, it was within a reasonable range to continue with *in vivo* testing [220] given the trend of the hydrogel having lower endotoxin levels than the starting material, along with the improved endotoxin levels for the plant-based cellulose hydrogels after implementation of aseptic handling procedures described above. Additional techniques to reduce the endotoxin levels will be explored for any future testing with BC hydrogels.

7. 3. 3. Rat subcutaneous implantation model

The implants all showed acute inflammation with increased number of immune cells at the 3- and 7-day time points (Figure 7.3). In addition, inflammation surrounding cellulose implants was more severe than that of conventional contact lenses soon after implantation, but less severe than the contact lens group at day 7. This suggests that all cellulose implants cause a moderate acute immune response but are tolerated by the host tissue over time. When compared to the conventional contact lens, all three types of cellulose showed acceptable biocompatibility.

7. 3. 4. Contact lens geometry and rabbit ocular irritation study

Based on the high oxygen permeability (Table 7.2), acceptable endotoxin level, and *in vivo* biocompatibility results, Avicel 101 was selected as the cellulose source for the hydrogel lenses. Contact lens–shaped hydrogels were successfully prepared from a 5% Avicel 101 solution, using modified aseptic synthesis procedures described above, and a lens-shaped mold (Figure 7.4A). Preliminary fit tests were done using an adult rabbit cadaver eye and showed that the geometry of the lens was appropriate for further *in vivo* testing (Figure 7.4B).

Owing to the specificity of the ocular environment, the degree of ocular irritation in rabbits was investigated according to ISO #9394. An initial ophthalmic examination showed all eyes were clear of ophthalmic problems. It has been well established that poor fitting contact lenses cause irritation, discomfort, decreased contact lens stability, and could be associated with ocular problems, including limbal hyperemia and corneal staining [225]. Because poor lens fitting could distort the results of the irritation study, creating a contact lens which fits the contour of rabbit cornea was essential. The shaping procedures developed during this work successfully generated cellulose contact lenses with curvature corresponding to the contour of rabbit cornea, as did the control contact lens. The fitting test with fluorescein dye proved that both control and experimental contact lenses had proper curvature without any lifting areas or bubbles under the contact lens (Figure 7.4C).

Cellulose contact lenses did not cause corneal abrasion, as indicated by corneal staining with fluorescein (Figure 7.4D and E). During the irritation study with ISO 9394, the rate of lens retention, i.e., no dislocation during the 7 hour application time was 90.9% for cellulose contact lenses and 68.1% for control lenses. The McDonald-Shadduck

scores for slit lamp biomicroscopy are presented in Table 7.3. Despite some mild symptoms, all eyes were within normal variations (Figure 7.4F). No serious lesions, including corneal ulcer, corneal haze, conjunctival chemosis, aqueous flare, or iris lesions were found in either group. Throughout the study, only mild (Score 1 out of 4 on Draize scale) conjunctival redness (Figure 7.4G) and ocular discharge (Figure 7.4H) were found in the gross ocular examination. However, the cellulose contact lens groups showed redness and discharge more frequently than the control group (Table 7.4).

The pathological examinations confirmed mild irritation caused by both the control and experimental contact lenses. There was no evidence of an inflammatory response or toxic effects in either the experimental or control corneas. Additionally, Masson's trichrome and PAS staining proved corneas from both groups did not include scar tissue formation in the stromal layer and there was no abnormal glycogen metabolism around the corneal epithelium (Figure 7.5). However, five to seven layers of moderate hypertonic epithelium, representing irritation of the corneal surface, were found in the cellulose contact lens group, whereas four to five layers of mild hypertonic epithelium were found in the control group (Figure 7.5). This may have been a function of the cellulose lens fitting too tightly against the corneal surface, something that could be easily corrected.

7. 4. Conclusions

Cellulose hydrogels with optimized material properties, including high oxygen permeability and low endotoxin levels, were synthesized using aseptic methods. In rats, the hydrogels were biocompatible. Cellulose hydrogels with contact lens geometry were

successfully tested *in vivo* and showed no evidence of material toxicity after daily wear for 22 days. Although further refinements to the contact lens fit will be needed to reduce irritation and redness, we have established biocompatibility of the cellulose hydrogels. Future investigations will be twofold. First, while BC does not seem ideal for ocular wear at this time, given its healing benefits, additional synthesis options will be investigated in attempts to optimize the oxygen permeability and other properties for this application. Second, the healing efficacy of the cellulose hydrogels will be studied; if healing efficacy is shown, cellulose hydrogels have the potential to not only be used as a bandage material, but may provide a platform for drug delivery, which has been challenging with currently used contact lens materials [226].

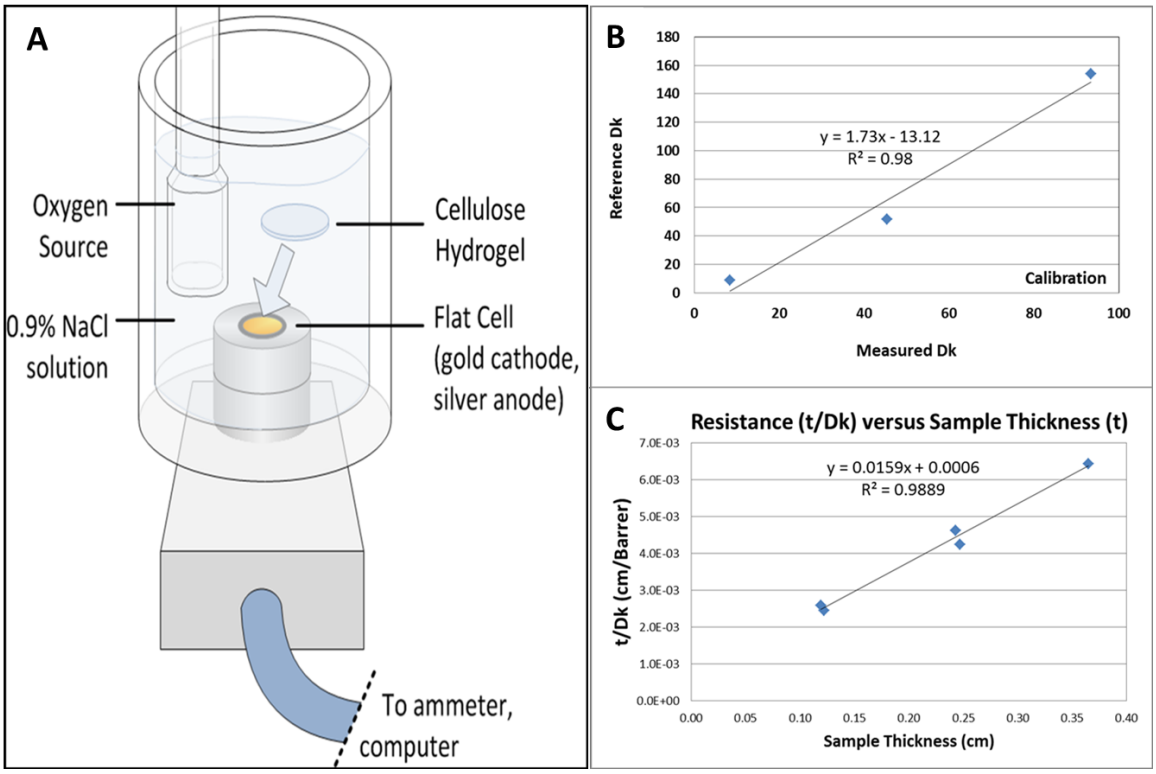

Figure 7. 1. Oxygen permeability measurements. A) Diagram of the polarographic cell used with components labeled. B) Best fit linear equation derived from the measured and established standard Dk values of the rigid gas permeable reference materials from which the oxygen permeability of the samples was calibrated. C) Representative best fit linear regression plot of the edge-corrected resistance (t/Dk) versus sample thickness (t) from which the oxygen permeability of cellulose-based hydrogels was derived.

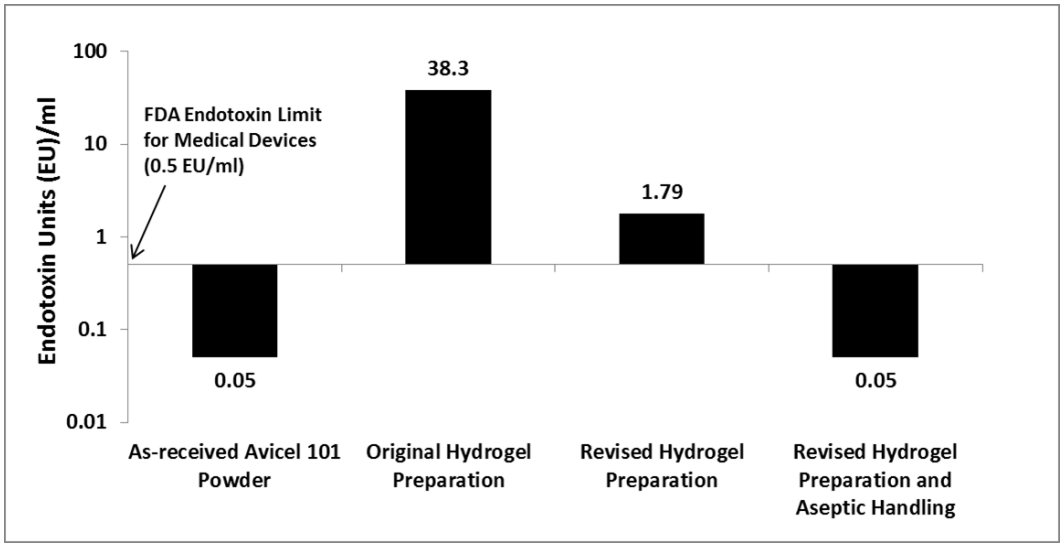

Figure 7. 2. Bacterial endotoxin level for cellulose-based hydrogels. Data are from Avicel 101 at different preparations, showing the decrease in endotoxin level after revising the synthesis protocol (n = 1).

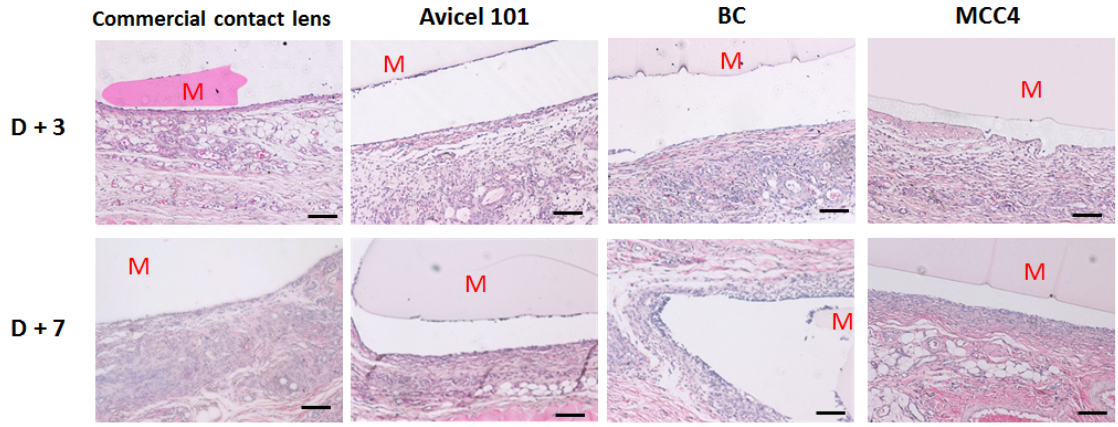

Figure 7. 3. Pathological examination of material implanted rats. Images of H&E-stained implants and surrounding tissue are shown. Commercial balafilcon A contact lens, Avicel 101, BC, and MCC4 hydrogels were implanted and analyzed 3 days (D + 3) and 7 days (D + 7) later. M: area of material. Scale bars: 100 μm.

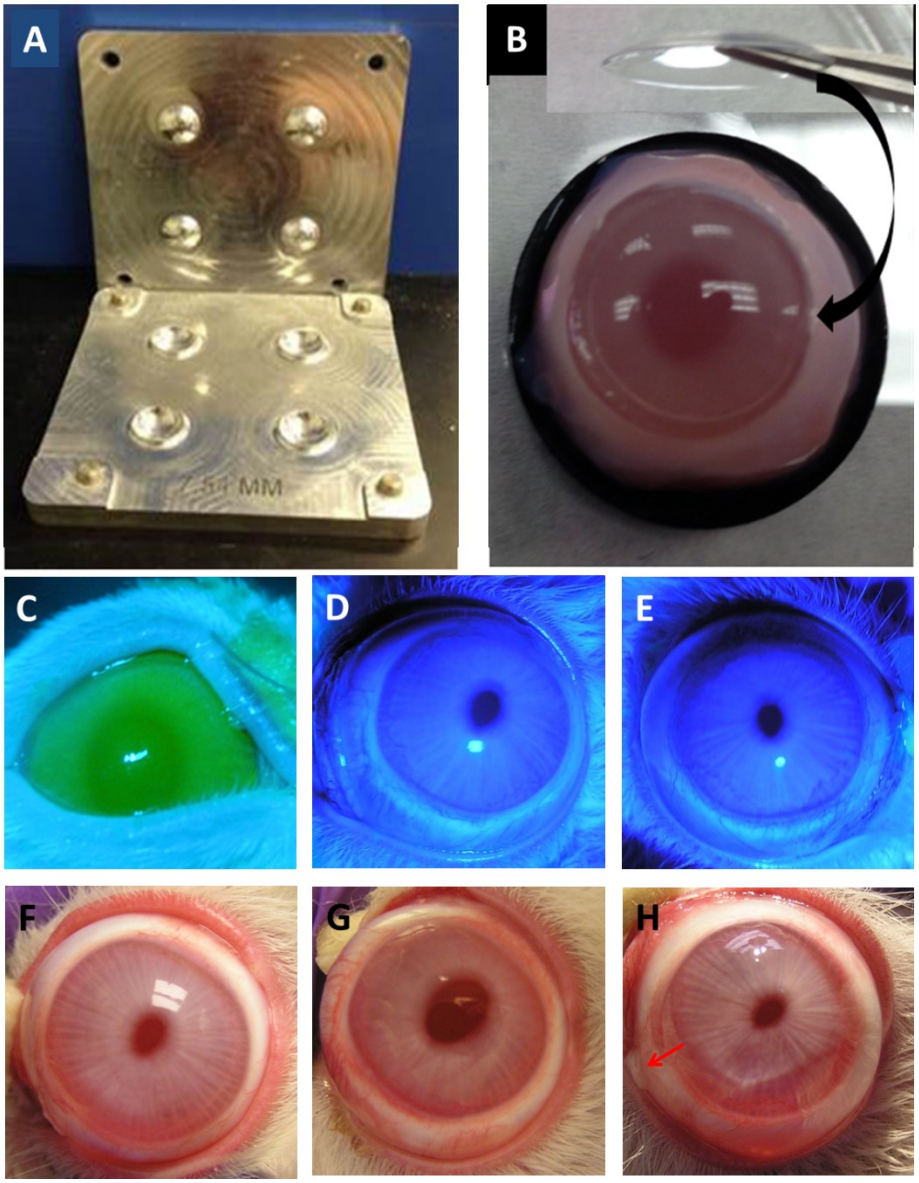

Figure 7. 4. Hydrogels with contact lens geometry and *in vivo* ocular irritation study. A) Contact lens shaped mold. B) Contact lens hydrogel fit-tested using a cadaver rabbit eye. C) Contact lens hydrogel fit-tested in live rabbit. D) & F) Abrasion test of the cellulose hydrogel lens (D) and control (E). F) – H) Representative pictures of rabbit eyes in the cellulose contact lens group with no lesions (F) and mild conjuctival redness (G) without the cellulose contact lens, and mild ocular discharge (H) denoted by red arrow with the cellulose contact lens.

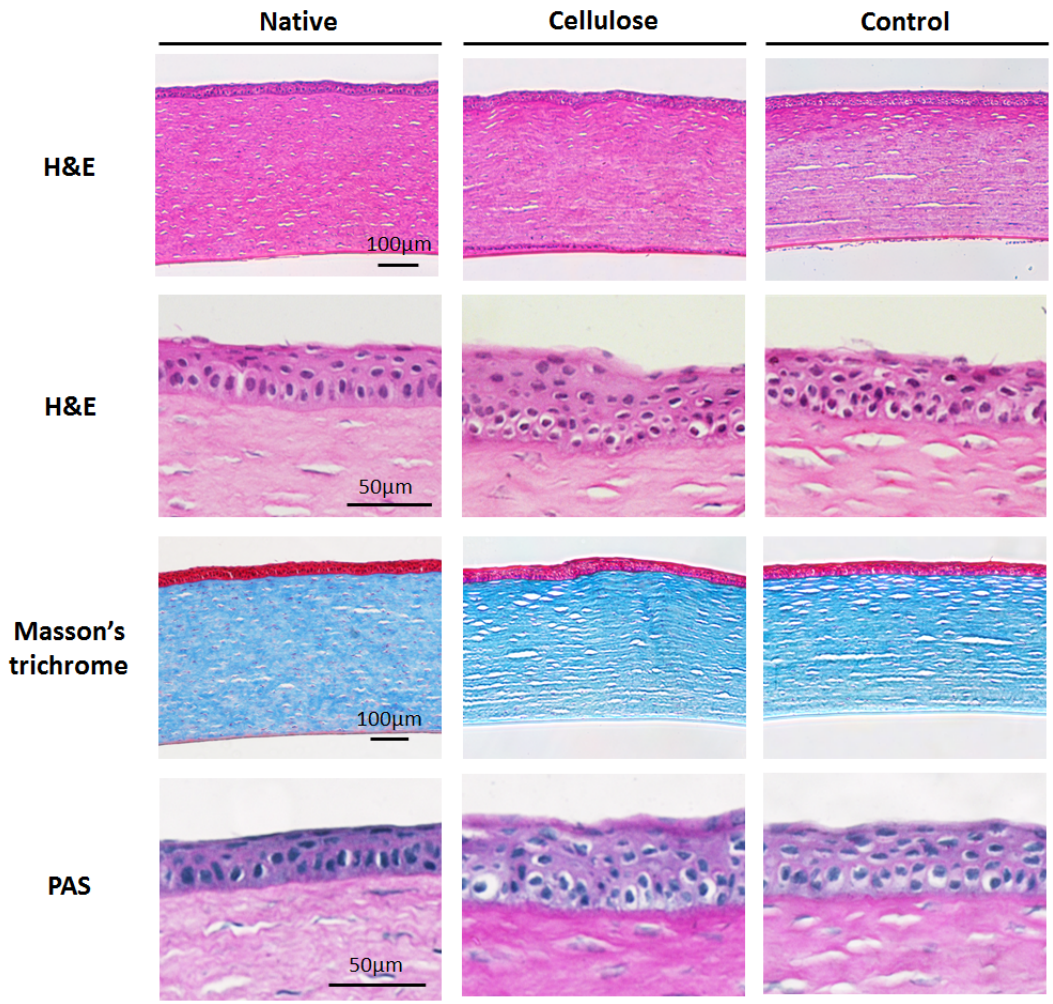

Figure 7. 5. Pathological examination for the native cornea, cellulose-derived and conventional contact lens (control) applied corneas. Tissues were stained with H&E, Masson's trichrome, and Periodic acid–Schiff (PAS).

Table 7. 1. Oxygen permeability measured for rigid gas permeable reference materials. The permeability values (Dk) are the inversion of the slope from the corresponding edge-corrected resistance (t/Dk) versus sample thickness (t) linear regression plot of the number of thicknesses tested (N) for each material. The measured Dk was plotted against the established Dk value[206] and used to develop the calibration curve shown in Figure 7.1B.

Material	Number of Thicknesses Tested (N)	Measured Oxygen Permeability (Dk)	Established Oxygen Permeability (Dk)
Silafocon A	4	8.3	8.8
Itafluorofocon A	4	45.4	51.8
Tisilfocon A	4	93.4	154

Table 7. 2. Oxygen permeability and confidence limits for regenerated cellulose hydrogels. The permeability values (Dk) are the inversion of the slope from the corresponding edge-corrected resistance (t/Dk) versus sample thickness (t) linear regression plot of the number of thicknesses tested (N) for each material. The confidence limits were derived from ±2 standard deviations surrounding the slope of the regression line (as shown in Figure 7.1C).

Material	Number of Thicknesses Tested (N)	Corrected, Calibrated Oxygen Permeability (Dk)	95% Confidence Limits
2% Avicel 101	4	115.2	92.6 - 150.5
3% Avicel 101	5	101.8	98.5 - 105.2
5% Avicel 101	5	95.9	83.9 - 111.1
5% MCC4	4	86.0	71.3 - 107.1
0.5% BC	5	54.9	27.0 - 206.2

Table 7. 3. Ophthalmic observation by slit lamp biomicroscopy with the McDonald-Shadduck score system. Data reported are the number of eyes that present ocular lesion (i.e. either conjuctival congestion or discharge) on day 8, 15 and 22 (n=4 per group). Except mild conjunctival congestion and discharge, other responses were not found.

Response	Day	Cellulose group (number of eyes)	Control group) (number of eyes)
Conjunctival congestion (Score 1)	8	1	2
	15	4	0
	22	1	0
Conjunctival discharge (Score 1)	8	2	2
	15	3	1
	22	1	1

Table 7. 4. Gross ocular observation by the Draize Scale. Data presented are the frequency of finding for eye responses (conjunctival redness and discharges) for 22 days (n=4 per group). Except conjunctival redness and discharge, other responses were not found during the experiment.

Response	Cellulose group (times for 22 days)	Control group (times for 22 days)
Conjunctival redness (Score 1)	32	13
Conjunctival discharge (Score 1)	56	25

Bibliography

1. Ruberti JW, Roy AS, Roberts CJ. Corneal biomechanics and biomaterials. *Annu Rev Biomed Eng*. 2011; 13: 269-295.
2. Hendrix DVH. Canine conjuntiva and nictitating membrane. In: *Veterinary Ophthalmology*. (ed. Gelatt KM). 4th ed. Blackwell: Ames, Iowa, 2007; 675.
3. Hanna C, Bicknell DS, O'Brien JE. Cell turnover in the adult human eye. *Arch Ophthalmol*. 1961; 65: 695-698.
4. Wiley L, SundarRaj N, Sun TT, Thoft RA. Regional heterogeneity in human corneal and limbal epithelia: an immunohistochemical evaluation. *Invest Ophthalmol Vis Sci*. 1991; 32: 594-602.
5. Tseng SC. Concept and application of limbal stem cells. *Eye (Lond)*. 1989; 3 (Pt 2): 141-157.
6. Li W, Hayashida Y, Chen YT, Tseng SC. Niche regulation of corneal epithelial stem cells at the limbus. *Cell Res*. 2007; 17: 26-36.
7. DelMonte DW, Kim T. Anatomy and physiology of the cornea. *J Cataract Refract Surg*. 2011; 37: 588-598.
8. Dyrlund TF, Poulsen ET, Scavenius C, Nikolajsen CL, Thogersen IB, Vorum H, Enghild JJ. Human cornea proteome: identification and quantitation of the proteins of the three main layers including epithelium, stroma, and endothelium. *J Proteome Res*. 2012; 11: 4231-4239.
9. Boote C, Dennis S, Newton RH, Puri H, Meek KM. Collagen fibrils appear more closely packed in the prepupillary cornea: optical and biomechanical implications. *Invest Ophthalmol Vis Sci*. 2003; 44: 2941-2948.
10. Maurice DM. The transparency of the corneal stroma. *Vision Res*. 1970; 10: 107-108.
11. Jester JV, Petroll WM, Cavanagh HD. Corneal stromal wound healing in refractive surgery: the role of myofibroblasts. *Prog Retin Eye Res*. 1999; 18: 311-356.
12. Samuelson D. Ophthalmic anatomy. In: *Veterinary Ophthalmology*. (ed. Gelatt KM). 4th ed. Blackwell: Ames, Iowa, 2007; 37.
13. Watsky MA, McDermott ML, Edelhauser HF. In vitro corneal endothelial permeability in rabbit and human: the effects of age, cataract surgery and diabetes. *Exp Eye Res*. 1989; 49: 751-767.
14. Stiemke MM, Edelhauser HF, Geroski DH. The developing corneal endothelium: correlation of morphology, hydration and Na/K ATPase pump site density. *Current Eye Research*. 1991; 10: 145-156.
15. Geroski DH, Matsuda M, Yee RW, Edelhauser HF. Pump function of the human corneal endothelium. Effects of age and cornea guttata. *Ophthalmology*. 1985; 92: 759-763.
16. Tuft SJ, Coster DJ. The corneal endothelium. *Eye (Lond)*. 1990; 4 (Pt 3): 389-424.
17. Yee RW, Matsuda M, Schultz RO, Edelhauser HF. Changes in the normal corneal endothelial cellular pattern as a function of age. *Current Eye Research*. 1985; 4: 671-678.
18. Kraljevic Pavelic S, Klobucar M, Sedic M, Micek V, Gehrig P, Grossman J, Pavelic K, Vojnikovic B. UV-induced retinal proteome changes in the rat model of age-related macular degeneration. *Biochim Biophys Acta*. 2015; 1852: 1833-1845.

19. Marshall J. Radiation and the ageing eye. *Ophthalmic Physiol Opt*. 1985; 5: 241-263.
20. Muller LJ, Pels E, Vrensen GF. The specific architecture of the anterior stroma accounts for maintenance of corneal curvature. *Br J Ophthalmol*. 2001; 85: 437-443.
21. Carroll JP. On emmetropization. *J Theor Biol*. 1982; 95: 135-144.
22. Grosvenor T. Reduction in axial length with age: an emmetropizing mechanism for the adult eye? *Am J Optom Physiol Opt*. 1987; 64: 657-663.
23. Richdale K, Bullimore MA, Sinnott LT, Zadnik K. The Effect of Age, Accommodation, and Refractive Error on the Adult Human Eye. *Optom Vis Sci*. 2016; 93: 3-11.
24. Griffith M, Harkin DG. Recent advances in the design of artificial corneas. *Curr Opin Ophthalmol*. 2014; 25: 240-247.
25. Tan DT, Dart JK, Holland EJ, Kinoshita S. Corneal transplantation. *Lancet*. 2012; 379: 1749-1761.
26. Burton MJ. Trachoma: an overview. *Br Med Bull*. 2007; 84: 99-116.
27. Grunauer-Kloevekorn C, Duncker GI. [Keratoconus: epidemiology, risk factors and diagnosis]. *Klin Monbl Augenheilkd*. 2006; 223: 493-502.
28. Kelliher C, Chakravarti S, Vij N, Mazur S, Stahl PJ, Engler C, Matthaei M, Yu SM, Jun AS. A cellular model for the investigation of Fuchs' endothelial corneal dystrophy. *Exp Eye Res*. 2011; 93: 880-888.
29. Alldredge OC, Krachmer JH. Clinical types of corneal transplant rejection. Their manifestations, frequency, preoperative correlates, and treatment. *Arch Ophthalmol*. 1981; 99: 599-604.
30. Carlsson DJ, Li F, Shimmura S, Griffith M. Bioengineered corneas: how close are we? *Curr Opin Ophthalmol*. 2003; 14: 192-197.
31. Espandar L, Carlson AN. Lamellar keratoplasty: a literature review. *J Ophthalmol*. 2013; 2013: 894319.
32. Armitage WJ, Dick AD, Bourne WM. Predicting endothelial cell loss and long-term corneal graft survival. *Invest Ophthalmol Vis Sci*. 2003; 44: 3326-3331.
33. Patel SV, Hodge DO, Bourne WM. Corneal endothelium and postoperative outcomes 15 years after penetrating keratoplasty. *Trans Am Ophthalmol Soc*. 2004; 102: 57-65; discussion 65-56.
34. Price MO, Gorovoy M, Benetz BA, Price FW, Jr., Menegay HJ, Debanne SM, Lass JH. Descemet's stripping automated endothelial keratoplasty outcomes compared with penetrating keratoplasty from the Cornea Donor Study. *Ophthalmology*. 2010; 117: 438-444.
35. Terry MA. Endothelial keratoplasty: history, current state, and future directions. *Cornea*. 2006; 25: 873-878.
36. Gomaa A, Comyn O, Liu C. Keratoprostheses in clinical practice - a review. *Clin Experiment Ophthalmol*. 2010; 38: 211-224.
37. Ruberti JW, Zieske JD. Prelude to corneal tissue engineering - gaining control of collagen organization. *Prog Retin Eye Res*. 2008; 27: 549-577.
38. Khan B, Dudenhoefer EJ, Dohlman CH. Keratoprosthesis: an update. *Curr Opin Ophthalmol*. 2001; 12: 282-287.
39. Aquavella JV, Qian Y, McCormick GJ, Palakuru JR. Keratoprosthesis: the Dohlman-Doane device. *Am J Ophthalmol*. 2005; 140: 1032-1038.

40. Yaghouti F, Nouri M, Abad JC, Power WJ, Doane MG, Dohlman CH. Keratoprosthesis: preoperative prognostic categories. *Cornea*. 2001; 20: 19-23.
41. Strampelli B, Valvo A, Tusa E. [Osteo-odonto-keratoprosthesis in a case treated for anchylobepharon and total simbleraphon]. *Ann Ottalmol Clin Ocul*. 1965; 91: 462-479.
42. Michael R, Charoenrook V, de la Paz MF, Hitzl W, Temprano J, Barraquer RI. Long-term functional and anatomical results of osteo- and osteoodonto-keratoprosthesis. *Graefes Arch Clin Exp Ophthalmol*. 2008; 246: 1133-1137.
43. Falcinelli G, Falsini B, Taloni M, Colliardo P, Falcinelli G. Modified osteo-odonto-keratoprosthesis for treatment of corneal blindness: long-term anatomical and functional outcomes in 181 cases. *Arch Ophthalmol*. 2005; 123: 1319-1329.
44. Hicks C, Crawford G, Chirila T, Wiffen S, Vijayasekaran S, Lou X, Fitton J, Maley M, Clayton A, Dalton P, Platten S, Ziegelaar B, Hong Y, Russo A, Constable I. Development and clinical assessment of an artificial cornea. *Prog Retin Eye Res*. 2000; 19: 149-170.
45. Jiraskova N, Rozsival P, Burova M, Kalfertova M. AlphaCor artificial cornea: clinical outcome. *Eye (Lond)*. 2011; 25: 1138-1146.
46. Griffith M, Jackson WB, Lagali N, Merrett K, Li F, Fagerholm P. Artificial corneas: a regenerative medicine approach. *Eye (Lond)*. 2009; 23: 1985-1989.
47. Fagerholm P, Lagali NS, Merrett K, Jackson WB, Munger R, Liu Y, Polarek JW, Soderqvist M, Griffith M. A biosynthetic alternative to human donor tissue for inducing corneal regeneration: 24-month follow-up of a phase 1 clinical study. *Sci Transl Med*. 2010; 2: 46ra61.
48. Takezawa T, Ozaki K, Nitani A, Takabayashi C, Shimo-Oka T. Collagen vitrigel: a novel scaffold that can facilitate a three-dimensional culture for reconstructing organoids. *Cell Transplant*. 2004; 13: 463-473.
49. Takezawa T, Nishikawa K, Wang PC. Development of a human corneal epithelium model utilizing a collagen vitrigel membrane and the changes of its barrier function induced by exposing eye irritant chemicals. *Toxicol In Vitro*. 2011; 25: 1237-1241.
50. Guo Q, Phillip JM, Majumdar S, Wu PH, Chen J, Calderon-Colon X, Schein O, Smith BJ, Trexler MM, Wirtz D, Elisseeff JH. Modulation of keratocyte phenotype by collagen fibril nanoarchitecture in membranes for corneal repair. *Biomaterials*. 2013; 34: 9365-9372.
51. McIntosh Ambrose W, Salahuddin A, So S, Ng S, Ponce Marquez S, Takezawa T, Schein O, Elisseeff J. Collagen Vitrigel membranes for the in vitro reconstruction of separate corneal epithelial, stromal, and endothelial cell layers. *J Biomed Mater Res B Appl Biomater*. 2009; 90: 818-831.
52. Kim MK, Wee WR, Park CG, Kim SJ. Xenocorneal transplantation. *Curr Opin Organ Transplant*. 2011; 16: 231-236.
53. Badylak SF, Taylor D, Uygun K. Whole-organ tissue engineering: decellularization and recellularization of three-dimensional matrix scaffolds. *Annu Rev Biomed Eng*. 2011; 13: 27-53.
54. Mendelson K, Schoen FJ. Heart valve tissue engineering: concepts, approaches, progress, and challenges. *Ann Biomed Eng*. 2006; 34: 1799-1819.

55. Pang K, Du L, Wu X. A rabbit anterior cornea replacement derived from acellular porcine cornea matrix, epithelial cells and keratocytes. *Biomaterials*. 2010; 31: 7257-7265.
56. Fu Y, Fan X, Chen P, Shao C, Lu W. Reconstruction of a tissue-engineered cornea with porcine corneal acellular matrix as the scaffold. *Cells Tissues Organs*. 2010; 191: 193-202.
57. Gonzalez-Andrades M, de la Cruz Cardona J, Ionescu AM, Campos A, Del Mar Perez M, Alaminos M. Generation of bioengineered corneas with decellularized xenografts and human keratocytes. *Invest Ophthalmol Vis Sci*. 2011; 52: 215-222.
58. Oh JY, Kim MK, Lee HJ, Ko JH, Wee WR, Lee JH. Processing porcine cornea for biomedical applications. *Tissue Eng Part C Methods*. 2009; 15: 635-645.
59. Sasaki S, Funamoto S, Hashimoto Y, Kimura T, Honda T, Hattori S, Kobayashi H, Kishida A, Mochizuki M. In vivo evaluation of a novel scaffold for artificial corneas prepared by using ultrahigh hydrostatic pressure to decellularize porcine corneas. *Mol Vis*. 2009; 15: 2022-2028.
60. Hashimoto Y, Funamoto S, Sasaki S, Honda T, Hattori S, Nam K, Kimura T, Mochizuki M, Fujisato T, Kobayashi H, Kishida A. Preparation and characterization of decellularized cornea using high-hydrostatic pressurization for corneal tissue engineering. *Biomaterials*. 2010; 31: 3941-3948.
61. Ponce Marquez S, Martinez VS, McIntosh Ambrose W, Wang J, Gantxegui NG, Schein O, Elisseeff J. Decellularization of bovine corneas for tissue engineering applications. *Acta Biomater*. 2009; 5: 1839-1847.
62. Choi HJ, Kim MK, Lee HJ, Ko JH, Jeong SH, Lee JI, Oh BC, Kang HJ, Wee WR. Efficacy of pig-to-rhesus lamellar corneal xenotransplantation. *Invest Ophthalmol Vis Sci*. 2011; 52: 6643-6650.
63. Daoud YJ, Smith R, Smith T, Akpek EK, Ward DE, Stark WJ. The intraoperative impression and postoperative outcomes of gamma-irradiated corneas in corneal and glaucoma patch surgery. *Cornea*. 2011; 30: 1387-1391.
64. Chae JJ, Choi JS, Lee JD, Lu Q, Stark WJ, Kuo IC, Elisseeff JH. Physical and Biological Characterization of the Gamma-Irradiated Human Cornea. *Cornea*. 2015; 34: 1287-1294.
65. Oelkera AM, Grinstaff MW. Ophthalmic adhesives: a materials chemistry perspective. *J Mater Chem*. 2008; 18: 2521-2536.
66. Peng HT, Shek PN. Novel wound sealants: biomaterials and applications. *Expert Rev Med Devices*. 2010; 7: 639-659.
67. Chan SM, Boisjoly H. Advances in the use of adhesives in ophthalmology. *Curr Opin Ophthalmol*. 2004; 15: 305-310.
68. Kumar N, Al Sabti K. Fibrin glue in ophthalmology. *Indian J Ophthalmol*. 2010; 58: 176.
69. Grinstaff MW. Designing hydrogel adhesives for corneal wound repair. *Biomaterials*. 2007; 28: 5205-5214.
70. Reyes JM, Herretes S, Pirouzmanesh A, Wang DA, Elisseeff JH, Jun A, McDonnell PJ, Chuck RS, Behrens A. A modified chondroitin sulfate aldehyde adhesive for sealing corneal incisions. *Invest Ophthalmol Vis Sci*. 2005; 46: 1247-1250.

71. Strehin I, Ambrose WM, Schein O, Salahuddin A, Elisseeff J. Synthesis and characterization of a chondroitin sulfate-polyethylene glycol corneal adhesive. *J Cataract Refract Surg*. 2009; 35: 567-576.
72. Chae JJ, Mulreany DG, Guo Q, Lu Q, Choi JS, Strehin I, Espinoza FA, Schein O, Trexler MM, Bower KS, Elisseeff JH. Application of a collagen-based membrane and chondroitin sulfate-based hydrogel adhesive for the potential repair of severe ocular surface injuries. *Mil Med*. 2014; 179: 686-694.
73. Mader TH, Carroll RD, Slade CS, George RK, Ritchey JP, Neville SP. Ocular war injuries of the Iraqi Insurgency, January-September 2004. *Ophthalmology*. 2006; 113: 97-104.
74. Thach AB, Johnson AJ, Carroll RB, Huchun A, Ainbinder DJ, Stutzman RD, Blaydon SM, Demartelaere SL, Mader TH, Slade CS, George RK, Ritchey JP, Barnes SD, Fannin LA. Severe eye injuries in the war in Iraq, 2003-2005. *Ophthalmology*. 2008; 115: 377-382.
75. Blanch RJ, Scott RA. Military ocular injury: presentation, assessment and management. *J R Army Med Corps*. 2009; 155: 279-284.
76. Thomas R, McManus JG, Johnson A, Mayer P, Wade C, Holcomb JB. Ocular Injury Reduction From Ocular Protection Use in Current Combat Operations. *J Trauma*. 2009; 66: S99-S103.
77. Johnson AJ. Eye trauma management - OIF clinical considerations. *J Trauma*. 2007; 62: S20.
78. Weichel ED, Colyer MH. Combat ocular trauma and systemic injury. *Curr Opin Ophthalmol*. 2008; 19: 519-525.
79. Mansour AM, Hamade H, Ghaddar A, Mokadem AS, El Hajj Ali M, Awwad S. Cluster bomb ocular injuries. *Middle East Afr J Ophthalmol*. 2012; 19: 153-157.
80. Bhatia SS. Ocular surface sealants and adhesives. *Ocul Surf*. 2006; 4: 146-154.
81. Byun YS, Kim MS. Superimposed fungal ulcer after fibrin glue sealant in infectious corneal ulcer. *Korean J Ophthalmol*. 2011; 25: 447-450.
82. Berdahl JP, Johnson CS, Proia AD, Grinstaff MW, Kim T. Comparison of sutures and dendritic polymer adhesives for corneal laceration repair in an in vivo chicken model. *Arch Ophthalmol*. 2009; 127: 442-447.
83. Noguera G, Lee WS, Castro-Combs J, Chuck RS, Soltz B, Soltz R, Behrens A. Novel laser-activated solder for sealing corneal wounds. *Invest Ophthalmol Vis Sci*. 2007; 48: 1038-1042.
84. Rossi F, Matteini P, Ratto F, Menabuoni L, Lenzetti I, Pini R. Laser tissue welding in ophthalmic surgery. *J Biophotonics*. 2008; 1: 331-342.
85. Guo Q, Aly A, Schein O, Trexler MM, Elisseeff JH. Moxifloxacin in situ gelling microparticles–bioadhesive delivery system. *Results in Pharma Sciences*. 2012; 2: 66–71.
86. Strehin I, Nahas Z, Arora K, Nguyen T, Elisseeff J. A versatile pH sensitive chondroitin sulfate-PEG tissue adhesive and hydrogel. *Biomaterials*. 2010; 31: 2788-2797.
87. Takezawa T, Ozaki K, Nitani A, Takabayashi C, Shimo-Oka T. Collagen vitrigel: A novel scaffold that can facilitate a three-dimensional culture for reconstructing organoids. *Cell Transplantation*. 2004; 13: 463-473.
88. Calderon-Colon X, Xia Z, Breidenich JL, Mulreany DG, Guo Q, Uy OM, Tiffany JE, Freund DE, McCally RL, Schein OD, Elisseeff JH, Trexler MM. Structure and

properties of collagen vitrigel membranes for ocular repair and regeneration applications. *Biomaterials*. 2012; 33: 8286-8295.
89. Bartholomew LR, Pang DX, Sam DA, Cavender JC. Ultrasound biomicroscopy of globes from young adult pigs. *Am J Vet Res*. 1997; 58: 942-948.
90. McMenamin PG, Steptoe RJ. Normal anatomy of the aqueous humour outflow system in the domestic pig eye. *J Anat*. 1991; 178: 65-77.
91. Li B, Brown KV, Wenke JC, Guelcher SA. Sustained release of vancomycin from polyurethane scaffolds inhibits infection of bone wounds in a rat femoral segmental defect model. *J Control Release*. 2010; 145: 221-230.
92. Hilber D, Mitchener TA, Stout J, Hatch B, Canham-Chervak M. Eye injury surveillance in the U.S. Department of Defense, 1996-2005. *Am J Prev Med*. 2010; 38: S78-85.
93. Weichel ED, Colyer MH, Ludlow SE, Bower KS, Eiseman AS. Combat ocular trauma visual outcomes during operations iraqi and enduring freedom. *Ophthalmology*. 2008; 115: 2235-2245.
94. Sharma A, Kaur R, Kumar S, Gupta P, Pandav S, Patnaik B, Gupta A. Fibrin glue versus N-butyl-2-cyanoacrylate in corneal perforations. *Ophthalmology*. 2003; 110: 291-298.
95. Krachmer JH, Mannis MJ, Holland EJ. Cornea. In: *Surgical Management and Rehabilitation of Anterior Segment Trauma*. (ed. Macsai MS). 3rd ed. Mosby: Philadelphia, 2005; 1655-1669.
96. Grau AE, Duran JA. Treatment of a Large Corneal Perforation With a Multilayer of Amniotic Membrane and TachoSil. *Cornea*. 2012; 31: 98-100.
97. Sharma A, Mohan K, Nirankari VS. Management of nontraumatic corneal perforation with tectonic drape patch and cyanoacrylate glue. *Cornea*. 2012; 31: 465-466.
98. Khalifa YM, Bailony MR, Bloomer MM, Killingsworth D, Jeng BH. Management of nontraumatic corneal perforation with tectonic drape patch and cyanoacrylate glue. *Cornea*. 2010; 29: 1173-1175.
99. Su CY, Lin CP. Combined use of an amniotic membrane and tissue adhesive in treating corneal perforation: A case report. *Ophthalmic Surg Lasers*. 2000; 31: 151-154.
100. Kim HK, Park HS. Fibrin glue-assisted augmented amniotic membrane transplantation for the treatment of large noninfectious corneal perforations. *Cornea*. 2009; 28: 170-176.
101. Griffith M, Harkin DG. Recent advances in the design of artificial corneas. *Current Opinion in Ophthalmology*. 2014; 25: 240-247.
102. Garg P, Krishna PV, Stratis AK, Gopinathan U. The value of corneal transplantation in reducing blindness. *Eye (Lond)*. 2005; 19: 1106-1114.
103. Ritterband DC, Shah MK, Meskin SW, Shapiro DE, Seedor JA, Koplin RS, Hu DN, Shao S, Dahl P, McCormick S. Efficacy and safety of moxifloxacin as an additive in Optisol-GS a preservation medium for corneal donor tissue. *Cornea*. 2006; 25: 1084-1089.
104. Stevenson W, Cheng SF, Emami-Naeini P, Hua J, Paschalis EI, Dana R, Saban DR. Gamma-irradiation reduces the allogenicity of donor corneas. *Invest Ophthalmol Vis Sci*. 2012; 53: 7151-7158.
105. Utine CA, Tzu JH, Akpek EK. Lamellar Keratoplasty Using Gamma-Irradiated Corneal Lenticules. *American Journal of Ophthalmology*. 2011; 151: 170-174.

106. Nikolaeva SS, Kondakova NV, Khoroshkov Iu A, Dubinskaia VA, Koroleva OA. [Effect of ionizing radiation on the structure of the collagen fibers of human tendons]. *Radiobiologiia*. 1988; 28: 483-488.
107. Russell NA, Pelletier MH, Bruce WJ, Walsh WR. The effect of gamma irradiation on the anisotropy of bovine cortical bone. *Med Eng Phys*. 2012; 34: 1117-1122.
108. McDonald AA, Kunz MD, McLoon LK. Dystrophic Changes in Extraocular Muscles after Gamma Irradiation in mdx:utrophin(+/-) Mice. *Plos One*. 2014; 9.
109. Maslennikova A, Kochueva M, Ignatieva N, Vitkin A, Zakharkina O, Kamensky V, Sergeeva E, Kiseleva E, Bagratashvili V. Effects of gamma irradiation on collagen damage and remodeling. *Int J Radiat Biol*. 2015; 91: 240-247.
110. Shah NB, Wolkers WF, Morrissey M, Sun WQ, Bischof JC. Fourier Transform Infrared Spectroscopy Investigation of Native Tissue Matrix Modifications Using a Gamma Irradiation Process. *Tissue Engineering Part C-Methods*. 2009; 15: 33-40.
111. Gouk SS, Lim TM, Teoh SH, Sun WQ. Alterations of human acellular tissue matrix by gamma irradiation: Histology, biomechanical property, stability, in vitro cell repopulation, and remodeling. *Journal of Biomedical Materials Research Part B-Applied Biomaterials*. 2008; 84B: 205-217.
112. Aquino KAS. Sterilization by Gamma Irradiation. In: *Gamma Radiation*. (ed. Feriz A). InTech: Rijeka, Croatia, 2012; 171-206.
113. Bowes JH, Moss JA. The effect of gamma radiation on collagen. *Radiation Research*. 1962; 16: 211-223.
114. Bailey AJ, Rhodes DN, Cater CW. Irradiation-Induced Crosslinking of Collagen. *Radiation Research*. 1964; 22: 606-621.
115. Karring H, Thogersen I, Klintworth G, Moller-Pedersen T, Enghild J. The human cornea proteome: Bioinformatic analyses indicate import of plasma proteins into the cornea. *Molecular Vision*. 2006; 12: 451-460.
116. Sikder S, McCally RL, Engler C, Ward D, Jun AS. Evaluation of Irradiated Corneas Using Scatterometry and Light and Electron Microscopy. *Cornea*. 2011; 30: 503-507.
117. Calhoun WR, Akpek EK, Weiblinger R, Ilev IK. Evaluation of Broadband Spectral Transmission Characteristics of Fresh and Gamma-Irradiated Corneal Tissues. *Cornea*. 2015; 34: 228-234.
118. Doughty MJ. Averaged Spacing and 2-D Organization of Collagen Fibrils in the Posterior Cornea of the Rabbit Eye Assessed by Transmission Electron Microscopy. *Curr Eye Res*. 2014; 39: 329-339.
119. Wu I, Nahas Z, Kimmerling KA, Rosson GD, Elisseeff JH. An injectable adipose matrix for soft-tissue reconstruction. *Plast Reconstr Surg*. 2012; 129: 1247-1257.
120. Charulatha V, Rajaram A. Influence of different crosslinking treatments on the physical properties of collagen membranes. *Biomaterials*. 2003; 24: 759-767.
121. Wollensak G, Aurich H, Pham DT, Wirbelauer C. Hydration behavior of porcine cornea crosslinked with riboflavin and ultraviolet A. *J Cataract Refract Surg*. 2007; 33: 516-521.
122. Wollensak G, Spoerl E, Seiler T. Stress-strain measurements of human and porcine corneas after riboflavin-ultraviolet-A-induced cross-linking. *Journal of Cataract and Refractive Surgery*. 2003; 29: 1780-1785.

123. Kohlhaas M, Spoerl E, Schilde T, Unger G, Wittig C, Pillunat LE. Biomechanical evidence of the distribution of cross-links in corneas treated with riboflavin and ultraviolet A light. *Journal of Cataract and Refractive Surgery*. 2006; 32: 279-283.
124. Buehler MJ. Nanomechanics of collagen fibrils under varying cross-link densities: atomistic and continuum studies. *J Mech Behav Biomed Mater*. 2008; 1: 59-67.
125. Ignati'eva NY, Danilov NA, Lunin VV, Obrezkova MV, Averkiev SV, I. CT. Alteration of the Thermodynamic Characteristics of Corneal Collagen Denaturation as a Result of Nonenzymatic Glycation. *Moscow Univ Chem Bull*. 2006; 62: 63–66.
126. Rufer F, Schroder A, Bader C, Erb C. Age-related changes in central and peripheral corneal thickness: determination of normal values with the Orbscan II topography system. *Cornea*. 2007; 26: 1-5.
127. Boote C, Dennis S, Newton RH, Puri H, Meek KM. Collagen fibrils appear more closely packed in the prepupillary cornea: Optical and biomechanical implications. *Investigative Ophthalmology & Visual Science*. 2003; 44: 2941-2948.
128. Boote C, Kamma-Lorger CS, Hayes S, Harris J, Burghammer M, Hiller J, Terrill NJ, Meek KM. Quantification of Collagen Organization in the Peripheral Human Cornea at Micron-Scale Resolution. *Biophysical Journal*. 2011; 101: 33-42.
129. Kikkawa Y, Hirayama K. Uneven swelling of the corneal stroma. *Invest Ophthalmol*. 1970; 9: 735-741.
130. Freund DE, Mccally RL, Farrell RA, Cristol SM, Lhernault NL, Edelhauser HF. Ultrastructure in Anterior and Posterior Stroma of Perfused Human and Rabbit Corneas - Relation to Transparency. *Investigative Ophthalmology & Visual Science*. 1995; 36: 1508-1523.
131. Oelker AM, Grinstaff MW. Synthesis, Characterization, and In Vitro Evaluation of a Hydrogel-Based Corneal Onlay. *IEEE Trans Nanobioscience*. 2012; 11: 37-45.
132. Chae JJ, Ambrose WM, Espinoza FA, Mulreany DG, Ng S, Takezawa T, Trexler MM, Schein OD, Chuck RS, Elisseeff JH. Regeneration of corneal epithelium utilizing a collagen vitrigel membrane in rabbit models for corneal stromal wound and limbal stem cell deficiency. *Acta Ophthalmol*. 2015; 93: e57-66.
133. Yokomise H, Inui K, Wada H, Goh T, Yagi K, Hitomi S, Takahashi M. High-dose irradiation prevents rejection of canine tracheal allografts. *J Thorac Cardiovasc Surg*. 1994; 107: 1391-1397.
134. Ishii KJ, Akira S. Innate immune recognition of, and regulation by, DNA. *Trends Immunol*. 2006; 27: 525-532.
135. Takaoka A, Wang Z, Choi MK, Yanai H, Negishi H, Ban T, Lu Y, Miyagishi M, Kodama T, Honda K, Ohba Y, Taniguchi T. DAI (DLM-1/ZBP1) is a cytosolic DNA sensor and an activator of innate immune response. *Nature*. 2007; 448: 501-505.
136. Jeng BH. Preserving the cornea: corneal storage media. *Current Opinion in Ophthalmology*. 2006; 17: 332-337.
137. Alldredge OC, Krachmer JH. Clinical Types of Corneal Transplant Rejection - Their Manifestations, Frequency, Preoperative Correlates, and Treatment. *Archives of Ophthalmology*. 1981; 99: 599-604.
138. Hicks CR, Crawford GJ, Lou X, Tan DT, Snibson GR, Sutton G, Downie N, Werner L, Chirila TV, Constable IJ. Corneal replacement using a synthetic hydrogel cornea, AlphaCor (TM) device, preliminary outcomes and complications. *Eye*. 2003; 17: 385-392.

139. Chow CC, Kulkarni AD, Albert DM, Darlington JK, Hardten DR. Clinicopathologic correlation of explanted AlphaCor artificial cornea after exposure of implant. *Cornea*. 2007; 26: 1004-1007.
140. Avadhanam VS, Smith HE, Liu C. Keratoprostheses for corneal blindness: a review of contemporary devices. *Clin Ophthalmol*. 2015; 9: 697-720.
141. Liu W, Merrett K, Griffith M, Fagerholm P, Dravida S, Heyne B, Scaiano JC, Watsky MA, Shinozaki N, Lagali N, Munger R, Li F. Recombinant human collagen for tissue engineered corneal substitutes. *Biomaterials*. 2008; 29: 1147-1158.
142. Vrana NE, Builles N, Justin V, Bednarz J, Pellegrini G, Ferrari B, Damour O, Hulmes DJ, Hasirci V. Development of a reconstructed cornea from collagen-chondroitin sulfate foams and human cell cultures. *Invest Ophthalmol Vis Sci*. 2008; 49: 5325-5331.
143. Lawrence BD, Marchant JK, Pindrus MA, Omenetto FG, Kaplan DL. Silk film biomaterials for cornea tissue engineering. *Biomaterials*. 2009; 30: 1299-1308.
144. Merna N, Fung KM, Wang JJ, King CR, Hansen KC, Christman KL, George SC. Differential beta3 Integrin Expression Regulates the Response of Human Lung and Cardiac Fibroblasts to Extracellular Matrix and Its Components. *Tissue Eng Part A*. 2015; 21: 2195-2205.
145. Kim MK, Oh JY, Lee HI, Ko JH, Lee HJ, Lee JH, Wee WR. Susceptibility of porcine keratocytes to immune-mediated damage in xeno-related rejection. *Transplant Proc*. 2008; 40: 564-569.
146. Hashimoto Y, Funamoto S, Sasaki S, Negishi J, Honda T, Hattori S, Nam K, Kimura T, Mochizuki M, Kobayashi H, Kishida A. Corneal Regeneration by Deep Anterior Lamellar Keratoplasty (DALK) Using Decellularized Corneal Matrix. *Plos One*. 2015; 10.
147. Du L, Wu X, Pang K, Yang Y. Histological evaluation and biomechanical characterisation of an acellular porcine cornea scaffold. *Br J Ophthalmol*. 2011; 95: 410-414.
148. Guo QY, Phillip JM, Majumdar S, Wu PH, Chen JS, Calderon-Colon X, Schein O, Smith BJ, Trexler MM, Wirtz D, Elisseeff JH. Modulation of keratocyte phenotype by collagen fibril nanoarchitecture in membranes for corneal repair. *Biomaterials*. 2013; 34: 9365-9372.
149. Coburn JM, Bernstein N, Bhattacharya R, Aich U, Yarema KJ, Elisseeff JH. Differential Response of Chondrocytes and Chondrogenic-Induced Mesenchymal Stem Cells to C1-OH Tributanoylated N-Acetylhexosamines. *Plos One*. 2013; 8.
150. Garavito RM. Detergents and lipids as tools for handling integral membrane proteins. *Abstracts of Papers of the American Chemical Society*. 2005; 229: U717-U717.
151. Fu Y, Fan XQ, Chen P, Shao CY, Lu WJ. Reconstruction of a Tissue-Engineered Cornea with Porcine Corneal Acellular Matrix as the Scaffold. *Cells Tissues Organs*. 2010; 191: 193-202.
152. Lynch AP, Ahearne M. Strategies for developing decellularized corneal scaffolds. *Exp Eye Res*. 2013; 108: 42-47.
153. Shao Y, Quyang L, Zhou Y, Tang J, Tan Y, Liu Q, Lin Z, Yin T, Qiu F, Liu Z. Preparation and physical properties of a novel biocompatible porcine corneal acellularized matrix. *In Vitro Cell Dev Biol Anim*. 2010; 46: 600-605.

154. Shafiq MA, Gemeinhart RA, Yue BY, Djalilian AR. Decellularized human cornea for reconstructing the corneal epithelium and anterior stroma. *Tissue Eng Part C Methods*. 2012; 18: 340-348.
155. Gui L, Chan SA, Breuer CK, Niklason LE. Novel utilization of serum in tissue decellularization. *Tissue Eng Part C Methods*. 2010; 16: 173-184.
156. Tanaka Y, Kubota A, Yokokura S, Uematsu M, Shi D, Yamato M, Okano T, Quantock AJ, Nishida K. Optical mechanical refinement of human amniotic membrane by dehydration and cross-linking. *J Tissue Eng Regen Med*. 2012; 6: 731-737.
157. Zucker BB. Hydration and transparency of corneal stroma. *Arch Ophthalmol*. 1966; 75: 228-231.
158. Griffith M, Hakim M, Shimmura S, Watsky MA, Li F, Carlsson D, Doillon CJ, Nakamura M, Suuronen E, Shinozaki N, Nakata K, Sheardown H. Artificial human corneas: scaffolds for transplantation and host regeneration. *Cornea*. 2002; 21: S54-61.
159. Majumdar S, Guo Q, Garza-Madrid M, Calderon-Colon X, Duan D, Carbajal P, Schein O, Trexler M, Elisseeff J. Influence of collagen source on fibrillar architecture and properties of vitrified collagen membranes. *J Biomed Mater Res B Appl Biomater*. 2016; 104: 300-307.
160. Fitton JH, Ziegelaar BW, Hicks CR, Clayton AB, Crawford GJ, Constable IJ, Chirila TV. Assessment of anticollagenase treatments after insertion of a keratoprosthetic material in the rabbit cornea. *Cornea*. 1998; 17: 108-114.
161. Ljubimov AV, Saghizadeh M. Progress in corneal wound healing. *Prog Retin Eye Res*. 2015; 49: 17-45.
162. Spoerl E, Wollensak G, Seiler T. Increased resistance of crosslinked cornea against enzymatic digestion. *Current Eye Research*. 2004; 29: 35-40.
163. Choi JS, Williams JK, Greven M, Walter KA, Laber PW, Khang G, Soker S. Bioengineering endothelialized neo-corneas using donor-derived corneal endothelial cells and decellularized corneal stroma. *Biomaterials*. 2010; 31: 6738-6745.
164. Jester JV, Petroll WM, Cavanagh HD. Corneal stromal wound healing in refractive surgery: the role of myofibroblasts. *Prog Retin Eye Res*. 1999; 18: 311-356.
165. Ioannidis JP. Extrapolating from animals to humans. *Sci Transl Med*. 2012; 4: 151ps115.
166. Umeda Y, Nakamura S, Fujiki K, Toshida H, Saito A, Murakami A. Distribution of goblet cells and MUC5AC mRNA in the canine nictitating membrane. *Exp Eye Res*. 2010; 91: 721-726.
167. McCanna DJ, Driot JY, Hartsook R, Ward KW. Rabbit models of contact lens-associated corneal hypoxia: a review of the literature. *Eye Contact Lens*. 2008; 34: 160-165.
168. Helper LC, Magrane WG, Koehm J, Johnson R. Surgical induction of keratoconjunctivitis sicca in the dog. *J Am Vet Med Assoc*. 1974; 165: 172-174.
169. Barabino S, Chen Y, Chauhan S, Dana R. Ocular surface immunity: homeostatic mechanisms and their disruption in dry eye disease. *Prog Retin Eye Res*. 2012; 31: 271-285.
170. Li L, Ren DH, Ladage PM, Yamamoto K, Petroll WM, Jester JV, Cavanagh HD. Annexin V binding to rabbit corneal epithelial cells following overnight contact lens wear or eyelid closure. *CLAO J*. 2002; 28: 48-54.

171. Efron N, Carney LG. Oxygen levels beneath the closed eyelid. *Invest Ophthalmol Vis Sci*. 1979; 18: 93-95.
172. Yamamoto K, Ladage PM, Ren DH, Li L, Petroll WM, Jester JV, Cavanagh HD. Effect of eyelid closure and overnight contact lens wear on viability of surface epithelial cells in rabbit cornea. *Cornea*. 2002; 21: 85-90.
173. Robertson DM, Zhu M, Wu YC, Cavanagh HD. Hypoxia-induced downregulation of DeltaNp63alpha in the corneal epithelium. *Eye Contact Lens*. 2012; 38: 214-221.
174. Park SA, Lee I, Lee YL, Jeong MB, Kim WT, Kim SE, Park YW, Seo KM. Combination auriculopalpebral nerve block and local anesthesia for placement of a nictitating membrane-to-superotemporal bulbar conjunctiva flap in dogs. *J Am Anim Hosp Assoc*. 2009; 45: 164-167.
175. Maitchouk DY, Beuerman RW, Ohta T, Stern M, Varnell RJ. Tear production after unilateral removal of the main lacrimal gland in squirrel monkeys. *Arch Ophthalmol*. 2000; 118: 246-252.
176. Sapienza JS, Mayordomo A, Beyer AM. Suture anchor placement technique around the insertion of the ventral rectus muscle for the replacement of the prolapsed gland of the third eyelid in dogs: 100 dogs. *Veterinary Ophthalmology*. 2014; 17: 81-86.
177. McLaughlin SA, Brightman AH, 2nd, Helper LC, Primm ND, Brown MG, Greeley S. Effect of removal of lacrimal and third eyelid glands on Schirmer tear test results in cats. *J Am Vet Med Assoc*. 1988; 193: 820-822.
178. Ladage PM, Ren DH, Petroll WM, Jester JV, Bergmanson JP, Cavanagh HD. Effects of eyelid closure and disposable and silicone hydrogel extended contact lens wear on rabbit corneal epithelial proliferation. *Invest Ophthalmol Vis Sci*. 2003; 44: 1843-1849.
179. Carvalho IM, Marques CS, Oliveira RS, Coelho PB, Costa PC, Ferreira DC. Sustained drug release by contact lenses for glaucoma treatment-a review. *J Control Release*. 2015; 202: 76-82.
180. Grinninger P, Verbruggen AMJ, Kraijer-Huver IMG, Djajadiningrat-Laanen SC, Teske E, Boeve MH. Use of bandage contact lenses for treatment of spontaneous chronic corneal epithelial defects in dogs. *Journal of Small Animal Practice*. 2015; 56: 446-449.
181. Patchan M, Graham JL, Xia Z, Maranchi JP, McCally R, Schein O, Elisseeff JH, Trexler MM. Synthesis and properties of regenerated cellulose-based hydrogels with high strength and transparency for potential use as an ocular bandage. *Mater Sci Eng C Mater Biol Appl*. 2013; 33: 3069-3076.
182. Menghini M, Knecht PB, Kaufmann C, Kovacs R, Watson SL, Landau K, Bosch MM. Treatment of traumatic corneal abrasions: a three-arm, prospective, randomized study. *Ophthalmic Res*. 2013; 50: 13-18.
183. Petersen N, Gatenholm P. Bacterial cellulose-based materials and medical devices: current state and perspectives. *Applied Microbiology and Biotechnology*. 2011; 91: 1277-1286.
184. Klemm D, Heublein B, Fink H-P, Bohn A. Cellulose: Fascinating Biopolymer and Sustainable Raw Material. *Angewandte Chemie International Edition*. 2005; 44: 3358-3393.
185. Thoorens G, Krier F, Leclercq B, Carlin B, Evrard B. Microcrystalline cellulose, a direct compression binder in a quality by design environment—A review. *International Journal of Pharmaceutics*. 2014; 473: 64-72.

186. Simmons PA, Donshik PC, Kelly WF, Vehige JG. Conditioning of hydrogel lenses by a multipurpose solution containing an ocular lubricant. *Clao J*. 2001; 27: 192-194.
187. Okan D, Woo K, Ayello EA, Sibbald G. The role of moisture balance in wound healing. *Adv Skin Wound Care*. 2007; 20: 39-53.
188. Sibbald RG, Elliott JA, Ayello EA, Somayaji R. Optimizing the Moisture Management Tightrope with Wound Bed Preparation 2015(c). *Adv Skin Wound Care*. 2015; 28: 466-476.
189. Tammelin T, Abburi R, Gestranius M, Laine C, Setala H, Osterberg M. Correlation between cellulose thin film supramolecular structures and interactions with water. *Soft Matter*. 2015; 11: 4273-4282.
190. She Y, Li J, Xiao B, Lu H, Liu H, Simmons PA, Vehige JG, Chen W. Evaluation of a Novel Artificial Tear in the Prevention and Treatment of Dry Eye in an Animal Model. *J Ocul Pharmacol Ther*. 2015; 31: 31.
191. Czaja W, Krystynowicz A, Bielecki S, Brown RM, Jr. Microbial cellulose--the natural power to heal wounds. *Biomaterials*. 2006; 27: 145-151.
192. Pal K, Banthia AK, Majumdar DK. Polymeric Hydrogels: Characterization and Biomedical Applications. *Designed Monomers and Polymers*. 2009; 12: 197-220.
193. Chang C, Zhang L. Cellulose-based hydrogels: Present status and application prospects. *Carbohydrate Polymers*. 2011; 84: 40-53.
194. Oprea A-M, Ciolacu D, Neamtu A, Mungiu O, Stoica B, Vasile C. Cellulose/Chondroitin Sulfate Hydrogels: Synthesis, Drug Loading/Release Properties, and Biocompatibility. *Cellulose Chemistry and Technology*. 2010; 44: 369-378.
195. Lacin NT. Development of biodegradable antibacterial cellulose based hydrogel membranes for wound healing. *Int J Biol Macromol*. 2014; 67: 22-27.
196. Ballios Brian G, Cooke Michael J, Donaldson L, Coles Brenda LK, Morshead Cindi M, van der Kooy D, Shoichet Molly S. A Hyaluronan-Based Injectable Hydrogel Improves the Survival and Integration of Stem Cell Progeny following Transplantation. *Stem Cell Reports*.
197. Frankel V, Serafica G, Damien C. Development and testing of a novel biosynthesized XCell for treating chronic wounds. *Surg Technol Int*. 2004; 12: 27-33.
198. Klemm D, Schumann D, Udhardt U, Marsch S. Bacterial synthesized cellulose - artificial blood vessels for microsurgery. *Progress in Polymer Science*. 2001; 26: 1561-1603.
199. Svensson A, Nicklasson E, Harrah T, Panilaitis B, Kaplan DL, Brittberg M, Gatenholm P. Bacterial cellulose as a potential scaffold for tissue engineering of cartilage. *Biomaterials*. 2005; 26: 419-431.
200. Gulrez SKH, Phillips GO, Al-Assaf S. *Hydrogels: Methods of Preparation, Characterisation and Applications* INTECH Open Access Publisher, 2011.
201. Helenius G, Backdahl H, Bodin A, Nannmark U, Gatenholm P, Risberg B. In vivo biocompatibility of bacterial cellulose. *J Biomed Mater Res A*. 2006; 76: 431-438.
202. Miyamoto T, Takahashi S, Ito H, Inagaki H, Noishiki Y. Tissue biocompatibility of cellulose and its derivatives. *J Biomed Mater Res*. 1989; 23: 125-133.
203. Chhabra M, Prausnitz JM, Radke CJ. Polarographic Method for Measuring Oxygen Diffusivity and Solubility in Water-Saturated Polymer Films: Application to

Hypertransmissible Soft Contact Lenses. *Industrial & Engineering Chemistry Research*. 2008; 47: 3540-3550.
204. Gonzalez-Meijome JM, Compañ-Moreno V, Riande E. Determination of Oxygen Permeability in Soft Contact Lenses Using a Polarographic Method: Estimation of Relevant Physiological Parameters. *Industrial & Engineering Chemistry Research*. 2008; 47: 3619-3629.
205. Hadassah J, Sehgal PK. A novel method to measure oxygen permeability and transmissibility of contact lenses. *Clin Exp Optom*. 2006; 89: 374-380.
206. ANSI. Z80.20 - for Ophthalmics In: - *Contact Lenses - Standard Terminology, Tolerances, Measurements, and Physicochemical Properties* American National Standards Institute, 2004.
207. Benjamin WJ, Cappelli QA. Oxygen permeability (Dk) of thirty-seven rigid contact lens materials. *Optom Vis Sci*. 2002; 79: 103-111.
208. Lonza Walkersville I. Limulus Amebocyte Lysate (LAL) Kinetic-QCLÔ Product Guide. 2014.
209. Lonza Walkersville I. B-G-Blocker Product Guide. 2014.
210. Trexler MM, Graham JL, Breidenich JL, Maranchi JP, Patrone JB, Patchan MW, Elisseeff JH, Calderon-Colon X. Cellulose-Based Hydrogels and Methods of Making Thereof. Google Patents, 2013.
211. Bozkir G, Bozkir M, Dogan H, Aycan K, Guler B. Measurements of axial length and radius of corneal curvature in the rabbit eye. *Acta Med Okayama*. 1997; 51: 9-11.
212. Olsson B, Sliwkowski A, Langeland K. Subcutaneous implantation for the biological evaluation of endodontic materials. *J Endod*. 1981; 7: 355-367.
213. Macleod TM, Williams G, Sanders R, Green CJ. Histological evaluation of Permacol as a subcutaneous implant over a 20-week period in the rat model. *Br J Plast Surg*. 2005; 58: 518-532.
214. ISO 9394. Ophthalmic Optics - Contact Lenses and Contact Lens Care Products-Determination of Biocompatibility by Ocular Study Using Rabbit Eyes. In: *International Organization for Standardization*. Geneva, Switzerland, 2012.
215. Matsubara M, Kamei Y, Takeda S, Mukai K, Ishii Y, Ito S. Histologic and histochemical changes in rabbit cornea produced by an orthokeratology lens. *Eye Contact Lens*. 2004; 30: 198-204; discussion 205-196.
216. French K. Contact lens material properties: part 3. Oxygen performance. *Optician*. 2005; 230: 16-21.
217. EFRON N, MORGAN PB, CAMERON ID, BRENNAN NA, GOODWIN M. Oxygen Permeability and Water Content of Silicone Hydrogel Contact Lens Materials. *Optometry & Vision Science*. 2007; 84: E328-E337.
218. Xia Z, Patchan M, Maranchi J, Elisseeff J, Trexler M. Determination of crosslinking density of hydrogels prepared from microcrystalline cellulose. *Journal of Applied Polymer Science*. 2013; 127: 4537-4541.
219. USFDA. Guidance for Industry Pyrogen and Endotoxins Testing. June 2012.
220. Malyala P, Singh M. Endotoxin limits in formulations for preclinical research. *J Pharm Sci*. 2008; 97: 2041-2044.
221. Coté RJ. Aseptic Technique for Cell Culture. In: *Current Protocols in Cell Biology*. John Wiley & Sons, Inc., 2001.

222. Gao C, Wan Y, Lei X, Qu J, Yan T, Dai K. Polylysine coated bacterial cellulose nanofibers as novel templates for bone-like apatite deposition. *Cellulose*. 2011; 18: 1555-1561.
223. Li Y, Tian C, Tian H, Zhang J, He X, Ping W, Lei H. Improvement of bacterial cellulose production by manipulating the metabolic pathways in which ethanol and sodium citrate involved. *Applied Microbiology and Biotechnology*. 2012; 96: 1479-1487.
224. Zhijiang C, Guang Y. Bacterial cellulose/collagen composite: Characterization and first evaluation of cytocompatibility. *Journal of Applied Polymer Science*. 2011; 120: 2938-2944.
225. Belda-Salmeron L, Drew T, Hall L, Wolffsohn JS. Objective analysis of contact lens fit. *Cont Lens Anterior Eye*. 2015; 38: 163-167.
226. Guzman-Aranguez A, Colligris B, Pintor J. Contact lenses: promising devices for ocular drug delivery. *J Ocul Pharmacol Ther*. 2013; 29: 189-199.

Curriculum Vitae

DATE OF BIRTH: January 8th, 1977

PLACE OF BIRTH: Seoul, Republic of Korea

EDUCATIONAL BACKGROWND

Feb 2016	**Ph.D. Biomedical Engineering**, Johns Hopkins University School of Medicine
2008	**M.S. Veterinary Surgery**, Seoul National University, Seoul, Korea
1999	**D.V.M. Veterinary Medicine**, Konkuk University, Seoul, Korea

RESEARCH EXPERIENCE

Sep.09 ~ Feb 16	**Fellow / Research assistant,** Johns Hopkins University, MD, Baltimore
	Mentor: Jennifer Elisseeff, Ph. D.
	Development of corneal equivalents with tissue engineering approaches
	Evaluations of biomaterials using animal models
Mar.08 ~ Sep.09	**Fellow,** Wilmer Eye Institute, MD, Baltimore
	Mentor: Roy S. Chuck M.D., Ph. D.
	Investigation of pathological mechanism of dry eye syndrome using a Botulinum toxin B-induced murine model
	Evaluation of redox state for cultured human corneal endothelial cells
Sep.05 ~ Feb.08	**Research assistant,** Seoul National University, Seoul, Korea
	Mentor: Kangmoon Seo, D.V.M., Ph. D.
	Establishment of clinical criteria for veterinary ophthalmic practice
	Conduction of veterinary clinical trails for biomaterials.
Oct.96 ~ Sep.98	**Undergraduate student researcher,** Konkuk University, Seoul, Korea
	Mentor: Jin-Suk Kim, D.V.M., Ph. D.
	Evaluation of melatonin's effects in the neurotoxicity of methyl-mercury

WORKING EXPERIENCE

May.05~Feb.08	**Veterinary surgeon** (specialty: Veterinary ophthalmology) Section of surgery and ophthalmology, Veterinary teaching hospital at Seoul National University, Seoul, Korea
Sep.99~ Aug.04	**Veterinary officer** (Captain) Army, Korean National defense, Korea United nation army, United Nation Mission supporting East-Timor (UNMSET), East-Timor (2002/2 – 2002/10)

TEACHING EXPERIENCE

Fall 2013	**Tissue engineering,** Johns Hopkins University, MD, Baltimore
Spring 2014	**Molecular and cell biology,** Johns Hopkins University, MD, Baltimore

SELECTED PROFICIENCIES

Selected Laboratory skill: Corneal cell culture (Limbal stem cell, Epithelial cell, Keratocyte, Endothelial cell), Gene work (PCR, RT-PCR, electrophoresis), Pathological work (chemical staining, Immunohistochemistry), Animal surgery (soft tissue, orthopedic, thoracic and ophthalmic surgery) and anesthesia (large animal, rodent, carnivore and non-human primate), Physicomechanial work (differential scanning calorimetry, rheometer, compressive modulus test)

ORGANIZATIONS AND MEMBERSHIP

2008 - Present	Association for research in vision and ophthalmology (ARVO)

HONORS AND AWARDS

May. 2010	Mok-Am scientific foundation scholarship
Apr. 2008	Wilmer research association, Wilmer research grant
Feb. 2002	Military prize from Chief of General Staff in Korea Medal of honor - Peace Keeping Operation (Korean Army) Medal of peace (United Nation)

Mar 1998 KonKuk memorial Scholarship (scholarship tenure: 1998 ~ 1999)

Mar 1995 KonKuk foundation Scholarship (scholarship tenure: 1995 ~ 1997)

PUBLICATIONS (*co-first author)

Published:

1. Kim C*, Jeon OH*, Kim DH, Chae JJ, Shores L, Bernstein N, Bhattacharya R, Coburn JM, Yarema KJ, Elisseeff JH (2016), Local delivery of a carbohydrate analog for reducing arthritic inflammation and rebuilding cartilage, Biomaterials, 83 (3): 93–101

2. Patchan MW*, **Chae JJ***, Lee JD, Calderon-Colon X, Maranchi JP, McCally RL, Schein OD, Elisseeff JH, Trexler MM (2015), Evaluation of the biocompatibility of regenerated cellulose hydrogels with high strength and transparency for ocular applications, Journal of Biomaterials Applications, In press

3. **Chae JJ**, Choi Lee JD, Lu Q, Stark WJ, Kuo IC, MD, Elisseeff JH (2015), Physical and biological characterization of the gamma-irradiated human cornea, Corne, 34 (10): 1287-1294

4. **Chae JJ***, McIntosh Ambrose W*, Espinoza FA, Mulreany DG, Ng S, Takezawa T, Trexler MM, Schein OD, Chuck RS, Elisseeff JH (2015), Regeneration of Corneal Epithelium Utilizing a Collagen Vitrigel Membrane in Rabbit Models for Corneal Stromal Wound and Limbal Stem Cell Deficiency. Acta ophthalmologica, 93 (1): e57-66

5. Zhou H, Lu Q, Guo Q, Chae JJ, Fan X, Elissseeff JH, Grant MP (2014). Vitrified collagen-based conjunctival equivalent for ocular surface reconstruction. Biomaterial, 35 (26): 7398-406

6. **Chae JJ**, Mulreany DG, Guo Q, Lu Q, Choi JS, Strehin I, Espinoza FA, Schein OD, Trexler MM, Bower KS, Elisseeff JH (2014). Application of a Collagen-Based Membrane and Chondroitin Sulfate-Based Hydrogel Adhesive for the Potential Repair of Severe Ocular Surface Injuries. Mil Med, 179 (6): 686–694

7. Condé-Green A, Wu I, Graham I, Chae JJ, Drachenberg CB, Singh DP, Holton L 3rd, Slezak S, Elisseeff J (2013). Comparison of 3 Techniques of Fat Grafting and Cell-Supplemented Lipotransfer in Athymic Rats: A Pilot Study. Aesthet Surg J 33(5):713-21

8. **Chae JJ**, Jeong MB, Choi JS, Park SA, Yi NY, Kim WT, Seo K (2013). Seasonal Variations of Intraocular Pressure in Normal Sapsaree Dogs. J Vet Clin 30(2):95-9

9. Elisseeff J, Madrid MG, Lu Q, Chae JJ, Guo Q (2013). Future perspectives for regenerative medicine in ophthalmology. Middle East Afr J Ophthalmol 20(1):38-45

10. Hillel AT, Unterman S, Nahas Z, Reid B, Coburn JM, Axelman J, Chae JJ, Guo Q, Trow R, Thomas A, Hou Z, Lichtsteiner S, Sutton D, Matheson C, Walker P, David N, Mori S, Taube JM, Elisseeff JH (2010). Photoactivated composite biomaterial for soft tissue restoration in rodents and in humans. Sci Transl Med 3(93):93ra67

11. Park SA, Yi NY, Jeong MB, Kim WT, Kim SE, Chae JM, Seo KM (2009). Clinical manifestations of cataracts in small breed dogs. Vet Ophthalmol 12(4):205-10

12. Yi NY, Park SA, Jeong MB, Kim WT, Kim SE, Kim JY, Chae JM, Jang KJ, Seong JK, Seo KM (2009). Comparison of orbital prosthesis motility following enucleation or evisceration with sclerotomy with or without a motility coupling post in dogs. Vet Ophthalmol 12(3):139-51

13. Hongyok T, Chae JJ, Shin YJ, Na D, Li L, Chuck RS (2009). Effect of chitosan-N-acetylcysteine conjugate in a mouse model of botulinum toxin B-induced dry eye. Arch Ophthalmol 127(4):525-32

14. Jeong MB, Narfström K, Park SA, Chae JM, Seo KM (2009). Comparison of the effects of three different combinations of general anesthetics on the electroretinogram of dogs. Doc Ophthalmol 119(2):79-88

15. **Chae JM**, Kim WT, Jeong MB, Yi NY, Park SA, Kim SE, Park YW, Han KI, Ha JH, Seo KM (2008). Ophthalmic examination findings in 547 Korean Sapsaree Dogs, J Vet Clin 25(6):481-6

16. Kim SE, Park SA, Kim WT, Jeong MB, Chae JM, Park YW, Seo KM (2008). Retrospective study of anterior lens luxation in 8 dogs J Vet Clin 25(4):292-4

17. Kim HA, Jeong MB, Yi NY, Park SA, Kim WT, Kim SE, Chae JM, Seo KM (2008). Effects of stimulus intensity for Electroretinogram in conscious Miniature Schnauzers. J Vet Med Sci 70(8):857-9

18. Yu HA, Jeong MB, Park SA, Kim WT, Kim SE, Chae JM, Yi NY, Seo KM (2008). The determination of dark adaptation time using Electroretinography in conscious miniature Schnauzer dogs. J Vet Sci 8(4):409-14

19. Kim WT, Park SA, Jeon MB, Yi NY, Kim SE, Chae JM, Kang MS, Kim DY, Seo KM (2007). Multiple ocular defects in a cat J Vet Clin 24(4):640-3

20. **Chae JM**, Jeong MB, Yi NY, Park SA, Kim WT, Kim HA, Kim SE, Seo KM (2007). Prevalence of corneal diseases in dogs in Korea, J Vet Clin 24(3):557-62

21. Kim SE, Park SA, Jeong MB, Yi NY, Kim WT, Chae JM, Seo KM (2007). Idiopathic postganglionic Horner's syndrome in dogs: 3 cases J Vet Clin 24(3):441-3

22. Jeong MB, Kim YJ, Yi NY, Park SA, Kim WT, Kim SE, Chae JM, Kim JT, Lee H, Seo KM (2007). Comparison of the rebound tonometer (TonoVet) with the applanation tonometer (TonoPen XL) in normal Eurasian Eagle owls (Bubo bubo), Vet ophthalmology 10(6):376-9

23. Yi NY, Park SA, Jeong MB, Kim WT, Kim SE, Chae JM, Seo KM (2006). Phacoemulsification and acryl foldable intraocular lens implantation in dogs: 32 cases. J Vet Sci 7(3):281-5

Submitted or to be submitted:

1. Kim C, Shores L, Guo Q, Aly A, Jeon OH, Kim DH, Bernstein N, Bhattacharya R, Chae JJ, Yarema KJ, Elisseeff JH. Electrospun microfiber scaffolds with anti-inflammatory tributanoylated N-acetyl-D-glucosamine promote cartilage regeneration

2. **Chae JJ**, Lee JD, Shin Y, Seo K, Elisseeff JH. Nictitating membrane fixation improves stability of the contact lens on the corneal surface.

3. **Chae JJ**, Shin Y, Chon G, Jeon OH, Kang JU, Elisseeff JH. Reconstructed decellularized tissue for corneal regeneration.

4. Jeon OH, Panicker LM, Lu Q, Chae JJ, Feldman RA, Elisseeff JH, Well-orchestrated coupling of osteoblast to osteoclast derived from human iPSCs promotes bone regeneration